Assessment of Sequential and Simultaneous Ensemble-based History Matching Methods for Weakly Non-linear Problems

Kristian Fossum

Dissertation for the degree of Philosophiae Doctor (PhD)

Department of Mathematics
University of Bergen

November 2014

Dissertation date: 02.13.2015

Preface

The work documented in this thesis is a partial fulfilment of the requirements for the degree of Philosophiae Doctor (PhD) in Applied and Computational Mathematics at the University of Bergen (UiB), Norway.

The PhD project has been supported by Uni Research CIPR through the Research Council of Norways Centre of Excellence grant (#146029/V30).

The supervising committee for this PhD work has been Trond Mannseth (Uni Research CIPR,UiB), Dean S. Oliver (Uni Research CIPR), and Hans J. Skaug (UiB).

Outline

The thesis consists of two parts. Part I is devoted to background theory required for the collection of research papers given in Part II, and is structured as follows. Chapter 1 give an introduction to reservoir modelling and history matching, and motivates the use of stochastic methods.

In Chapter 2, we provide a brief introduction to inverse problems from a Bayesian point of view. Here the filter and smoother approaches are introduced.

Chapter 3 is devoted to parameter estimation problems, considering both the classical and the stochastic approach.

Various sampling method are considered in Chapter 4, and a special emphasis is given to the Markov chain Monte Carlo (MCMC) methods.

In Chapter 5, we introduce ensemble-based methods that either assimilate data sequentially or simultaneously, and we discuss how these methods can be used for parameter estimation problems.

In Chapter 6, we discuss several methods for evaluating sampling performance. Here, it is assumed that the MCMC methods provide exact samples, and that the ensemble-based methods generate approximate samples from some high-dimensional probability distribution function.

The ensemble-based methods depend on the non-linearity of the forward model, in Chapter 7 we introduce two different measures for the degree of non-linearity in the forward model.

In Chapter 8, we provide a brief introduction to mathematical and numerical models for two-phase flow in a porous media.

Abstract

The ensemble Kalman filter (EnKF) has, since its introduction in 1994, gained much attention as a tool for sequential data assimilation in many scientific areas. In recent years, the EnKF has been utilized for estimating the poorly known petrophysical parameters in petroleum reservoir models. The ensemble based methodology has inspired several related methods, utilized both in data assimilation and for parameter estimation. All these methods, including the EnKF, can be shown to converge to the correct solution in the case of a Gaussian prior model, Gaussian data error, and linear model dynamics. However, for many problems, where the methods are applied, this is not satisfied. Moreover, several numerical studies have shown that, for such cases, the different methods have different approximation error.

Considering parameter estimation for problems where the model depends on the parameters in a non-linear fashion, this thesis explore the similarities and differences between the EnKF and the alternative methods. Several characteristics are established, and it is shown that each method represents a specific combination of these characteristics. By numerical comparison, it is further shown that a variation of the characteristics produce a variation of the approximation error.

A special emphasis is put on the effect of one characteristic, whether data are assimilated sequentially or simultaneously. Typically, several data types are utilized in the parameter estimation problem. In this thesis, we assume that each data depends on the parameters in a specific non-linear fashion. Considering the assimilation of two weakly non-linear data with different degree of non-linearity, we show, through analytical studies, that the difference between sequential and simultaneous assimilation depends on the combination of data.

Via numerical modelling, we investigate the difference between sequential and simultaneous assimilation on toy models and simplified reservoir problems. Utilizing realistic reservoir data, we show that the assumption of difference in non-linearity for different data holds. Moreover, we demonstrate that, for favourable degree of non-linearity, it is beneficial to assimilate the data ordered after ascending degree of non-linearity.

List of papers

Paper A: K. Fossum, T. Mannseth, D. S. Oliver, and H. J. Skaug, *Numerical Comparison of Ensemble Kalman Filter and Randomized Maximum Likelihood*, in Proceedings of the 13th European Conference on the Mathematics of Oil Recovery (ECMOR XIII), Biarritz, France, 10-13 September 2012.

Paper B: K. Fossum, and T. Mannseth, *Parameter sampling capabilities of sequential and simultaneous data assimilation. Part I: analytical comparison*, Inverse Problems **30**, 114002, 2014.

Paper C: K. Fossum, and T. Mannseth, *Parameter sampling capabilities of sequential and simultaneous data assimilation. Part II: statistical analysis of numerical results* Inverse Problems **30**, 114003, 2014.

Paper D: K. Fossum, and T. Mannseth, *Evaluation of ordered sequential assimilation for improved EnKF sampling*, in Proceedings of the 14th European Conference on the Mathematics of Oil Recovery (ECMOR XIV), Catania, Sicily, Italy, 8-11 September 2014.

Paper E: K. Fossum, and T. Mannseth, *Assessment of ordered sequential data assimilation*, submitted to Computational Geosciences, 2014.

Acknowledgements

I would first and foremost like to thank my supervisors: Trond Mannseth, Dean S. Oliver, and Hans J. Skaug for guiding me and sharing their knowledge during my years as a PhD student. I would especially like to thank Trond Mannseth, my principal supervisor, for his great insight and for always inspiring me to seek deeper knowledge of problems.

I'm deeply grateful for all my friends and colleagues at Uni Research Centre for Integrated Petroleum Research and at the University of Bergen. I have enjoyed every day of my PhD studies due to the good research and social environment you provide. I would especially like to thank Svenn and Trine for sharing eight years with me as students at the University of Bergen.

This work would never have been completed without the support from my friends and family. A special thanks to my parents for encouraging my curiosity, and to Siren for her constant support.

Kristian Fossum,
Bergen, November 2014

Contents

C Parameter sampling capabilities of sequential and simultaneous data assimilation. Part II: statistical analysis of numerical results

D Evaluation of ordered sequential assimilation for improved EnKF sampling

E Assessment of ordered sequential data assimilation

"We should not be ashamed to acknowledge truth from whatever source it comes to us, even if it is brought to us by former generations and foreign people. For him who seeks the truth there is nothing of higher value than truth itself."

Abu Yussuf Yaakoub Ibn Ishaq as-Sabbah Al-Kindi (801–873)

Part I

Scientific background

Chapter 1

Introduction

A steady and reliable supply of energy is essential for the global community. Ideally, this supply should come from renewable sources such as wind or solar power. However, non-renewable sources, such as hydrocarbons, will, for the foreseeable future, continue to play a fundamental role in the global energy mix. Hydrocarbons have, for the last century, been one of the worlds most important sources of energy. The chemical composition of hydrocarbons, allowing safe transportation and storage, makes them an ideal energy carrier. This ensures that hydrocarbons will keep their role as an elemental part of the gradually more renewable energy mix, and that they will continue to be one of the most sought after commodities worldwide. Exploration after and production of hydrocarbons is, therefore, still an important activity for a wide range of companies and countries.

Hydrocarbons, in the form of oil and gas, have been produced from underground reservoirs for more than 150 years. During these years, increased industry competence has made production from off-shore reservoirs, such as the oil and gas fields on the Norwegian continental shelf, possible. The increased complexity associated with the production from off-shore oil and gas fields induce higher costs, especially related to drilling of wells. In order to be economically feasible, a typical off-shore reservoir has to contain a minimum number of wells which must produce a maximum amount or hydrocarbons. Unfortunately, the success of any well depends on the properties of the subsurface, which are, generally, poorly known.

There is a large risk associated with exploration and production of hydrocarbons, and methods for predicting future production with associated uncertainty are needed to mitigate this risk. In this regard, reservoir modelling plays a vital part in the petroleum industry work-flow. Reservoir modelling consists of representing multiphase fluid-flow in the porous media (the reservoir) via mathematical formulae. Solving these formulae with correct initial and boundary conditions enables, in principle, the prediction of any dynamic quantities, such as pressures and fluid saturations, in both space and time. Moreover, this framework enables the reservoir engineer to assess the effects of different production strategies, e.g., different well positions, production rates, etc., with a minimum cost.

With the exception of the simplest cases, the mathematical formulae cannot be solved analytically; they need to be solved numerically. The reservoir model is then represented by a 3D grid consisting of cells, where each cell is associated with a number of constant parameters and dynamical states. By discretizing the mathematical

equations, the numerical solution consists of estimating the time evolution of the dynamical states, e.g., the pressure and saturation, in each cell.

There are many sources of uncertainty in this setup. Several simplifications are needed to derive the mathematical formulae; hence, the formulae never represent the real world exactly. Moreover, the numerical schemes utilized for solving the equations involve approximations, and the solution always contain some numerical error. Finally, the grid will only approximate the subsurface, especially the petrophysical quantities, assumed to be constant within the cells, are only known approximately. The error caused by the final approximation is the main concern in this thesis.

Production of hydrocarbons is a dynamic process. Hence, as time evolves, one can observe the true values of the dynamic process. Such observations can, for example, consist of pressure measurements made in the wells. These observations, or data, can then be compared with the predictions made by the numerical model. One can then adjust the model such that the error between predictions and data is minimized; this process is referred to as *history matching* or *data assimilation*. Since data contain information about the real world, it is reasonable to assume that history matching will reduce the uncertainty in the numerical model, and, thus, reduce the error in the predictions made by the model.

The process of collecting data is never exact. We must always assume that the data contain error, arising from several sources. Firstly, no observation apparatus is able to measure the dynamical state in an exact manner, which introduces error. Secondly, indirect measurements are often utilized. That is, the measured quantities are connected to the dynamic state via a functional relationship. Extraction of the correct information relies on correct modelling of this functional relationship. Error in the data can be introduced by this modelling step for the same reasons as above. Thirdly, the measurement and the grid cell are represented on different scales in the computational model. Compared to the size of the grid cell, the measurement can be considered as a point measurement. Moreover, this point may or may not be centred in the grid cell, and extrapolation methods may be needed to properly represent the measurement in the cell. This process is never exact and will also introduce error in the data.

Since both the numerical model and the data contain error, it is advantageous to consider them as stochastic variables. In this framework, the history matching problem can be solved by Bayes' theorem. Under some general assumptions, this procedure consists of estimating the conditional probability density function (PDF) of the unknown quantities in the numerical model – denoted the posterior – given the PDF of the data – denoted the likelihood – and the PDF of predicted numerical quantities – denoted the prior. Typically, this procedure, referred to as the *analysis step*, is expressed as

$$\text{Posterior} = \text{Const} \times \text{Prior} \times \text{Likelihood}, \tag{1.1}$$

where Const denotes a normalizing constant. The numerical reservoir model will then, when considered as a stochastic model, be used for modelling the temporal evolution of the PDF of model quantities, mapping the posterior PDF at the current data-assimilation time to the prior PDF at the next data-assimilation time. This procedure is referred to as the *forecast step*. Note that the initial PDF must contain all prior information regarding the subsurface. (This PDF is often referred to as the initial prior PDF.)

Even though Bayes' theorem provides the correct solution to the history matching problem, it is generally impossible to calculate the posterior PDF without extra assump-

tions. The computational complexity is mainly caused by the normalizing constant, which, for any realistic reservoir case, involves the solution of a high-dimensional integral. As an alternative to a full evaluation of the posterior PDF, one can rely on methods that draw samples from the PDF. Utilizing such methods, one can obtain estimates of statistical quantities, such as mean and variance, via Monte Carlo (MC) methods (see, Chapter 4). Unfortunately, methods that sample exactly from a general PDF are computationally demanding and difficult to utilize for realistic cases.

The Bayesian approach can be significantly simplified by making assumptions on the structure of the prior model, the likelihood model, and the numerical model. If the prior model for the unknown quantities is Gaussian, the data errors are Gaussian, and the forward model is linear in the unknown quantities (preserving Gaussianity), all PDFs involved in the forecast and analysis steps are Gaussian. This is denoted a Gauss-linear problem. If these assumptions hold, the history matching problem is solved by the well known Kalman filter (KF) equations [54]. Since a Gaussian PDF is completely described by its mean and covariance matrix, the KF provides equations for the forecast and analysis of the mean and covariance.

For many interesting problems the assumptions made by the KF are not valid. Typically, the forward model depends non-linearly on the unknown quantities, and Gaussianity is not preserved. For such problems, the KF cannot be utilized directly. A common solution is to linearize the model. This allows calculation of linearized forecasts of the covariance, and it enables a linearized analysis step. This approach is generally known as the extended Kalman Filter (ExKF). However, the linearization will introduce additional error in the model, and for highly non-linear problems the approximation error is high. For realistic models there are typically a large number of unknown quantities, e.g. reservoir models that contain a high number of grid cell with corresponding values for the petrophysical and dynamic quantities. Both the KF and the ExKF require the storage and update of the covariance matrix, and for large models the covariance matrices cannot be stored in the computer memory.

As a solution to the storage problem, the ensemble Kalman Filter (EnKF) was introduced by Evensen in [27]. Here, the PDF is approximated by an ensemble of models. Each ensemble member is evolved in time, approximating the forecast step. Following this, each ensemble member is analysed utilizing an approximation to the KF equations. Throughout, the mean and covariance are approximated via an MC approach. The EnKF avoids formulating the full covariance matrices, and the method only needs to store the ensemble of models. Since one usually apply much fewer ensemble members than unknown quantities, the computational savings are significant. If the KF assumptions of Gaussianity are satisfied, the EnKF estimate of mean and covariance converge to the KF solution when the number of ensemble members goes to infinity. Hence, for Gauss-linear problems the EnKF has well defined asymptotic properties. The EnKF forecast does not make any assumptions on the forward model, and it can therefore be directly implemented, without derivatives, even if the forward model is non-linear. For this reason, the EnKF is well suited as an alternative to the ExKF for data assimilation of large scale problems such as atmospheric and oceanographic models or petroleum reservoirs. However, for non-linear forward models the asymptotic property of the EnKF is not known, and it is reasonable to assume that the EnKF only provides an approximation to the posterior PDF, for such cases. Unfortunately, for non-linear models one does not know how large this approximation error is.

The EnKF is only one of several methods that can be utilized for solving the Bayesian history matching problem. If one (in addition) restrain the problem to only estimating the petrophysical quantities, which are constant in time, the number of alternative ensemble-based algorithms becomes even higher. All these methods are based on the Bayesian approach, and they are designed to solve the same problem. If the KF assumptions of Gaussianity are valid all the methods considered in this thesis have well-defined asymptotic behaviour, but for non-linear forward models the methods only provide approximations. Similar to the EnKF, one does not know the size of the approximation error, but numerical experiments have shown that different methods provide different degrees of error.

Since all methods seek the solution to the same problem, there are some clear similarities between the methods. Nevertheless, they all differ with regards to some key characteristics, which can be considered as defining for the individual methods. The emphasis of this thesis is to investigate the effects of these characteristics with regards to the approximation error. Analytical and numerical investigations are conducted to explore if some characteristics lead to a reduction of the approximation error. There is a special emphasis on the characteristic of whether data are assimilated sequentially or simultaneously, and Papers B–E are only concerned with this characteristic.

Chapter 2

Inverse problem

Modelling of natural phenomenons constitute the basis of natural science, and successful models are essential for understanding and describing the behaviour of any physical system. Generally, the derivation of such models follow three main steps with related uncertainties [96]. The first step, typically referred to as *parametrisation*, is to identify a minimal set of model quantities, $\boldsymbol{y} \in \mathbb{R}^{n_y}$, that completely defines the natural phenomenon. The model quantities can typically be split into two according to the following principle. If the quantity varies as the model evolves through time it is defines as a model *state*. If, on the other hand, the quantity stays constant in time it is defined as a model *parameter*. In the following, all model quantities $\boldsymbol{y}$ are considered jointly. One can, unfortunately, not guarantee that $\boldsymbol{y}$ properly represents the natural phenomenon. For this reason, it is reasonable to assume that the parametrisation contains some representation error.

The second step, referred to as *forward modelling*, is to define mathematical models such that, for given values of $\boldsymbol{y}$, observable quantities, $\boldsymbol{d} \in \mathbb{R}^{n_d}$, can be predicted by solving the mathematical equations. For most problems, it would be impossible to solve the mathematical models without making additional simplifications or assumptions. In addition, the equations must often be solved via numerical methods. For these reasons, one must assume that, in addition to the representation error, the forward model contains modelling errors.

The final step, referred to as *inverse modelling*, consists of utilizing actual observations of the natural phenomenon, $\boldsymbol{d}$, to infer the values of $\boldsymbol{y}$. However, observations are never generated without some error, either caused by the instruments or by the representation of observations in the numerical model. Thus, one must always assume that the observations contain measurement errors. These three steps are closely related, as the inverse modelling relies on both parametrisation and forward modelling. For this reason, inverse modelling depends on a correct inclusion of the uncertainties.

Considering the definition of a well-posed problem in the terms of [46], that is,

- the problem has a solution,
- the solution is unique, and
- the solution is a continuous function of the data,

it is well-known that most inverse-modelling problems, when no assumptions are made with regards to the various error terms, are ill-posed problems. The current chapter pro-

vides the reader with a brief overview of probabilistic methods for solving the inverse problem, focussing on the Bayesian framework.

2.1 Bayesian formulation

Mathematically, the relationship between the observations, $\boldsymbol{d}$, and the model quantities, $\boldsymbol{y}$, can be defined as

$$\boldsymbol{d} = G(y). \tag{2.1}$$

Here, $G(\cdot)$ can be thought of as the combination of two operators, $H(F(\cdot))$, where $H(\cdot)$ is the measurement operator, and $F(\cdot)$ is the forward-model operator, defined by the discretized mathematical model. The inverse problem consists of estimating $\boldsymbol{y}$ given observations $\boldsymbol{d}$. From the above discussion, it is clear that this system contains several sources of error. A more appropriate relation between $\boldsymbol{d}$ and $\boldsymbol{y}$ is therefore

$$\boldsymbol{d} = G(\boldsymbol{y}) + \boldsymbol{\xi}, \tag{2.2}$$

where $\boldsymbol{\xi}$ is an unknown error term, and it is assumed that the error is additive. If one considers $\boldsymbol{\xi}$ as a random variable with zero mean and known statistical properties, we can derive a well-defined solution to the inverse problem (2.2) by posing it in a Bayesian framework.

Random variables are defined by their probability measure μ, defined on a measurable space by the pair $(\Omega, \mathcal{F})$, where Ω is the sample space, and $\mathcal{F}$ is a sigma-algebra. For our applications we consider the cases where Ω is a separable finite dimensional Banach space, $\mathcal{F}$ is a Borel sigma-algebra generated by the open sets, and μ is absolutely continuous with respect to the Lebesque measure. The measure can then be defined via the well known PDF, p,

$$\mu(\mathcal{X}) = \int_{\mathcal{X}} p(\boldsymbol{x}) \mathrm{d}\boldsymbol{x}, \tag{2.3}$$

for $\mathcal{X} \in \mathcal{F}$. For more details regarding probability measures, see, e.g., [68, 94].

Solving the inverse problem using the Bayesian framework consists of finding the posterior PDF, i.e., the conditional PDF of $\boldsymbol{y}$ given $\boldsymbol{d}$, written as $p(\boldsymbol{y}|\boldsymbol{d})$. This is easily formulated via Bayes' theorem

$$p(\boldsymbol{y}|\boldsymbol{d}) = \frac{p(\boldsymbol{d}|\boldsymbol{y})\, p(\boldsymbol{y})}{\int_{\mathbb{R}^{n_y}} p(\boldsymbol{d}|\boldsymbol{y})\, p(\boldsymbol{y}) \mathrm{d}\boldsymbol{y}}. \tag{2.4}$$

By defining a suitable data likelihood,

$$p(\boldsymbol{d}|\boldsymbol{y}) = p(\boldsymbol{\xi} = \boldsymbol{d} - G(\boldsymbol{y})), \tag{2.5}$$

and incorporating all prior information into $p(\boldsymbol{y})$ it is, conceptually, possible to calculate the posterior PDF.

With the Bayesian approach it is possible to show that for some cases where the inverse problem (2.1) is ill-posed, the inverse problem (2.2) might be well posed in a probabilistic setting [94].

2.2 Smoothing

For many cases, the model quantities and the data vary in time, and $G(\cdot)$ represents a dynamical system. For such cases, the inverse problem consists of estimating $y(t)$ conditioned to $d(t)$, where t denotes time. In the dynamical system, it is beneficial to separate $G(\cdot)$ into a prediction model and an observation model. Let us assume that the observations are available at n_a discrete points in time, $\boldsymbol{d}_{t_k}$, for $k = 1,\ldots,n_a$, and let us, for simplicity, assume that the model equations are solved at the same time as data are available. Throughout, we will, for notational convenience, write k as short for the discretized time step t_k. The system evolution from the $(k-1)$'th time step to the k'th time step is then given as

$$\boldsymbol{y}_k = F(\boldsymbol{y}_{k-1}) + \boldsymbol{\eta}_k, \tag{2.6}$$

and the observations at the k'th time step are given as

$$\boldsymbol{d}_k = H(\boldsymbol{y}_k) + \boldsymbol{\epsilon}_k. \tag{2.7}$$

Here $\boldsymbol{\eta}$ denotes a combination of the modelling error and the representation error, and $\boldsymbol{\epsilon}$ denotes the measurement error.

In this setting, the inverse problem consists of finding the PDF of $\boldsymbol{y}_k$ conditioned to $\boldsymbol{d}_k$ for $k = 1,\ldots,n_a$. This is easy to formulate utilizing Bayes' theorem, omitting the normalizing constant,

$$p\left(\boldsymbol{y}_{1:n_a}|\boldsymbol{d}_{1:n_a}\right) \propto p\left(\boldsymbol{d}_{1:n_a}|\boldsymbol{y}_{1:n_a}\right) p\left(\boldsymbol{y}_{1:n_a}\right), \tag{2.8}$$

where the subscripts are shorthand notation for the joint distribution, i.e.,

$$p\left(\boldsymbol{y}_{1:n_a}|\boldsymbol{d}_{1:n_a}\right) = p\left(\boldsymbol{y}_1,\boldsymbol{y}_2,\ldots,\boldsymbol{y}_{n_a}|\boldsymbol{d}_1,\boldsymbol{d}_2,\ldots,\boldsymbol{d}_{n_a}\right). \tag{2.9}$$

For some problems, one may only be interested in the model quantities at a specific time. Utilizing (2.8) one can easily find the expression for $\boldsymbol{y}$ at the k'th time step by integrating (2.8) with respect to $\boldsymbol{y}_1,\ldots,\boldsymbol{y}_{k-1},\boldsymbol{y}_{k+1},\ldots,\boldsymbol{y}_{n_a}$. This is generally referred to as the *smoother* solution of the inverse problem. A special feature of the smoother solution is that $\boldsymbol{y}_k$ will be calculated utilizing data from both previous, current, and subsequent time steps.

The smoother expression can either be calculated by all data simultaneously as in (2.8), or by utilizing data as they become available [30]. This last approach is shown by rewriting (2.8) as

$$p\left(\boldsymbol{y}_{1:n_a}|\boldsymbol{d}_{1:n_a}\right) \propto p\left(\boldsymbol{d}_{n_a}|\boldsymbol{y}_{1:n_a}\right) p\left(\boldsymbol{y}_{n_a}|\boldsymbol{y}_{1:n_a-1}\right) p\left(\boldsymbol{y}_{1:n_a-1}|\boldsymbol{d}_{1:n_a-1}\right). \tag{2.10}$$

By assuming that $p\left(\boldsymbol{y}_{1:n_a-1}|\boldsymbol{d}_{1:n_a-1}\right)$ is obtained at the previous time step, it is clear that $p\left(\boldsymbol{y}_{1:n_a}|\boldsymbol{d}_{1:n_a}\right)$ can be obtained by calculating the transition PDF, $p\left(\boldsymbol{y}_{n_a}|\boldsymbol{y}_{1:n_a-1}\right)$, and the data PDF, $p\left(\boldsymbol{d}_{n_a}|\boldsymbol{y}_{1:n_a}\right)$, when $\boldsymbol{d}_{n_a}$ become available.

Equation (2.10) is simplified significantly by assuming that the PDFs at time step k only depend on the PDF at $k-1$. Models that have this property are called Markov processes [68]. If one additionally assumes that measurements collected at different time steps are independent from each other, and that $\boldsymbol{d}_k$ only depends on $\boldsymbol{y}_k$ for $k = 1,\ldots,n_a$, (2.10) reduces to

$$p\left(\boldsymbol{y}_{1:n_a}|\boldsymbol{d}_{1:n_a}\right) \propto p\left(\boldsymbol{d}_{n_a}|\boldsymbol{y}_{n_a}\right) p\left(\boldsymbol{y}_{n_a}|\boldsymbol{y}_{n_a-1}\right) p\left(\boldsymbol{y}_{1:n_a-1}|\boldsymbol{d}_{1:n_a-1}\right). \tag{2.11}$$

2.3 Filtering

Contrary to the smoother solution, the filter solution is defined as the conditional density of the model quantities at the final time step given all data up to and including that time step. Hence, when solving the filter problem one seeks the conditional density $p\left(\boldsymbol{y}_{n_a}|\boldsymbol{d}_{1:n_a}\right)$. Assuming that the smoother PDF is known up to a normalizing constant, the filter solution is written as

$$\begin{aligned} p\left(\boldsymbol{y}_k|\boldsymbol{d}_{1:k}\right) &\propto \int_{\boldsymbol{y}_{1:k-1}} p\left(\boldsymbol{y}_{1:k}|\boldsymbol{d}_{1:k}\right)\mathrm{d}\boldsymbol{y}_{1:k-1}, \\ &\propto \int_{\boldsymbol{y}_{1:k-1}} p\left(\boldsymbol{y}_{1:k-1}|\boldsymbol{d}_{1:k-1}\right) p\left(\boldsymbol{y}_k|\boldsymbol{y}_{k-1}\right)\mathrm{d}\boldsymbol{y}_{1:k-1} p\left(\boldsymbol{d}_k|\boldsymbol{y}_k\right), \\ &\propto \int_{\boldsymbol{y}_{1:k-1}} p\left(\boldsymbol{y}_{1:k}|\boldsymbol{d}_{1:k-1}\right)\mathrm{d}\boldsymbol{y}_{1:k-1} p\left(\boldsymbol{d}_k|\boldsymbol{y}_k\right), \\ &= c\, p\left(\boldsymbol{y}_k|\boldsymbol{d}_{1:k-1}\right) p\left(\boldsymbol{d}_k|\boldsymbol{y}_k\right). \end{aligned} \tag{2.12}$$

If we assume that $\boldsymbol{\eta}$ is a vector Brownian motion with $\mathbb{E}\left[\mathrm{d}\boldsymbol{\eta}_t \mathrm{d}\boldsymbol{\eta}_t^T\right] = Q_y(t)\mathrm{d}t$, the time evolution of the prior PDF, $p\left(\boldsymbol{y}_k|\boldsymbol{d}_{1:k-1}\right)$, satisfies Kolmogorov's forward equation and can be written as [53]

$$\mathrm{d}p\left(\boldsymbol{y}_k|\boldsymbol{d}_{1:k-1}\right) = l\left(p\right)\mathrm{d}t, \qquad k-1 \le t < k, \tag{2.13}$$

where

$$l\left(p\right) = -\sum_{j=1}^{\mathbb{R}^{n_y}} \frac{\partial pF}{\partial y_j} + \frac{1}{2}\sum_{i,j=1}^{\mathbb{R}^{n_y}} \frac{\partial^2\left(pQ_y\right)_{i,j}}{\partial y_i \partial y_j}. \tag{2.14}$$

Hence, solving the filter at time step k is a two-step process. Firstly, the prior PDF, $p\left(\boldsymbol{y}_k|\boldsymbol{d}_{k-1:1}\right)$, is calculated utilizing Kolmogorov's forward equation; this corresponds to the prediction step. Secondly, the filter solution is calculated by (2.12); this corresponds to the analysis step.

Since the filter solution is defined as the marginal of the smoother, one can in principle calculate the filter solution by assimilating all data simultaneously. However, the filter solution usually assimilated data sequentially, calculating the prediction and analysis each time data becomes available. Note that the filter and smoother solution defined at the final data assimilation step are identical.

2.4 Filtering for Gauss-linear problems

As shown in the previous section, it is easy to derive the filter equations. Unfortunately, the filter solution is not easy to evaluate since it involves the evaluation of several high-dimensional integrals, both in (2.12) and in the normalizing constant.

However, for a special case, there exists a closed-form solution to the filter problem. The solution procedure, known as the Kalman filter (KF), can be derived by numerous approaches. In the following, we outline the version provided in [53]. Let us assume that the model is described by a linear stochastic differential equation

$$\mathrm{d}\boldsymbol{y}_t = F\boldsymbol{y}_t\mathrm{d}t + \mathrm{d}\boldsymbol{\eta}_t, \qquad t \ge t_0, \tag{2.15}$$

where F represents a linear function, and $\{\boldsymbol{\eta}_t,\, t \geq t_0\}$ is a vector Brownian motion process with $\mathbb{E}\left[\mathrm{d}\boldsymbol{\eta}_t \mathrm{d}\boldsymbol{\eta}_t^T\right] = Q_\eta\,(t)\,\mathrm{d}t$. Furthermore, let the observations be given by

$$\boldsymbol{d}_k = H\boldsymbol{y}_k + \epsilon_k, \qquad t = 1, \cdots, n_a \tag{2.16}$$

where H represents a linear function, and the sequence $\{\boldsymbol{\epsilon}_n\}_{n=1}^{n_a}$ is a white Gaussian sequence with $\boldsymbol{\epsilon}_k \sim N\left(\mathbf{0}, Q_{d_k}\right)$. In addition, let us assume that the prior PDF of y_{t_0} is Gaussian $\boldsymbol{y}_{t_0} \sim N\left(\boldsymbol{\mu}_{y_{t_0}}, Q_{y_{t_0}}\right)$, and that y_{t_0}, $\{\eta_t\}$, and $\{\epsilon_k\}$ are independent.

With these assumptions all the densities in (2.12) are Gaussian, and to find $p\left(\boldsymbol{y}_k|\boldsymbol{d}_{1:k-1}\right)$ we only need to consider the time evolution of the mean and covariance matrix, given as

$$\frac{\mathrm{d}\boldsymbol{\mu}_{y_t}}{\mathrm{d}t} = F\boldsymbol{\mu}_{y_t}, \qquad \frac{\mathrm{d}Q_{y_t}}{\mathrm{d}t} = FQ_{y_t} + Q_{y_t}F^T + Q_\eta, \tag{2.17}$$

where the solution to (2.17), the forecast mean and covariance at time k, are denoted $\boldsymbol{\mu}_{y_k^*}$ and $Q_{y_k^*}$. Throughout this introduction, we will, to differentiate between the prediction and the analysis, denote the prediction with a superscripted $*$. Since the observation error is Gaussian, the PDF for $p\left(\boldsymbol{d}_k|\boldsymbol{y}_k\right)$ is given as

$$p\left(\boldsymbol{d}_k|\boldsymbol{y}_k\right) \propto \exp\left(-\frac{1}{2}\left(\boldsymbol{d}_k - H\boldsymbol{y}_k\right)^T Q_{d_k}^{-1}\left(\boldsymbol{d}_k - H\boldsymbol{y}_k\right)\right). \tag{2.18}$$

If one in addition notes that the normalizing constant in (2.12) is given as

$$p\left(\boldsymbol{d}_k|\boldsymbol{d}_{k:1}\right) = N\left(H\boldsymbol{\mu}_{y_k^*}, HQ_{y_k^*}H^T + Q_{d_k}\right), \tag{2.19}$$

it is possible to derive the PDF for the filter analysis. Inserting the above expressions into (2.12) gives

$$p\left(\boldsymbol{y}_k|\boldsymbol{d}_{k:1}\right) \propto \exp\left(-\frac{1}{2}[\cdot]\right) \tag{2.20}$$

where

$$\begin{aligned}[\cdot] = &\left(\boldsymbol{d}_k - H\boldsymbol{y}_k\right)^T Q_{d_k}^{-1}\left(\boldsymbol{d}_k - H\boldsymbol{y}_k\right) + \left(\boldsymbol{y}_k - \boldsymbol{\mu}_{y_k^*}\right)^T Q_{y_k^*}^{-1}\left(\boldsymbol{y}_k - \boldsymbol{\mu}_{y_k^*}\right) \\ &- \left(\boldsymbol{d}_k - H\boldsymbol{\mu}_{y_k^*}\right)^T \left(HQ_{y_k^*}H^T + Q_{d_k}\right)^{-1}\left(\boldsymbol{d}_k - H\boldsymbol{\mu}_{y_k^*}\right).\end{aligned} \tag{2.21}$$

Since all PDFs in (2.12) are Gaussian, we must have

$$p\left(\boldsymbol{y}_k|\boldsymbol{d}_{k:1}\right) \sim N\left(\boldsymbol{\mu}_{y_k}, Q_{y_k}\right), \tag{2.22}$$

and (2.21) must have the form

$$[\cdot] = \left(\boldsymbol{y}_k - \boldsymbol{\mu}_{y_k}\right)^T Q_{y_k}^{-1}\left(\boldsymbol{y}_k - \boldsymbol{\mu}_{y_k}\right). \tag{2.23}$$

As shown in [53], it is possible to rewrite (2.21) in the form of (2.23) by completing the square. The equation for the analyzed mean and covariance are then given as

$$\boldsymbol{\mu}_{y_k} = \left(H^T Q_{d_k}^{-1} H + Q_{y_k^*}^{-1}\right)^{-1}\left(H^T Q_{d_k}^{-1}\boldsymbol{d}_k + Q_{y_k^*}^{-1}\boldsymbol{\mu}_{y_k^*}\right), \tag{2.24}$$

$$Q_{y_k}^{-1} = Q_{y_k^*}^{-1} + H^T Q_{d_k}^{-1} H. \tag{2.25}$$

The equations for the analysed mean and covariance require the inversion of the $n_y \times n_y$ matrix in (2.24). In a filter, data are assimilated sequentially and usually $n_y > n_d$. For such cases one can, utilizing the Woodburry formula (see, e.g., [47]) rewrite (2.24) and (2.25) such that it is only necessary to invert a $n_d \times n_d$ matrix. This version of the analysis equations corresponds to the well known Kalman filter equations [54]

$$\boldsymbol{\mu}_{y_k} = \boldsymbol{\mu}_{y_k^*} + K\left(\boldsymbol{d}_k - H\boldsymbol{\mu}_{y_k^*}\right), \tag{2.26}$$

$$Q_{y_k} = Q_{y_k^*} - KHQ_{y_k^*}, \tag{2.27}$$

where

$$K = Q_{y_k^*}H^T\left(HQ_{y_k^*}H^T + Q_{d_k}\right)^{-1}, \tag{2.28}$$

is denoted the Kalman gain.

2.5 Smoothing for Gauss-linear problems

As discussed in Section 2.2, the smoothing estimate is concerned with finding the conditional PDF of $\boldsymbol{y}$ at any time step given data at all n_a observation points. Compared to the filter solution, which only contains information from previous time steps, the smoother improves the estimate of $\boldsymbol{y}_k$ for $k < n_a$ by including information available at subsequent time steps in the analysis.

Smoothing can be performed in several ways depending on the problem and, especially, on the operational setting, see, e.g., [65, 90]. To discuss the various smoothing methods, let us consider a satellite that is gathering measurements at discrete time steps. Post-processing of a measurement requires accurate estimates of the satellites position at the time when the measurement was obtained. For this reason, one observes the trajectory of the satellite and gathers observations of the trajectory at the same discrete times as the satellite is taking measurements.

Let us assume that, for some operational reason, after the measurement is gathered there is a fixed lag of n time steps before the measurement can be transmitted. Since accurate post-processing of the satellite measurement requires high accuracy of the satellite trajectory, it is possible to improve this results by including the n extra observations of the satellite trajectory that are available due to the lag. In formal terms, one seeks the estimate of $\boldsymbol{y}_{k-n}$ given $\boldsymbol{d}_{1:k}$, where n is fixed. This estimation procedure is referred to as *fixed lag smoothing*.

Alternatively, one might be interested in a certain point fixed in time, e.g., a special measurement made by a satellite at time step k. As observations of the satellite trajectory are made at $k+j$, where $j = 1, 2, \ldots$, one seeks to improve post-processing of the measurement made at time step k by updating the estimate of the satellite position $\boldsymbol{y}_k$. This smoothing procedure is referred to as *fixed point smoothing*.

The final smoothing procedure we consider is *fixed interval smoothing*. Here it is assumed that we are only able to observe the satellite within a limited time interval. The fixed interval smoother then utilizes all these observations simultaneously to estimate the PDF of $\boldsymbol{y}$ at every time step within the interval. This smoothing procedure is well suited for weather prediction scenarios. Here a weather system is being observed in a fixed time window. At the end of the time window one can utilize all the observations to find the most accurate description of the weather system. This estimate is then used

as the initial conditions in the next weather forecasts. (The 4D-Var algorithm, currently utilized in several meteorological centres [22, 101], is formulated as a fixed interval smoother.)

For each smoothing scenario there exists at least one algorithm, see, e.g., [65, 90]. For completeness we describe the Rauch-Tung-Striebel (RTS) smoother [76], which is a fixed interval smoother. Let us, for simplicity, assume that the forward model, F, is discretized in both time and space, and that the solution of the forward-model equations and the observations occur at the same, discrete, time steps. Contrary to (2.15), the forward model is now described by the difference equation

$$\boldsymbol{y}_{k+1} = F\boldsymbol{y}_k + \eta_{k+1}, \tag{2.29}$$

where the model error, $\{\eta_n\}_{n=1}^{n_a}$, is a white Gaussian sequence, $\eta_k \sim N\left(0, Q_{\eta_k}\right)$. With these assumptions, the forward evolution of the model and covariance are given by

$$\boldsymbol{\mu}_{y_{k+1}} = F\boldsymbol{\mu}_{y_k}, \qquad Q_{y_{k+1}} = FQ_{y_k}F^T + Q_{\eta_{k+1}}. \tag{2.30}$$

The RTS smoother is calculated in two stages. Firstly, one calculates the analysed mean, $\boldsymbol{\mu}_{y_k^{KF}}$, and covariance, $Q_{y_k^{KF}}$, via the standard Kalman filter as defined in Section 2.4, for $k = 1, \cdots, n_a$. Secondly, one update the mean and covariance by the RTS smoother equations for $k = n_a - 1, \ldots, 1$ given as

$$\boldsymbol{\mu}_{y_k} = \boldsymbol{\mu}_{y_k^{KF}} + B_k\left(\boldsymbol{\mu}_{y_k+1} - F\boldsymbol{\mu}_{y_k^{KF}}\right), \tag{2.31}$$

$$Q_{y_k} = Q_{y_k^{KF}} + B_k\left(Q_{y_k+1} - FQ_{y_k^{KF}}F^T + Q_{\eta_{k+1}}\right)B_k, \tag{2.32}$$

where

$$B_k = Q_{y_k^{KF}}F^T\left(FQ_{y_k^{KF}}F^T + Q_{\eta_{k+1}}\right)^{-1}. \tag{2.33}$$

Hence, when estimating the sequence of model quantities the smoother represents an extension of the KF.

2.6 Filter approximation for non-linear problems

When deriving both (2.15) and (2.29) it was assumed that the forward model was linear. However, this assumption does not hold for a wide range of practical problems, and for such problems one cannot utilize the filter or smoother algorithms shown in the two preceding sections. In this section, we provide a brief introduction to the ExKF, which is an approximate algorithm for non-linear problems [19, 53, 65]. Let us assume that the forward model and observation model provided in (2.6) and (2.7) are differentiable non-linear functions, and let us, further, assume that the model and observation error are distributed as in section 2.4.

The update equation for the ExKF is, similar to the KF, performed in two steps. Let us assume that the previous analysis of the mean, $\boldsymbol{\mu}_{y_{k-1}}$, and the covariance, $Q_{y_{k-1}}$, are known. The predicted mean is obtained by direct application of the non-linear model operator

$$\boldsymbol{\mu}_{y_k^*} = F\left(\boldsymbol{\mu}_{y_{k-1}}\right), \tag{2.34}$$

and the predicted covariance is given by the linearized approximation

$$Q_{y_k^*} = \mathcal{F} Q_{y_{k-1}} \mathcal{F}^T + Q_{\eta_k}, \tag{2.35}$$

where

$$\mathcal{F} = \frac{\partial F\left(\boldsymbol{\mu}_{y_{k-1}}\right)}{\partial \boldsymbol{\mu}_{y_{k-1}}}. \tag{2.36}$$

The analysed mean and covariance are then given as

$$\boldsymbol{\mu}_{y_k} = \boldsymbol{\mu}_{y_k^*} + \mathcal{K}\left(\boldsymbol{d}_k - H\left(\boldsymbol{\mu}_{y_k^*}\right)\right) \tag{2.37}$$

$$Q_{y_k} = Q_{y_k^*} - \mathcal{K}\mathcal{H} Q_{y_k^*}, \tag{2.38}$$

where

$$\mathcal{H} = \frac{\partial H\left(\boldsymbol{\mu}_{y_k^*}\right)}{\partial \boldsymbol{\mu}_{y_k^*}}, \tag{2.39}$$

and

$$\mathcal{K} = Q_{y_k^*} \mathcal{H}^T \left(\mathcal{H} Q_{y_k^*} \mathcal{H}^T + Q_{d_k}\right)^{-1}. \tag{2.40}$$

The ExKF works by relinearizing the system at each assimilation step where linearized measurements are incorporated. For moderately non-linear systems, this procedure ensures that the deviation from the true solution remains small enough to allow for linearization. However, in the presence of significant non-linearities the procedure might fail. For such systems the estimate can be improved by incorporating iterations [53]. Note that the ExKF is not an optimal filter, that is, the mean and covariance will not provide a valid estimate of the true posterior mean and covariance, and since the true posterior density is not guaranteed to be Gaussian, it cannot be fully described using only the mean and covariance.

Chapter 3

Parameter estimation

The previous chapter introduced the general inverse problem, where we considered the estimation of the model quantity $\boldsymbol{y}$ given a time sequence of data. By assuming that all the error terms were clearly defined, we could pose the inverse problem in a stochastic framework and utilize the powerful methods that are available for dynamical stochastic systems. As briefly discussed in the previous chapter, the model quantity $\boldsymbol{y}$ can be split into two groups

$$\boldsymbol{y} = \begin{pmatrix} \boldsymbol{z} \\ \boldsymbol{m} \end{pmatrix}, \tag{3.1}$$

where the states, $\boldsymbol{z}$, represent quantities that vary in time according to the system equations, and the parameters, $\boldsymbol{m}$, represent coefficients in the system equations, which are constant in time.

The methods considered in the previous chapter are designed for state estimation problems. However, for many problems, estimating the poorly known parameters is of much higher importance than the estimation of the dynamic states. Examples of such problems are models for multiphase fluid flow in porous media, where important parameters, such as permeability and porosity, are poorly known. Contrary to, e.g., atmospheric models, such problems have (approximately) static initial conditions, and the model equations describing the fluid flow do not show chaotic behaviour. If the initial conditions are known, the dynamic quantities can be estimated at any point in time. The quality of this estimation, for non-chaotic problems, will mainly depend on the unknown parameters. However, the forward model equations can still contain large approximation errors. Typically, such errors are poorly understood, and their contribution is, therefore, often neglected.

In this section, we provide solution strategies for the parameter estimation problem considering both the classical and the stochastic approach. In addition, we will discuss two different formulations of the parameter estimation problem.

3.1 Classical approach

Even though the statistical approach is very powerful for solving inverse problems, it is still possible to find solutions where no assumptions are made regarding the nature of the error term in (2.2). Let us assume that we have some noisy measurements, $\boldsymbol{d}$, of

a physical problem, modelled as

$$\boldsymbol{d} = G(\boldsymbol{m}) + \boldsymbol{\xi}. \tag{3.2}$$

Contrary to (2.2), this model only depends on the unknown parameters, and we do not know if the error term arise from the forward-model operator or the measurement operator. The parameter estimation problem consists of estimating $\boldsymbol{m}$ from the noisy measurements, $\boldsymbol{d}$. This problem is generally ill-posed in the manner described in Chapter 2. Hence, a direct inversion of G might be impossible; if the inversion is possible, there may be more than one solution; and, in addition, the inversion methods themselves can be highly sensitive to small perturbations in $\boldsymbol{d}$.

The classical approach for solving the problem is to minimize the least-squares misfit between data and model predictions, see, e.g., [98]

$$\boldsymbol{m}^* = \arg\min_{\boldsymbol{m}} \|G(\boldsymbol{m}) - \boldsymbol{d}\|^2, \tag{3.3}$$

in the Euclidean norm. For a general forward model, the minimization is performed by some suitable optimization procedure. Unfortunately, this problem might still be ill-posed as the minimization can have multiple minima; the minimizing sequence may not converge; and the solution could still be highly sensitive to perturbations in the data. To circumvent these problems, regularization in the form of Tikhonov [98] can be introduced. One then seek the solution to the regularized minimization problem

$$\boldsymbol{m}^* = \arg\min_{\boldsymbol{m}} \|G(\boldsymbol{m}) - \boldsymbol{d}\|^2 + \left\|\Gamma\left(\boldsymbol{m} - \boldsymbol{m}^0\right)\right\|^2, \tag{3.4}$$

for some suitably chosen Tikhonov matrix Γ, centring parameter $\boldsymbol{m}^0$, and norm. These choices reflect which solution one is seeking, and there exists a vast amount of literature dedicated to this subject, see, e.g., [4, 26].

Let us consider the regularized parameter estimation problem where the parameters are related to the data through a linear forward model. For such problems it is possible to provide an expression for the solution. Let us assume that we are seeking a solution close to some prior value, i.e., $\boldsymbol{m}^0 = \boldsymbol{m}^{prior}$, weighted by a suitably chosen Γ. Inserting this into (3.4) gives

$$\boldsymbol{m}^* = \arg\min_{\boldsymbol{m}} \|G\boldsymbol{m} - \boldsymbol{d}\|^2 + \left\|\Gamma\left(\boldsymbol{m} - \boldsymbol{m}^{prior}\right)\right\|^2. \tag{3.5}$$

The solution to this problem is given by the normal equations, see, e.g., [4]

$$\boldsymbol{m}^* = \left(G^T G + \widehat{\Gamma}\right)^{-1}\left(G^T\boldsymbol{d} + \widehat{\Gamma}\boldsymbol{m}^{prior}\right), \tag{3.6}$$

where the matrix $\widehat{\Gamma}$ is given as $\widehat{\Gamma} = \Gamma^T\Gamma$.

3.2 Stochastic approach

We now consider the stochastic approach to parameter estimation. This method is similar to the classical approach. However, contrary to the classical approach, all error terms are now expressed as stochastic variables with well defined statistics.

Similar to the classical approach, the forward model is defined as (3.2). However, we now assume that $\boldsymbol{\xi} \sim N(\mathbf{0}, Q_d)$ represents the error caused by the joint effect of the forward-model operator and the measurement operator. Given a series of n_a independent observations, we seek the most likely parameter vector corresponding to the observations. Since the data are assumed to be stochastic, the conditional PDF of the data given a parameter vector $\boldsymbol{m}$ is

$$p(\boldsymbol{d}|\boldsymbol{m}) = p(\boldsymbol{d}_1|\boldsymbol{m}) \dots p(\boldsymbol{d}_{n_a}|\boldsymbol{m}) . \tag{3.7}$$

However, in our problems, the data are measured and we seek the parameter values that most likely produced the data values. For this reason, it is more suitable to consider the *likelihood function*, $L(\boldsymbol{m}|\boldsymbol{d})$. It is well known that

$$L(\boldsymbol{m}|\boldsymbol{d}) = p(\boldsymbol{d}|\boldsymbol{m}) = p(\boldsymbol{d}_1|\boldsymbol{m}) \dots p(\boldsymbol{d}_{n_a}|\boldsymbol{m}) . \tag{3.8}$$

Hence, one should find the parameter values $\boldsymbol{m}$ that maximizes the likelihood function. Since the observations have Gaussian errors, where σ_i is the standard deviation for observation i, the likelihood function can be written as

$$L(\boldsymbol{m}|\boldsymbol{d}) \propto \prod_{i=1}^{n_a} \exp\left(-\frac{(d_i - (G(\boldsymbol{m}))_i)^2}{2\sigma_i}\right). \tag{3.9}$$

The *maximum likelihood* (ML) estimate is given by the parameter vector maximizing (3.9). Hence, we seek the model

$$\boldsymbol{m}^* = \arg\min_{\boldsymbol{m}} \left\| Q_d^{-\frac{1}{2}} (G(\boldsymbol{m}) - \boldsymbol{d}) \right\|^2 , \tag{3.10}$$

in the Euclidean norm, where Q_d is a diagonal matrix consisting of the elements σ_i^2. If $\sigma_i = 1$, for $i = 1, \dots, n_a$, this is identical to the least-squared misfit in the classical approach (3.3). Clearly, weights different from 1 could have been included in the classical case. However, the values of such weights would have to be based on some notion of the problem. Contrary to this, for the stochastic approach all weights are defined based on well-defined statistics.

Similar to the classical approach, the stochastic approach might be ill-posed, and to deal with this problem one needs to include some sort of regularization. In the stochastic framework, regularization is provided through Bayes' theorem which incorporates prior information regarding the parameters $\boldsymbol{m}$. Let us, for simplicity, assume that the prior PDF for the unknown parameters can be written as the Gaussian

$$p(\boldsymbol{m}) \propto \exp\left(-\frac{1}{2} (\boldsymbol{m} - \boldsymbol{\mu}_{m^{prior}})^T Q_{m^{prior}}^{-1} (\boldsymbol{m} - \boldsymbol{\mu}_{m^{prior}})\right). \tag{3.11}$$

Following Bayes' formula, (2.4), the posterior PDF is given as

$$\begin{aligned} p(\boldsymbol{m}|\boldsymbol{d}) \propto \exp\Bigg(&-\frac{1}{2} (\boldsymbol{d} - G(\boldsymbol{m}))^T Q_d^{-1} (\boldsymbol{d} - G(\boldsymbol{m})) \\ &-\frac{1}{2} (\boldsymbol{m} - \boldsymbol{\mu}_{m^{prior}})^T Q_{m^{prior}}^{-1} (\boldsymbol{m} - \boldsymbol{\mu}_{m^{prior}})\Bigg). \end{aligned} \tag{3.12}$$

The posterior PDF will completely characterize the solution to the parameter estimation problem. However, for some applications, one is only interested in the most likely model. This model is denoted as the *maximum a posteriori* (MAP) solution. Defining the penalty function

$$J(\boldsymbol{m}) = \frac{1}{2}\Big((\boldsymbol{d} - G(\boldsymbol{m}))^T Q_d^{-1} (\boldsymbol{d} - G(\boldsymbol{m})) + (\boldsymbol{m} - \boldsymbol{\mu}_{m^{prior}})^T Q_{m^{prior}}^{-1} (\boldsymbol{m} - \boldsymbol{\mu}_{m^{prior}})\Big), \tag{3.13}$$

the MAP solution is provided by

$$\boldsymbol{m}^* = \arg\max_{\boldsymbol{m}} p(\boldsymbol{m}|\boldsymbol{d}) = \arg\min_{\boldsymbol{m}} J(\boldsymbol{m}). \tag{3.14}$$

Note that covariance matrices are always symmetric positive definite matrices, hence $Q^{-1/2}$ will always exist. Now define the norm

$$\|\cdot\|_Q = \left\|Q^{-1/2}\cdot\right\|, \tag{3.15}$$

where the Euclidean norm is used on the right hand side. Inserting this into (3.14), the MAP solution can be given as

$$\boldsymbol{m}^* = \arg\min_{\boldsymbol{m}} \|\boldsymbol{d} - G(\boldsymbol{m})\|_{Q_d}^2 + \|\boldsymbol{m} - \boldsymbol{\mu}_{m^{prior}}\|_{Q_{m^{prior}}}^2. \tag{3.16}$$

There are strong similarities between the MAP solution and the classical parameter estimation problem (3.5). The two are in-fact identical if we let $\boldsymbol{m}^{prior} = \boldsymbol{\mu}_{m^{prior}}$, $Q_d = I$, and $Q_{m^{prior}}^{-1} = \widehat{\Gamma}$. Similar to the ML, the weights on the data term in the MAP solution are chosen based on statistical information regarding the data error. Moreover, the MAP solution incorporates regularization naturally as prior information via Bayes' theorem. There are, therefore, fundamental differences between the stochastic and the classical approach.

3.3 Weak and strong constraint formulation

In the two previous sections, we discussed the classical and the stochastic approach to parameter estimation. It was shown that, given correct weights, both approaches could provide the same solution. As discussed, the stochastic approach is advantageous as it provides a good foundation for selecting the weights. Recall that we assumed that the term $\boldsymbol{\xi}$ represented both the error in the forward-model operator and the observation error. However, as seen in Chapter 2 it can often be advantageous to separate these two terms. In the parameter estimation setting, the data is given as

$$\boldsymbol{d} = H(\boldsymbol{z}) + \boldsymbol{\epsilon}, \tag{3.17}$$

while the forward model is given as

$$\boldsymbol{z} = F(\boldsymbol{m}) + \boldsymbol{\eta}, \tag{3.18}$$

where $\boldsymbol{\epsilon} \sim N(\mathbf{0}, Q_d)$, and $\boldsymbol{\eta} \sim N(\mathbf{0}, Q_z)$. Utilizing the least-squares estimator one can define the following objective function [29]

$$J(\boldsymbol{m}) = (\boldsymbol{d} - H(z))^T Q_d^{-1} (\boldsymbol{d} - H(z)) + (z - F(\boldsymbol{m}))^T Q_z^{-1} (z - F(\boldsymbol{m})) + (\boldsymbol{m} - \boldsymbol{\mu}_{m^{prior}})^T Q_{m^{prior}}^{-1} (\boldsymbol{m} - \boldsymbol{\mu}_{m^{prior}}) . \tag{3.19}$$

Finding the unknown parameter vector that minimize (3.19) is generally known as a weakly constrained problem. This is similar to the formulation utilized in Section 2.2, and the error both in the forward model and in the observation model are honoured. This formulation does not require the model equations to be matched exactly, which can be a great advantage for many problems.

Alternatively, one might assume that the forward model is exact, i.e., $z = F(\boldsymbol{m})$. Hence, removing the second term in (3.19). This is generally known as the strong constraint formulation. The solution to a parameter estimation problem, formulated with the strong constraint, must satisfy the model equations exactly. However, as discussed in Chapter 2, natural phenomenon can seldom be modelled exactly. Approximations, introduced by neglected physics or computational simplifications, are usually present in the forward model. If one utilize the strong constraint formulation for problems where the size of the model error is significant, one get estimates of $\boldsymbol{m}$ that attempt to correct for error not caused by the parameter value [29].

It is important to note the fundamental difference between the weak and strong formulation. With the classical and stochastic approach to parameter estimation, as introduced above, one does not separate between the two sources of error. When little is known regarding the nature of the error in the forward model, this term might be underestimated. Hence, for such cases, the strong formulation is utilized, both with the classic and the stochastic approach.

The error in the forward model is, however, always considered for the state estimation problems discussed in Chapter 2. Both in the filter and the smoother solution, the propagation of the model error is determined by the error in the forward-model operator. In Chapter 5, we will consider some methods that utilize the state estimation strategy for estimation of the parameters.

Chapter 4

Sampling from the posterior PDF

Utilizing the Bayesian formulation, it is (conceptually) simple to formulate the posterior PDF. Unfortunately, for most realistic problems this PDF cannot be evaluated due to its complex high-dimensional integrals (see, Section 2). For such problems, information regarding the posterior PDF can only be obtained by sampling.

In this chapter, we consider several methods that sample from the posterior PDF. A special emphasis is placed on various MCMC methods, which provide a robust, but computationally expensive, way of sampling from the posterior PDF.

4.1 MCMC

The MCMC methods relate to the general framework of methods introduced by Metropolis et al. [66], and Hastings [48] for MC integration. The concept of the MCMC method is simple. One designs a Markov chain with the property that a sequence of outputs from the chain are distributed according to a specified PDF. These outputs are then utilized for MC estimation. Clearly, with such a broad definition, there is room for significant innovation in the design of methods. However, they all share some common features.

Consider a stochastic process, that is, a sequence of random elements, $\boldsymbol{m}_1, \boldsymbol{m}_2, \ldots$, and assume that the conditional PDF of $\boldsymbol{m}_{n+1}$ given $\boldsymbol{m}_1, \ldots, \boldsymbol{m}_n$ only depends on $\boldsymbol{m}_n$. This stochastic process is referred to as a Markov chain, and the set in which $\boldsymbol{m}_j$ takes values is referred to as the state space of the Markov chain. The marginal PDF of $\boldsymbol{m}_1$ is referred to as the initial PDF, while the conditional PDF of $\boldsymbol{m}_{n+1}$ given $\boldsymbol{m}_n$ is referred to as the transition PDF.

The main kind of Markov chains of interest in MCMC have stationary transition PDFs, that is, the conditional PDF of $\boldsymbol{m}_{n+1}$ given $\boldsymbol{m}_n$ does not depend on n. A stochastic process is stationary if the joint PDF of $\boldsymbol{m}_{n+1}, \ldots, \boldsymbol{m}_{n+k}$ does not depend on n. The Markov chain is stationary if it is a stationary stochastic process. Moreover, the Markov chain is stationary, if and only if, the marginal PDF of $\boldsymbol{m}_n$ does not depend on n. A stationary process implies stationary transition probability, but not vice versa.

An initial PDF is defined as the stationary PDF, for some transition PDF, if the Markov chain specified by the combination of the specific initial PDF and transition PDF is stationary. Hence, the transition PDF preserves the initial PDF.

Consider a Markov chain with a given initial PDF. If the PDF of a pair in the sequence $(\boldsymbol{m}_n, \boldsymbol{m}_{n+1})$ is exchangeable, the transition PDF of the Markov chain is re-

versible with respect to the initial PDF. A Markov chain with reversible transition PDF is referred to as a reversible Markov chain. Reversibility implies that the sequence is stationary. Most MCMC algorithms rely on reversible transition probabilities.

A Markov chain is irreducible if there is a positive probability that the chain can go from element $\boldsymbol{m}_i$ to element $\boldsymbol{m}_j$ in finite time. The element $\boldsymbol{m}_j$ is recurrent if the chain returns to $\boldsymbol{m}_j$ with probability 1. If the expected time until the chain returns to $\boldsymbol{m}_j$ is finite the element is positive recurrent, with period defined as the greatest common divisor of the lengths of all paths starting and ending in the element $\boldsymbol{m}_j$. In an irreducible chain, all elements have equal periods, and the chain is aperiodic if this period is equal to 1. Positive recurrent, aperiodic elements are ergodic.

Since we are unable to sample from the desired stationary PDF (the posterior), we can never generate a Markov chain where the initial PDF is the stationary PDF. Hence, we never utilize stationary Markov chains in MCMC. Fortunately, an ergodic Markov chain eventually reach a unique stationary PDF, regardless of the initial element [77]. Therefore, if the transition PDF is defined in a suitable manner one is guaranteed, independent of the initial PDF, that the Markov chain generates samples from the stationary PDF, after some time. In the following, we introduce some MCMC algorithms that, when allowed to run for sufficiently long time, converge to the correct stationary PDF.

4.1.1 Metropolis-Hastings

The first method we consider is the well known Metropolis-Hastings (M-H), proposed in [48] as an extension of the method introduced in [66]. Suppose that we want samples from a stationary PDF that has unnormalized PDF a. This is the general situation when utilizing the Bayesian methods (see Section 2.1) where the normalizing factor is often impossible to calculate. Assume that the current element of the chain is $\boldsymbol{m}_n$, the M-H algorithm proposes a move to $\boldsymbol{m}_{n+1}^*$ having conditional probability density $q\left(\boldsymbol{m}_{n+1}^* | \boldsymbol{m}_n\right)$. This Markov-chain performs this move with probability

$$b\left(\boldsymbol{m}_n, \boldsymbol{m}_{n+1}^*\right) = \min\left(1, r\left(\boldsymbol{m}_n, \boldsymbol{m}_{n+1}^*\right)\right), \tag{4.1}$$

where the Hastings ratio r is defined as

$$r\left(\boldsymbol{m}_n, \boldsymbol{m}_{n+1}^*\right) = \frac{a\left(\boldsymbol{m}_{n+1}^*\right) q\left(\boldsymbol{m}_n | \boldsymbol{m}_{n+1}^*\right)}{a\left(\boldsymbol{m}_n\right) q\left(\boldsymbol{m}_{n+1}^* | \boldsymbol{m}_n\right)}. \tag{4.2}$$

If the move is not made $\boldsymbol{m}_{n+1} = \boldsymbol{m}_n$. Note that r is not defined for $a\left(\boldsymbol{m}_n\right) = 0$, and no candidate moves are made where $a\left(\boldsymbol{m}_{n+1}^*\right) = 0$. Hence, by ensuring that the initial element has $a\left(\boldsymbol{m}_1\right) > 0$ we are guaranteed that r is defined for all possible steps. The success of the method, therefore, relies on the definition of a suitable proposal PDF.

It is possible to show that the M-H update is reversible with respect to a. That is, the transition probability density that describes the update is reversible with respect to the PDF that has unnormalized density a [11]. Hence, the resulting Markov chain is ergodic, and the M-H algorithm samples from the stationary PDF.

A special case of the M-H, known as the Metropolis update, arises when $q\left(\boldsymbol{m}_n | \boldsymbol{m}_{n+1}^*\right) =$

$q\left(\boldsymbol{m}_{n+1}^{*}|\boldsymbol{m}_{n}\right)$ for all $\boldsymbol{m}_n$ and $\boldsymbol{m}_{n+1}^{*}$. For this special case, the Hastings ratio is given as

$$r\left(\boldsymbol{m}_{n},\boldsymbol{m}_{n+1}^{*}\right)=\frac{a\left(\boldsymbol{m}_{n+1}^{*}\right)}{a\left(\boldsymbol{m}_{n}\right)}. \tag{4.3}$$

This choice only simplifies the evaluation of the Hastings ratio.

4.1.2 Gibbs sampler

The M-H algorithm requires the user to define a suitable proposal PDF. In the Gibbs sampler, this is not necessary. Here, the candidates are drawn from the conditional stationary PDF, and they are always accepted. Typically, the Gibbs sampler draws from the conditional PDF of a single element, this is, however, not necessary and the candidates can be drawn from the conditional PDF of several elements.

One can easily observe that all candidates are accepted if one considers the Gibbs sampler as a special case of the M-H algorithm. Let us decompose the vector $\boldsymbol{m}_n$ into $(\boldsymbol{x}_n,\boldsymbol{y}_n)$, and let us factor the unnormalized PDF as $a\left(\boldsymbol{x}_n,\boldsymbol{y}_n\right)=g\left(\boldsymbol{y}_n\right)q\left(\boldsymbol{x}_n|\boldsymbol{y}_n\right)$, where $g\left(\boldsymbol{y}_n\right)$ is the unnormalized marginal PDF of $\boldsymbol{y}_n$, and $q\left(\boldsymbol{x}_n|\boldsymbol{y}_n\right)$ is the properly normalized PDF of $\boldsymbol{x}_n$ given $\boldsymbol{y}_n$. For the Gibbs sampler the proposed element is $\boldsymbol{m}_{n+1}^{*}=\left(\boldsymbol{x}_{n+1}^{*},\boldsymbol{y_n}\right)$ with proposal PDF $q\left(\boldsymbol{x}_{n}^{*}|\boldsymbol{y}_n\right)$. (Note that $\boldsymbol{x}$ is a vector, hence, we consider candidate given as the conditional PDF of several elements.) Inserting this into the Hastings ratio (4.2), we get

$$\begin{aligned} r\left(\boldsymbol{m}_{n},\boldsymbol{m}_{n+1}^{*}\right) &= \frac{a\left(\boldsymbol{x}_{n+1}^{*},\boldsymbol{y}_n\right)q\left(\boldsymbol{x}_n|\boldsymbol{y}_n\right)}{a\left(\boldsymbol{x}_n,\boldsymbol{y}_n\right)q\left(\boldsymbol{x}_{n+1}^{*}|\boldsymbol{y}_n\right)} \\ &= \frac{g\left(\boldsymbol{y}_n\right)q\left(\boldsymbol{x}_{n+1}^{*}|\boldsymbol{y}_n\right)q\left(\boldsymbol{x}_n|\boldsymbol{y}_n\right)}{g\left(\boldsymbol{y}_n\right)q\left(\boldsymbol{x}_n|\boldsymbol{y}_n\right)q\left(\boldsymbol{x}_{n+1}^{*}|\boldsymbol{y}_n\right)} \\ &= 1 \end{aligned} \tag{4.4}$$

The Gibbs sampler is very easy to use, and if one utilize the Gibbs sampler, no other algorithmic choices are needed. However, the Gibbs sampler requires a method of sampling from the conditional PDF and it may require a large number of iterations to converge.

4.1.3 Variable-at-a-time M-H

The most obvious difference between the original M-H algorithm and the Gibbs sampler is that the latter only alters a part of the element vector, drawing candidates from the conditional of the stationary PDF. However, there exist alternative versions of the M-H algorithm, utilizing different proposal PDFs, updating only parts of the element vector. Similar to the Gibbs sampler, let us decompose the element vector $\boldsymbol{m}_n$ into two parts $(\boldsymbol{x}_n,\boldsymbol{y}_n)$. We can now generate candidates where $\boldsymbol{x}_n$ is altered and $\boldsymbol{y}_n$ is left unchanged. The candidate sample is then $\boldsymbol{m}_{n+1}^{*}=\left(\boldsymbol{x}_{n+1}^{*},\boldsymbol{y}_n\right)$, where, contrary to the

Gibbs samples, the candidate $\boldsymbol{m}^*_{n+1}$ is drawn from the conditional probability density $q\left(\boldsymbol{x}^*_{n+1}|\boldsymbol{x}_n,\boldsymbol{y}_n\right)$. The Hastings ratio for the Variable-at-a-Time M-H is then

$$r\left(\boldsymbol{m}_n,\boldsymbol{m}^*_{n+1}\right)=\frac{a\left(\boldsymbol{x}^*_{n+1},\boldsymbol{y}_n\right)q\left(\boldsymbol{x}_n|\boldsymbol{x}^*_{n+1},\boldsymbol{y}_n\right)}{a\left(\boldsymbol{x}_n,\boldsymbol{y}_n\right)q\left(\boldsymbol{x}^*_{n+1}|\boldsymbol{x}_n,\boldsymbol{y}_n\right)}, \tag{4.5}$$

where a is, as in the previous cases, the unnormalized density for the desired stationary PDF.

An example of a variable-at-a-time MCMC algorithm was introduced in [71]. Here the candidates were drawn from the prior PDF via a standard Cholesky decomposition method, that is

$$\boldsymbol{m}^*_{n+1}=\boldsymbol{\mu}_m+L\boldsymbol{l}_{n+1}, \tag{4.6}$$

where $\boldsymbol{l}\sim N\left(\boldsymbol{0},I\right)$, and $Q_m=LL^T$. The proposal PDF is then

$$\begin{aligned}q\left(\boldsymbol{m}^*_{n+1}|\boldsymbol{m}_n\right)&=c\exp\left(-\frac{1}{2}\left(\boldsymbol{m}^*_{n+1}-\boldsymbol{\mu}_m\right)^TQ_m^{-1}\left(\boldsymbol{m}^*_{n+1}-\boldsymbol{\mu}_m\right)\right)\\&=c\exp\left(-\frac{1}{2}\boldsymbol{l}^T_{n+1}\boldsymbol{l}_{n+1}\right).\end{aligned} \tag{4.7}$$

Utilizing the fact that the candidate were fully characterized by the random vector, $\boldsymbol{l}_{n+1}$, [71] suggested a proposal PDF where a single element, k, of the random vector $(l_k)_{n+1}$, drawn uniformly from the n_m available elements, was perturbed in each candidate. Hence, the variable-at-a-time proposal PDF was given as [71]

$$q\left(\boldsymbol{x}^*_{n+1}|\boldsymbol{x}_n,\boldsymbol{y}_n\right)=\frac{1}{n_m\sqrt{2\pi}}\exp\left(-\frac{1}{2}\left(l^*_k\right)^2_{n+1}\right). \tag{4.8}$$

This MCMC algorithm was utilized in a Bayesian estimation problem in [71], with unnormalized stationary PDF given by (3.12). For this specific problem, the Hastings ratio reduced to

$$r\left(\boldsymbol{m}_n,\boldsymbol{m}^*_{n+1}\right)=\frac{\exp\left(-\frac{1}{2}\left(\boldsymbol{d}-G\left(\boldsymbol{m}^*_{n+1}\right)\right)^TQ_d^{-1}\left(\boldsymbol{d}-G\left(\boldsymbol{m}^*_{n+1}\right)\right)\right)}{\exp\left(-\frac{1}{2}\left(\boldsymbol{d}-G\left(\boldsymbol{m}_n\right)\right)^TQ_d^{-1}\left(\boldsymbol{d}-G\left(\boldsymbol{m}_n\right)\right)\right)}. \tag{4.9}$$

This MCMC algorithm was also utilized in paper A.

4.1.4 Adaptive MCMC

The M-H algorithm requires a choice of proposal PDF, and it is well known that some proposal PDFs work better than others. Intuitively, the most efficient way of running the MCMC would be to draw the candidates directly from the stationary PDF. However, the whole point of MCMC is that we cannot sample from the stationary PDF, and other approaches are needed. To highlight some issues related to the choice of proposal PDF let us consider one of the simplest methods, the scaled random walk (RW). Here, the candidate is given as

$$\boldsymbol{m}^*_{n+1}=\boldsymbol{m}_n+\boldsymbol{l}_{n+1}, \tag{4.10}$$

where

$$\boldsymbol{l}_n \sim N\left(\mathbf{0}, \sigma^2 I_d\right), \tag{4.11}$$

and σ is a scaling factor. Any MCMC algorithm needs to converge fast, that is, the chain should sample from the stationary PDF in few iterations. Moreover, a good MCMC algorithm allows for rapid exploration of the state space, that is, the chain should mix fast. A successful algorithm should, therefore, have few rejected moves (as this will not contribute to explore the state space) and few accepted moves that are small (as one needs a high number of small iterations to sample from the stationary PDF). In summary, one seeks an algorithm that proposes relatively large steps that have a high acceptance rate (fraction of proposed moves that are accepted). Our goal is therefore to choose σ in (4.11) such that the proposed steps are relatively large, while maintaining a relatively high acceptance rate. Clearly, if σ is chosen to large, most candidates are rejected, and if σ is chosen to small, the chain will not mix properly. However, the selection of σ is highly problem dependent. Clearly, the size of σ determines the acceptance rate. Under some assumptions on the stationary PDF, it has been shown that an acceptance rate of 0.234 is optimal for problems as $n_m \to \infty$ [79]. Numerical studies indicates that this choice is optimal even for n_m=5 [11, 33, 80], while for n_m= 1 the optimal acceptance rate is approximately 0.44 [11].

Finding an optimal σ, such that the acceptance rate is approximately 0.234, is not trivial. However, theoretical evidence suggest that σ should be selected such that the proposal covariance is approximately proportional to the stationary covariance [11]. Unfortunately, we do not know the stationary covariance. Two different approaches can be considered for tuning σ. The first approach is using trial and error, which can be difficult and time demanding for high-dimensional systems. Trial and error can be the best choice if the problem is low dimensional and one has some intuitive notion of the value σ. The second approach is based on an adaptive tuning of σ, and is therefore denoted adaptive MCMC. If the problem is high-dimensional and little is known regarding σ one can benefit from an adaptive MCMC algorithm.

Similarly to ordinary MCMC, there exist numerous adaptive MCMC algorithms. One can consider the adaptive MCMC algorithms as consisting of a family of individual Markov chains having the same stationary PDF, and where each adaptation corresponds to a member of the family. This mixture of chains does not necessarily converge to the stationary PDF for all cases as was exemplified in [81]. However, as shown in [82], the adaptive MCMC is ergodic under some assumptions, most importantly if the amount of adaptation is diminishing with the number of iterations.

A simple Metropolis algorithm that satisfies the diminishing adaptation condition was proposed in [83] as a variation of the adaptive Metropolis algorithm introduced in [45]. Here, the proposal PDF is a mixture of the form

$$\boldsymbol{m}_{n+1}^{*} \sim (1-\beta)\, N\left(\boldsymbol{m}_n, \left(\frac{2.38^2}{n_m}\right) C_{m_n}\right) + \beta N\left(\boldsymbol{m}_n, Q_{m_0}\right), \tag{4.12}$$

where C_{m_n} is the empirical covariance matrix calculated using all the preceding iterations, Q_{m_0} is some fixed nonsingular matrix, and $0 < \beta < 1$. Note that for the first iterations (until the empirical covariance is well established) one must set β=1. In [83], numerical experiments illustrated good results utilizing this algorithm for problems with n_m=100. This method was utilized in Paper C-E.

4.1.5 Preconditioned Crank-Nicolson MCMC

All the previous MCMC algorithms assume that the unknown, $\boldsymbol{m}$, is discretized in n_m dimensions and the methods are therefore exploring a finite dimensional space. With this assumption, the methods described above sample from the correct stationary PDF. However, this may not be the case if $\boldsymbol{m}$ is a continuous function, that is, before any discretization is performed. Moreover, the convergence properties of the algorithms defined previously depend heavily on the dimension of the state space. Considering MCMC methods defined for functions, [17] designed several algorithms that maintained robust convergence properties when applied to discrete models, independent of the dimension of the system.

To introduce these methods, the prior must be defined as a dominating measure, μ_0, and Bayes' theorem is given by the Radon-Nikodyn derivative

$$\frac{\mathrm{d}\,\mu}{\mathrm{d}\,\mu_0}(m) \propto \exp\left(-\Phi(m)\right), \tag{4.13}$$

where Φ is defined as some real-valued potential, and μ is the posterior measure. The key algorithmic idea introduced in [17] was to consider stochastic differential equations (SDEs) that preserved μ or μ_0, and to utilize a Crank-Nicolson (CN) discretization of the SDEs, which preserved the Gaussian reference measure μ_0 when $\Phi \equiv 0$, as proposals in Metropolis-Hastings methods. Several modifications of standard MCMC methods were proposed in [17], but, in the following, we only present the preconditioned CN (pCN) method, which was proposed as a modification of the standard random walk algorithm.

As discussed for the finite-dimensional adaptive MCMC algorithms it is advisable that the proposal variance is approximately a scalar multiple of the target covariance (or at least the prior covariance). This is not the case with the CN proposal, and preconditioning was included to make the proposal covariance equal to the prior covariance. The resulting pCN-MCMC algorithm generates candidates by

$$\boldsymbol{m}^*_{n+1} = \sqrt{(1-\sigma^2)}\boldsymbol{m}_n + \sigma \boldsymbol{l}_n, \tag{4.14}$$

where $\boldsymbol{l} \sim N\left(\boldsymbol{0}, Q_{prior}\right)$. The candidates are then accepted with probability

$$b\left(\boldsymbol{m}_n, \boldsymbol{m}^*_{n+1}\right) = \min\left\{1, \exp\left(\Phi(\boldsymbol{m}_n) - \Phi\left(\boldsymbol{m}^*_{n+1}\right)\right)\right\}. \tag{4.15}$$

This algorithm is very similar to the RW algorithm discussed above, however, the pCN-MCMC is independent of the dimension of the problem [17]. Unfortunately, the algorithm still depends on a scaling variable σ. Similar to the RW algorithm, selecting σ too large gives high rejection rates, while selecting a low value of σ does not provide sufficient mixing in the chain. Hence, both the RW and the pCN-MCMC algorithms require test runs to establish a good value for σ.

4.1.6 Evaluation of MCMC convergence

The start value for all MCMC algorithms is drawn from some initial PDF, which is different from the stationary PDF. For a general MCMC method, one does not know

how many iterations the chain needs before the samples are from the stationary PDF. The convergence of the chain must therefore be monitored. This is especially important for problems where parts of the state space is poorly connected, e.g., for a multimodal PDF. For such cases, the chain may appear to have converged when it is only stuck in parts of the state space. This problem is denoted pseudo-convergence, and can only be avoided by running the chain for sufficiently many iterations to ensure that the chain has explored the full space. There exists several methods for evaluating the convergence of an MCMC algorithm, see, e.g., [18]. In the following, we consider a method that is based on monitoring several parallel chains. This procedure is well suited for modern computers that easily allow for parallel runs.

Prior to the discussion of the convergence measure, we make some notes regarding the standard practice of discarding the initial iterations. Since the initial value of the MCMC algorithm is never a sample from the stationary PDF, any empirical estimation that includes all samples will be erroneous. To avoid this error, the initial iterations, denoted the burn-in, are discarded. The question is, however, how many samples should be discarded? In the following convergence measure, we discard the first half of the total iterations, which is a conservative choice.

A standard method for assessing MCMC convergence is to calculate the potential scale reduction factor [12, 34, 78]. This method is based on examining several parallel chains started from a set of initial values that are overdispersed with respect to the stationary PDF. From each of the parallel chains, one calculates the empirical mean and (co)variance of the chain output (either the parameters or some summary statistic). The chain convergence is then calculated by comparing these within chain estimates, to the approximation obtained by combining all the samples together, denoted the between-sequence estimate. It is assumed that the chain has converged if the two estimates are similar. This method is used both for assessing scalar quantities, denoted potential scale reduction factor (PSRF), and for assessing multivariate quantities, denoted multivariate PSRF (MPSRF).

Consider the output of n_c parallel MCMC chains, each of length n_{mcmc}, and let this be stored in the tensor $\{\underline{M}_{j,i,l} : j = 1,\ldots,n_m, i = 1,\ldots,n_c, l = 1,\ldots,n_{\text{mcmc}}\}$. The matrix containing the mean of each chain is then calculated as

$$\overline{M}_{j,i} = \frac{1}{n_{\text{mcmc}}} \sum_{l=1}^{n_{\text{mcmc}}} \underline{M}_{j,i,l} \tag{4.16}$$

and the vector containing the mean of all chain combined is calculated as

$$\overline{\boldsymbol{m}} = \frac{1}{n_c} \sum_{i=1}^{n_c} \overline{M}_{j,i} \tag{4.17}$$

By calculating the between-sequence covariance, B, as

$$B = \frac{n_{\text{mcmc}}}{n_c - 1} \sum_{i=1}^{n_c} \left(\overline{M}_{\cdot,i} - \overline{\boldsymbol{m}}\right)\left(\overline{M}_{\cdot,i} - \overline{\boldsymbol{m}}\right)^T, \tag{4.18}$$

and the within-sequence covariance, W, as

$$W = \frac{1}{n_c\,(n_{\text{mcmc}} - 1)} \sum_{j=1}^{n_c} \sum_{i=1}^{n_{\text{mcmc}}} \left(\underline{M}_{j,i,\cdot} - \overline{M}_{j,i}\right)\left(\underline{M}_{j,i,\cdot} - \overline{M}_{j,i}\right)^T, \tag{4.19}$$

it is possible to estimate the total posterior covariance matrix by

$$V = \frac{n_{\text{mcmc}} - 1}{n_{\text{mcmc}}} W + \left(1 + \frac{1}{n_c}\right) \frac{B}{n_{\text{mcmc}}}. \tag{4.20}$$

The MPSRF is based on a summarizing measure of the distance between V and B. There exist several such measures but [12] suggested to utilize the maximum root statistic

$$r = \frac{n_{\text{mcmc}} - 1}{n_{\text{mcmc}}} + \left(\frac{n_c + 1}{n_c}\right) \lambda_1, \tag{4.21}$$

where λ_1 is the largest eigenvalue of the symmetric, positive definite matrix $W^{-1}\,(B/n_{\text{mcmc}})$. Paper C, D, and E utilize the MPSRF for evaluating the convergence of the MCMC methods.

4.2 Importance sampling and sequential MC

The traditional MCMC methods, as described in the previous section, will sample from the stationary PDF. These samples can then be utilized to approximate some statistic, e.g., the empirical mean or (co)variance. An alternative approach is given by the importance sampling methods. Instead of generating a Markov chain that gradually converges towards its stationary PDF, importance sampling methods are based on the idea that any sample can be generated from any PDF [100]. Suppose that we have a sequence of independent identically distributed (i.i.d.) samples $\boldsymbol{m}_1, \boldsymbol{m}_2, \ldots$ that have an unnormalized stationary PDF (one can also consider samples from a normalized stationary PDF). Using these samples it is possible to calculate inference from any other PDF (as long as it is absolutely continuous with respect to the original PDF) applying only the original samples and some suitable weights. This simple observation is the basis of the importance sampling technique. Here the stationary PDF of the original sequence is called the importance function, and one often referrers to the, finite, sequence of samples as a swarm of particles.

Consider a swarm of n_e particles, $\boldsymbol{m}_1, \boldsymbol{m}_2, \ldots, \boldsymbol{m}_{n_e}$, distributed following the unnormalized importance function g. We wish to estimate the mean value of the parameter $\boldsymbol{m}^*$ distributed according to the unnormalized PDF g^*. We will now demonstrate how the importance sampling technique can be utilized to approximate this value. As mentioned above, to estimate the mean we need to define some suitable weights, referred to as the normalized importance weights. These weights are given as [35]

$$w\left(\boldsymbol{m}\right) = \frac{\frac{g^*(\boldsymbol{m})}{g(\boldsymbol{m})}}{\sum_{n=1}^{n_e} \frac{g^*(\boldsymbol{m}_n)}{g(\boldsymbol{m}_n)}}. \tag{4.22}$$

Utilizing the importance weights, the empirical mean of the parameters $\boldsymbol{m}^*$ can be calculated as

$$\overline{\boldsymbol{m}^*} = \sum_{n=1}^{n_e} w\left(\boldsymbol{m}_n\right) \boldsymbol{m}_n. \tag{4.23}$$

The quality of the empirical mean improves as n_e increase, and it is possible to show that, given some assumptions on the relationship between g and g^*, $\overline{\boldsymbol{m}^*} \rightarrow \boldsymbol{\mu}_{m^*}$ as $n_e \rightarrow \infty$, see, e.g., [11].

Recall the Bayesian filter problem discussed in Section 2.3. Here, the estimation of the posterior PDF was a dynamic process, and the posterior PDF was efficiently calculated by including data in a recursive manner whenever they were available. In Section 2.4, it was shown that, for Gauss-linear problems, the filter problem could be solved by the KF equations. However, for non-linear problems this method failed, and the solution could only be approximated by methods such as the ExKF, discussed in Section 2.6. To sample exactly from the filter solution, one would need to utilize either MCMC or importance sampler methods. Unfortunately, neither the importance sampler nor the MCMC methods can utilize the recursive nature of the filter problem. They are both designed to generate samples from a fixed posterior PDF, and it is only computationally efficient to sample from the posterior PDF when all data are available. To mitigate this problem, sequential MC (particle filter) methods have been introduced. Here, the evolution of the PDF (the solution to Kolmogorov's equation (2.13)) is approximated by a swarm of particles. When data are assimilated, the filter solution is calculated applying an importance sampling technique. Hence, one assigns weights to the particles so that they represent samples from the correct posterior PDF.

The first successful application of the sequential MC technique to a non-linear filtering problem was the bootstrap filter [38]. Even though many other sequential MC algorithms have been introduced (see, e.g., [3]) we only discuss two basic version, the sequential importance sampling (SIS) method, and the related sequential importance resampling (SIR) method, often, referred to as the standard particle filter.

Recall from Chapter 2 that the posterior PDF for the Markov process is easily formulated in a recursive form:

$$p\left(\boldsymbol{y}_{1:n_a}|\boldsymbol{d}_{1:n_a}\right) \propto p\left(\boldsymbol{d}_{n_a}|\boldsymbol{y}_{n_a}\right) p\left(\boldsymbol{y}_{n_a}|\boldsymbol{y}_{n_a-1}\right) p\left(\boldsymbol{y}_{1:n_a-1}|\boldsymbol{d}_{1:n_a-1}\right). \tag{4.24}$$

This formulation is now utilized to generate the SIS method. Let us assume that the importance function has the recursive form

$$g\left(\boldsymbol{y}_{1:k}|\boldsymbol{d}_{1:k}\right) = g\left(\boldsymbol{y}_k|\boldsymbol{y}_{1:k-1},\boldsymbol{d}_{1:k}\right) g\left(\boldsymbol{y}_{1:k-1},\boldsymbol{d}_{1:k-1}\right). \tag{4.25}$$

We can then calculate the importance weights sequentially as

$$\begin{aligned} w_{1:k}\left(\boldsymbol{y}_n\right) &= \frac{p\left(\boldsymbol{y}_{1:n_a}|\boldsymbol{d}_{1:n_a}\right)}{g\left(\boldsymbol{y}_{1:k}|\boldsymbol{d}_{1:k}\right)} \\ &\propto \frac{p\left(\boldsymbol{d}_{n_a}|\boldsymbol{y}_{n_a}\right) p\left(\boldsymbol{y}_{n_a}|\boldsymbol{y}_{n_a-1}\right) p\left(\boldsymbol{y}_{1:n_a-1}|\boldsymbol{d}_{1:n_a-1}\right)}{g\left(\boldsymbol{y}_k|\boldsymbol{y}_{1:k-1},\boldsymbol{d}_{1:k}\right) g\left(\boldsymbol{y}_{1:k-1},\boldsymbol{d}_{1:k-1}\right)} \\ &= \frac{p\left(\boldsymbol{d}_{n_a}|\boldsymbol{y}_{n_a}\right) p\left(\boldsymbol{y}_{n_a}|\boldsymbol{y}_{n_a-1}\right)}{g\left(\boldsymbol{y}_k|\boldsymbol{y}_{1:k-1},\boldsymbol{d}_{1:k}\right)} w_{1:k-1}\left(\boldsymbol{y}_n\right). \end{aligned} \tag{4.26}$$

If the evolution of the PDF has been approximated by the swarm of particles, it is natural to select an importance function equal to the prediction PDF, i.e., we select $g\left(\boldsymbol{y}_k|\boldsymbol{y}_{1:k-1},\boldsymbol{d}_{1:k}\right) = p\left(\boldsymbol{y}_{n_a}|\boldsymbol{y}_{n_a-1}\right)$. With this choice we get the following update for the weights

$$w_{1:k} = p\left(\boldsymbol{d}_{n_a}|\boldsymbol{y}_{n_a}\right) w_{1:k-1}\left(\boldsymbol{y}_n\right). \tag{4.27}$$

If we assume that it is possible to sample from the transition PDF, and if we know the observation operator with some known error, we can calculate the value for the weights.

Unfortunately, the weights in the SIS are known to degenerate rapidly with increasing time, and after the weights are normalized there will be a large difference between the highest and smallest values of the weights. Hence, after a while, most particles have weights that are almost zero, reducing the number of samples that are contributing to the estimation. To avoid this, [38] introduced a resampling step in the SIS algorithm, generating the SIR algorithm. Here, n_e independent samples are draw from the SIS estimate. The resamling step does not need to be performed at every assimilation step, and it is possible to measure the degeneracy of the weights, and perform resampling only when it is necessary. There exist numerous methods to perform the resampling step [21], all designed to avoid weight degeneration. The simplest approach is to draw, with replacement, n_e new samples with probability equal to the weights. Unfortunately, it is difficult to resample from high-dimensional PDFs, and the SIR method is therefore not suited for high-dimensional filter problems.

4.3 Randomized maximum likelihood

The randomized maximum likelihood (RML) is a non-recursive method for sampling from the posterior PDF. The method was introduced independently by Kitanidis [55] and Oliver et al. [72]. If the dynamic problem is linear, the prior model is Gaussian, and the observation errors are Gaussian, the RML samples exactly from the posterior PDF. For non-linear or non-Gaussian problems the method is approximate [69]. The approximation error is, however, low compared to other approximate methods, and it has been shown that the RML method can produce reliable samples from a multimodal PDF [107].

The RML method is based on two steps. Unconditional realizations are drawn from both the prior model and the data PDFs, then, via an optimization process, these realizations are used to generate samples that are conditioned to the data. That is, for the unconditional realizations $\boldsymbol{m}_{uc}^{prior}$ and $\boldsymbol{d}_{uc}$, the model minimizing

$$\begin{aligned} J(\boldsymbol{m}) = &\left(\boldsymbol{m} - \boldsymbol{m}_{uc}^{prior}\right)^T Q_{m^{prior}}^{-1} \left(\boldsymbol{m} - \boldsymbol{m}_{uc}^{prior}\right) \\ &+ \left(G(\boldsymbol{m}) - \boldsymbol{d}_{uc}\right)^T Q_d^{-1} \left(G(\boldsymbol{m}) - \boldsymbol{d}_{uc}\right) \end{aligned} \tag{4.28}$$

is an approximate sample from the posterior PDF. (For Gauss-linear problems the model is an exact sample from the posterior)

The RML method is significantly less expensive than MCMC methods, but for non-linear problems the method relies on sensitivities, which might be computationally demanding to calculate. The optimization step in the RML method is equivalent to finding the MAP solution in (3.16), and for non-linear problems this step requires a suitable optimization algorithm. The specific type of optimization is not given by the RML algorithm. Hence, even though any RML method follow the two steps given above, there exist as many implementations of the RML algorithm as there are optimization algorithms. In the following, we will discuss some general optimization algorithms.

4.3.1 Numerical optimization

Let us assume, that we are seeking the minimum of an objective function $J : \mathbb{R}^{n_m} \rightarrow \mathbb{R}$, with no restriction on the input variable $\boldsymbol{m}$. Mathematically this is formulated as

$$\min_{\boldsymbol{m}} J(\boldsymbol{m}) . \tag{4.29}$$

This problem can be solved by a range of methods, and in the following, we present some basic optimization methods. Note that the algorithms introduced here will only find local minima, and problems such as multiple local minima or non-unique global minima are present for all the different methods. Moreover, the following methods are deterministic optimization methods, i.e., the methods always produce the same result for a given starting location.

One usually differentiate between two types of optimization methods [67]. The first type is denoted *line search* methods. These methods are designed to search for a new iterate, given as a step υ in the direction $\boldsymbol{p}$ from the current iterate. The step is successful if the new iterate has a lower objective function value than the current iterate, i.e., if $J(\boldsymbol{m}^q + \upsilon \boldsymbol{p}) < J(\boldsymbol{m}^q)$, where q denotes the iteration number. The second type of optimization methods are denoted the *trust-region* methods. These are based on optimizing a local approximation to the objective function $\widetilde{J}(\boldsymbol{m}^q)$. The approximation is generated by utilizing information from J, and the approximation error is assumed to be low around iteration $\boldsymbol{m}^q$. Hence, the trust-region methods seek the update step $\boldsymbol{m}^{q+1} = \boldsymbol{m}^q + \boldsymbol{p}$ that minimize $\widetilde{J}$ in some (trusted) region around $\boldsymbol{m}^q$. If the minimum does not provide a sufficient reduction of J, we select a smaller trust region and find a new minimizer of $\widetilde{J}$.

Both the line search and the trust-region methods generate iteration steps with the help of a quadratic approximation to the objective function, and the methods will therefore have some clear similarities. The two methods will, however, utilize the quadratic approximation in different ways. Line search methods will find an approximate search direction, and then focus on finding a suitable step length. Trust-region methods choose a step that minimize the quadratic approximation within the trusted region. Hence, in general, a new direction if found whenever the size of the trust region is altered. In the following, we focus on finding the optimal update direction $\boldsymbol{p}$, and we will not provide details for finding either the step length or the trust region. For information related to this topics, see, e.g., [67, 73].

Steepest-descent method. The simplest choice of search direction is the direction where J decrease most rapidly, i.e., $\boldsymbol{p}_{SD} = -\nabla J$. Here ∇J denotes the gradient of the objective function with respect to $\boldsymbol{m}$. This search direction is often referred to as the steepest descent direction. Since we do not approximate J, this search direction leads to a line search method denoted the *steepest descent* method. Provided with some suitable stopping criteria, the algorithm is easy to implement and it only requires the gradients of J. However, the method converges relatively slowly (linear convergence).

Newton method. The usual choice of search direction for non-linear optimization problems is given by the Newton search direction. Let us consider the second order Taylor

series approximation to $J(\boldsymbol{m}^q + \boldsymbol{p})$, defined as the quadratic

$$J(\boldsymbol{m}^q + \boldsymbol{p}) \approx J(\boldsymbol{m}^q) + \nabla J(\boldsymbol{m}^q)^T \boldsymbol{p} + \frac{1}{2}\boldsymbol{p}^T H_N \boldsymbol{p}. \tag{4.30}$$

where H_N denotes the Hessian evaluated at m^q

$$H_N = \nabla\left(\nabla J(\boldsymbol{m}^q)^T\right). \tag{4.31}$$

(The subscript N denotes that this is the Newton Hessian.) Now, setting the gradient (with respect to $\boldsymbol{p}$) of the approximation (4.30) equal to zero we obtain the Newton search direction

$$\boldsymbol{p}_N = -H_N^{-1}\nabla J(\boldsymbol{m}^q). \tag{4.32}$$

Clearly, this method requires that the inverse of H_N exist, and to ensure that $\boldsymbol{p}$ is a descent direction, it is required that the Hessian is positive definite. Note that the approximation is only used to find a search direction. The Newton search direction is then applied in a line search algorithm. This method converges faster (quadratic convergence) than the steepest descent, with an additional cost of calculating the Hessian matrix. To mitigate this cost while retaining some of the convergence properties, one typically tries to approximate the Hessian.

Quasi-Newton approximations. The quasi-Newton methods represent one strategy for approximating the Newton Hessian. Starting with some initial guess, the methods will iteratively generate an improved approximation of the Hessian, $\widetilde{H}_{QN}$, by incorporating information from each iteration. (Here the subscript QN denotes the quasi-Newton approximation.) The search direction in the quasi-Newton method is then found as

$$\boldsymbol{p}_{QN} = -\widetilde{H}_{QN}^{-1}\nabla J(\boldsymbol{m}^q). \tag{4.33}$$

At each iterate, $\boldsymbol{m}^{q+1}$, the quasi-Newton method updates the approximate Hessian such that is satisfies the secant equation [67]

$$\widetilde{H}_{QN}\left(\boldsymbol{m}^{q+1} - \boldsymbol{m}^q\right) = \nabla J\left(\boldsymbol{m}^{q+1}\right) - \nabla J(\boldsymbol{m}^q). \tag{4.34}$$

Hence, the updates only require the gradient of J. This condition is satisfied by numerous algorithms, but one of the most reliable quasi-Newton method is the Broyden-Fletcher-Goldfarb-Shanno (BFGS), or the limited memory BFGS (LBFGS) [67, 73]. The BFGS method converges superlinearly.

Gauss-Newton approximation. Let us now consider a problem where the objective function, J, is given by (4.28). For this objective function the Newton Hessian matrix is given as

$$H_N = Q_m^{-1} + \mathcal{G}^T Q_d^{-1}\mathcal{G} + \nabla\mathcal{G}^T Q_d^{-1}(G(\boldsymbol{m}) - \boldsymbol{d}), \tag{4.35}$$

where $\mathcal{G}$ is the sensitivity matrix defined by

$$\mathcal{G} = \begin{pmatrix} (\nabla G_1(\boldsymbol{m}))^T \\ \vdots \\ (\nabla G_{n_D}(\boldsymbol{m}))^T \end{pmatrix}. \tag{4.36}$$

With this objective function, significant computational savings can be achieved by ignoring the terms involving the second order derivatives of G, resulting in the Gauss-Newton Hessian matrix

$$\widetilde{H}_{GN} = Q_m^{-1} + \mathcal{G}^T Q_d^{-1} \mathcal{G}. \tag{4.37}$$

(The subscript GN indicated that this is the Gauss-Newton Hessian.) Noting that for the objective function (4.28) the gradient is

$$\nabla J\left(\boldsymbol{m}^q\right) = Q_m^{-1}\left(\boldsymbol{m}^q - \boldsymbol{m}^{prior}\right) + \mathcal{G}^T Q_d^{-1}\left(G\left(\boldsymbol{m}^q\right) - \boldsymbol{d}\right), \tag{4.38}$$

the Gauss-Newton search direction is therefore given by

$$\boldsymbol{p}_{GN} = -\left(Q_m^{-1} + \mathcal{G}^T Q_d^{-1} \mathcal{G}\right)^{-1}\left(Q_m^{-1}\left(\boldsymbol{m}^q - \boldsymbol{m}^{prior}\right) + \mathcal{G}^T Q_d^{-1}\left(G\left(\boldsymbol{m}^q\right) - \boldsymbol{d}\right)\right). \tag{4.39}$$

Close to the minimum the value of the residuals, $\left(G\left(\boldsymbol{m}\right) - \boldsymbol{d}\right)$, is small and the neglected term in (4.35) is small. Hence, in a neighbourhood of the minimum, the Gauss-Newton Hessian is a good approximation to the Newton Hessian. The Gauss-Newton convergence is quadratic if the residual is zero, while the convergence is quotient-linear when the residual is non-zero [73].

Levenberg-Marquardt method. An alternative modification of the Newton algorithm is provided by the Levenberg-Marquardt algorithm. Here, an extra term is added to the Newton Hessian

$$H_{LM} = \alpha I + H_N. \tag{4.40}$$

This algorithm is a trust region method and, for this reason, no line search is performed. The value α controls both the step size and the search direction. If α has a low value, the method is similar to the Newton method, and if α has a high value, the method is similar to taking a small step in the steepest descent direction. Typically α change from one iteration to the next, and the Levenberg-Marquardt algorithm is, therefore, more flexible than the Newton or Gauss-Newton methods. A standard strategy for tuning α is to start with a high value and gradually decrease the value if $J\left(\boldsymbol{m}^q\right) > J\left(\boldsymbol{m}^{q+1}\right)$ [73]. For most high-dimensional problems where J is given by (4.28), it is computationally demanding to calculate the full Newton Hessian. For this reason, the Gauss-Newton Hessian is often utilized in the Levenberg-Marquardt algorithm. The convergence of the Levenberg-Marquardt algorithm is quotient-linear [73].

Sensitivity calculations. All the algorithms depend on reliable methods for obtaining the gradients of the objective function, and the Gauss-Newton method also requires the full sensitivity matrix $\mathcal{G}$. If the forward model equations are known, there are several methods available for establishing the sensitivity matrix, such as the direct (gradient simulation) method [99], and the adjoint method [73]. While for cases where the forward model equations is unknown or inaccessible, the sensitivity matrix must be approximated numerically by a suitable finite difference methods. The computational cost of the direct and the finite difference methods are proportional to the number of parameters, n_m, while the computational cost of the adjoint method is proportional to the number of data, n_d. For reservoir cases, n_m is typically much higher than n_d, favouring the adjoint method. Unfortunately, numerical implementation of the ajoint system can be very time consuming. This is especially true if one does not have access to the full numerical schemes utilized by the numerical solver.

Chapter 5

Ensemble-based methods

The ensemble-based methods are closely related to the importance sampling and sequential MC methods, discussed in Section 4.2. The methods are all based on a MC estimation of the smoother or filter PDF, utilizing an ensemble of models (denoted swarm of particles in Section 4.2). There is, however, one important difference. Contrary to the sequential MC methods, the ensemble-based methods will assign the same weight to each ensemble member, thus removing the resampling step. This avoids degeneration of the weights, making the ensemble-based methods more suitable for high-dimensional problems. Unfortunately, this robustness comes at a cost, and the ensemble-based methods can only be shown to have well defined asymptotic behaviour when the posterior PDF is Gaussian. In the following chapter, we introduce some widely used ensemble-based methods. The assumption of a Gaussian PDF was not needed for the sequential MC methods discussed in the previous chapter. For a method that combines the ensemble-based methods and the sequential MC in an adaptive manner, see [93].

Before we introduce the ensemble-based methods, we provide some notation which are utilized by all the methods. Throughout this chapter, we let

$$M = (\boldsymbol{m}_1, \ldots, \boldsymbol{m}_{n_e}) \in \mathbb{R}^{n_m \times n_e}, \tag{5.1}$$

denote an ensemble matrix containing the n_e ensemble members as column vectors. We let $\mathbf{1}_{n_m} \in \mathbb{R}^{n_m \times n_m}$ be a matrix where all elements are $1/n_m$. We can then define ensemble mean matrix, $\overline{M} \in \mathbb{R}^{n_m \times n_e}$, as

$$\overline{M} = M\mathbf{1}_{n_m}, \tag{5.2}$$

the ensemble perturbation matrix, $\Delta M \in \mathbb{R}^{n_m \times n_e}$, as

$$\Delta M = M - \overline{M} = M\left(I - \mathbf{1}_{n_m}\right), \tag{5.3}$$

and the empirical covariance matrix, $C_m \in \mathbb{R}^{n_m \times n_m}$, as

$$C_m = \frac{1}{n_m - 1} \Delta M \Delta M^T. \tag{5.4}$$

5.1 EnKF

The EnKF was briefly introduced in Chapter 1 as an MC approximation to the KF equations. In the following, we will discuss the method in more detail. Since the EnKF is

based on the KF, it is assumed that the posterior PDF is Gaussian. The method will, therefore, only generate correct samples for problems where the prior model is Gaussian and where both the forward model and observation operator are linear. Despite this, the EnKF has been used for a wide range of high-dimensional problems that have non-linear forward and observation models, such as, atmospheric [50] and oceanographic systems [10], as well as porous-media flow problems [1]. For such cases, the ExKF can also be utilized. However, one can easily show (see, e.g. [28]) that the EnKF only needs to store the $n_y \times n_e$ ensemble matrix, and not the $n_y \times n_y$ covariance matrix. Moreover, the EnKF does not require any sensitivity calculation. For typical cases where the method is applied, $n_y \gg n_e$ and compared to the ExKF the EnKF represent significant computational savings.

Assume that we have a time series of data, collected at n_a time steps $\{\boldsymbol{d}_i\}_{i=1}^{n_a}$. Similar to the KF, the EnKF seeks to estimate the posterior filter PDF, $p\left(\boldsymbol{y}_{n_a}|\boldsymbol{d}_1,\cdots,\boldsymbol{d}_{n_a}\right)$, by sequentially assimilating the data. This is performed by estimating the forecast and analysis of the mean and covariance via an ensemble of models.

Even thought the KF is based on state estimation, where all stochastic variables evolve in time, it is convenient to consider a combination of the state and parameter vectors $\left(\boldsymbol{z}^T,\boldsymbol{m}^T\right)^T \in \mathbb{R}^{n_z+n_m}$. Let the time evolution of the dynamic states be given as

$$\boldsymbol{z}_k = G\left(\boldsymbol{z}_{k-1},\boldsymbol{m}_{k-1}\right) + \boldsymbol{\eta}_k, \tag{5.5}$$

and let us assume that the observation are given as

$$\boldsymbol{d}_k = H\left(\boldsymbol{z}_k\right) + \boldsymbol{\epsilon}_k, \tag{5.6}$$

where $\boldsymbol{\eta}_k \sim N\left(\boldsymbol{0},Q_{z_k}\right)$ and $\boldsymbol{\epsilon}_k \sim N\left(\boldsymbol{0},Q_{d_k}\right)$. To ensure that there is a linear relationship between the joint state-parameter vector and the observations one combines the observations with the joint state-parameter vector, generating $\boldsymbol{y} \in \mathbb{R}^{n_y}$ defined as

$$\boldsymbol{y}_k = \begin{pmatrix} \boldsymbol{d}_k \\ \boldsymbol{z}_k \\ \boldsymbol{m}_k \end{pmatrix}. \tag{5.7}$$

Note that the time index on the constant parameter vector $\boldsymbol{m}$ is included to indicate that the parameter estimate can change as data are assimilated.

With this notation the forward model is given by

$$\boldsymbol{y}_k = G\left(\boldsymbol{y}_{k-1}\right) + \boldsymbol{\eta}_k, \tag{5.8}$$

and the observations are given by

$$\boldsymbol{d}_k = H\boldsymbol{y}_k + \boldsymbol{\epsilon}_k, \tag{5.9}$$

where the matrix H_k picks the correct data, ensuring that there is a linear relationship between the vector $\boldsymbol{y}_k$ and the data.

The EnKF algorithm starts by sampling an ensemble of n_e models from the initial prior PDF. Utilizing the ensemble notation provided above this is given as

$$Y_0 = \left(\boldsymbol{y}_1,\ldots,\boldsymbol{y}_{n_e}\right). \tag{5.10}$$

Kolmogorov's forward equation (2.13) for the PDF is now approximated by running the entire ensemble forward in time. For a general time step, the MC approximation to the forecast mean is given as

$$\overline{Y}_k^* = G\left(Y_{k-1}\right)\mathbf{1}_{n_y} = Y_k^*\mathbf{1}_{n_y}, \tag{5.11}$$

and the MC approximation of the forecast covariance is

$$C_{y_k^*} = \frac{1}{n_e - 1}\Delta Y_k^*\left(\Delta Y_k^*\right)^T, \tag{5.12}$$

where, in similar fashion as for the KF, the superscripted star denotes the predicted quantity. At this time-step, the vector of data $(\boldsymbol{d})_k$ is available for assimilation. To ensure that the EnKF samples correctly, we must add a realization of the data error to the observed data $(\boldsymbol{d}_n)_k = (\boldsymbol{d})_k + (\boldsymbol{\epsilon}_n)_k$. The ensemble of perturbed data can then be gathered in a suitable ensemble matrix

$$D_k = \left((\boldsymbol{d}_1)_k, \ldots, (\boldsymbol{d}_{n_e})_k\right). \tag{5.13}$$

The EnKF will now update the ensemble of forward models by the empirical approximation to the KF,

$$Y_k = Y_k^* + C_{y_k^*}H^T\left(HC_{y_k^*}H^T + Q_{d_k}\right)^{-1}\left(D_k - HY_k^*\right). \tag{5.14}$$

The analysed mean and covariance can now be estimated by their corresponding MC estimates

$$\overline{Y}_k = Y_k\mathbf{1}_{n_e}, \qquad C_{y_k} = \frac{1}{n_e - 1}\Delta Y_k\Delta Y_k^T. \tag{5.15}$$

In the limit $n_e \to \infty$, it can be shown that the empirical estimates of the analyzed mean (one column of $\overline{Y}_k$) and analyzed covariance converge to the KF equations for analyzed mean and covariance given by (2.26) and (2.27), see, e.g., [13, 63].

As mentioned, the EnKF typically utilize a moderately sized ensemble. This is one of the main computational advantages with the method. There are, however, some problems related to the estimation of a high-dimensional covariance matrices applying a small ensemble. One such problem is spurious correlations, that is, artificial correlations in the empirical covariance that, when utilized in the update, causes changes to variables or parameters in regions of no real influence [1]. Considering a linear case with negligible observation error, [56, 57] derived an analytic error bound for the error caused by a small ensemble in the analysis step.

Another problem is caused by the rank of the approximate covariance matrix. Since this matrix is calculated from the ensemble, the number of ensemble members provides a limit for the degrees of freedom available for updating the vector $\boldsymbol{y}$. Moreover, after the analysis step, each ensemble member is a linear combination of the n_e initial ensemble member. For this reason, there are only n_e coefficients that can be adjusted to match the data. This can cause problems if one assimilate large amounts of independent data, such as time-lapse seismic data [92]. For such cases, it is possible to utilize sub-space approximations, see, e.g., [28].

The EnKF is commonly used for problems where the Gaussian assumptions are violated, e.g., fluid flow in porous media. For such problems, the EnKF provides a linear update to elements of the vector $\boldsymbol{y}$ when the relationship to the measurements are highly non-linear. The error caused by this approximation can be significant, and is independent of the number of ensemble members.

5.1.1 EnKF for parameter estimation

As mentioned in Chapter 3, for some problems, e.g., parameter estimation in porous media, one are mainly interested in the estimation of the constant parameters and not the states. Due to the formulation of $\boldsymbol{y}$, it is possible to utilize the EnKF as a method for parameter estimation.

Recall that the KF assumes that the forward model is stochastic, hence, the parameter estimation problems are formulated as weakly constrained problems. Unfortunately, for problems where the EnKF is applied, one generally have no information regarding the errors in the forward model. Although this error might be significant, one, typically, neglects the error completely [1]. Hence, the EnKF parameter estimation problem is typically formulated as a strong constrained problem.

As mentioned above, the linear observation operator H selects the correct data when applied to the vector $\boldsymbol{y}$. Hence, it is clear that

$$H = \begin{pmatrix} I & \mathbf{0} \end{pmatrix}, \tag{5.16}$$

where $I \in \mathbb{R}^{n_d \times n_d}$ is an identity matrix, and $\mathbf{0}$ is a suitably sized zero-matrix. Inserting this into (5.14), one obtains

$$M_k = C_{m_k d_k^*} \left(C_{d_k^*} + Q_{d_k} \right)^{-1} \left(D_k - H Y_k^* \right), \tag{5.17}$$

where $C_{m_k d_k^*}$ denotes the cross-covariance matrix between the predictions and the parameters, and $C_{d_k^*}$ denotes the auto-covariance matrix of the predicted data. Note that, since the full analysis of $\boldsymbol{y}$ is needed to restart the forward model, a pure parameter update will not work in the sequential estimation procedure.

5.1.2 HIEnKF

For a single EnKF update step, both the state and parameters are updated. The ensemble of updated states and parameters are then inserted into the forward model to predict the dynamic states at the next assimilation time. If the forward-model operator represents a non-linear relationship between the states and parameters, the analysis produce inconsistencies between the updated states and parameters. That is, the states estimated by rerunning the forward model from initial time, utilizing the updated parameters, would not correspond to the updated states, see, e.g., [97]. When the EnKF is utilized for estimation of both states and parameters, e.g., in a porous-media application, this inconsistency can make it computationally demanding to restart the numerical models [91]. Hence, in addition to the error caused in the future predictions, the inconsistency removes some of the computational advantages of the sequential scheme.

To remove the consistency problem, while retaining the advantages of a sequential approach, the half-iteration EnKF (HIEnKF) was introduced in [105]. Here, each prediction is generated by restarting the forward model from initial time. The parameter update equation for the HIEnKF is obtained by replacing $H_k Y_k^*$ with $G\left(M_k^*\right)$ in (5.17).

5.2 Ensemble Smoother

The ensemble smoother (ES) was proposed in [102] as an ensemble approximation to the fixed interval smoother (discussed in Section 2.5). Similar to the EnKF, the ES approximates Kolmogorov's equation by evolving the ensemble of prior models forward in time via the model dynamics. However, contrary to the EnKF, the ES is non-sequential, and predicts the data for all time-steps using the prior ensemble. The full state trajectory is then updated when all available data are assimilated into the system in a simultaneous manner.

Since the ES assimilates all data simultaneously, we have the prediction ensemble matrix

$$\widehat{Y}^* = \begin{pmatrix} \widehat{D} \\ \widehat{Z} \\ M \end{pmatrix} \in \mathbb{R}^{n_{\widehat{y}} \times n_e}, \tag{5.18}$$

where a single column of $\widehat{D}$ and $\widehat{Z}$ are given as (omitting the ensemble index)

$$\widehat{\boldsymbol{d}} = \begin{pmatrix} \boldsymbol{d}_1 \\ \boldsymbol{d}_{t_2} \\ \vdots \\ \boldsymbol{d}_{t_{na}} \end{pmatrix} \in \mathbb{R}^{n_D}, \qquad \widehat{\boldsymbol{z}} = \begin{pmatrix} G_{t_1}\left(\boldsymbol{y}_{prior}\right) \\ G_{t_2}\left(\boldsymbol{y}_{prior}\right) \\ \vdots \\ G_{t_{na}}\left(\boldsymbol{y}_{prior}\right) \end{pmatrix} \in \mathbb{R}^{n_D}, \tag{5.19}$$

and $n_D = \left(\sum_{k=1}^{n_a} n_{d_k}\right)$. The ES analysis equation is given as

$$\widehat{Y} = \widehat{Y}^* + C_{\widehat{y}^*}\widehat{H}^T\left(\widehat{H}C_{\widehat{y}^*}\widehat{H}^T + Q_{\widehat{d}}\right)^{-1}\left(\widehat{D} - \widehat{HY}^*\right), \tag{5.20}$$

where the observation operator $\widehat{H} \in \mathbb{R}^{n_D \times n_{\widehat{y}}}$ selects the correct data from the vector $\widehat{\boldsymbol{y}}$ (one column of $\widehat{Y}$), the empirical covariance matrix $C_{\widehat{y}^*} \in \mathbb{R}^{n_{\widehat{y}} \times n_{\widehat{y}}}$ is calculated based on the ensemble of predictions, and the data covariance matrix $Q_{\widehat{d}} \in \mathbb{R}^{n_D \times n_D}$ is a diagonal matrix.

For state estimation problems, considering any time step apart from the last (where the smoother and filter estimate are identical), smoothers generally produce superior results when compared with the filter [90]. This difference is caused by the fact that smoothers can adjust a model state utilizing both past, present, and future data. However, for non-linear dynamical models, particularly with chaotic dynamics, the EnKF was shown to perform better than the ES [30, 102]. This was contributed to the sequential assimilation scheme in the EnKF, which prevented strongly non-Gaussian contributions, arising from chaotic models with long unconstrained integration time, in the ensemble of predictions. For non-chaotic models, e.g., fluid flow in porous-media, numerical experiments produce similar results from EnKF and ES when considering data-match [91]. But as shown by numerical experiments in Paper A, C, D, and E, this is not always the case when comparing the approximate posterior PDFs of the parameters.

The ES can be derived with simultaneous or sequential assimilation of the data [30], and an alternative smoother algorithm denoted the ensemble Kalman smoother (EnKS), based on sequential assimilation of data, was derived in [30]. Numerical experiments

showed that this algorithm performed even better than the EnKF, suggesting that a combination of smoothing and sequential assimilation of data provides optimal results. Fixed-point or fixed-lag smoothers, as discussed in Section 2.5, can easily be implemented in the ES or EnKS framework [30].

5.2.1 ES for parameter estimation

As mentioned above, there exist several problems where the primary interest is in the static parameter vector. In similar fashion as for the EnKF, it is relatively easy to derive the parameter update for the ES. This is given as

$$M = C_{m\widehat{d}^*}\left(C_{\widehat{d}^*} + Q_{\widehat{d}}\right)^{-1}\left(\widehat{D} - \widehat{HY}^*\right), \tag{5.21}$$

where $C_{m\widehat{d}^*}$ denotes the empirical cross-covariance matrix between the parameters and all predicted data, while $C_{\widehat{d}^*}$ denotes the auto-covariance matrix for all predicted data. Note that all available data are assimilated simultaneously and the algorithm contains no restart step. Since one typically ignores the error in the forward model for reservoir problems, the ES parameter estimation problem is typically formulated as a strong constrained problem.

5.3 Ensemble Randomized Maximum Likelihood

The ensemble randomized maximum likelihood (EnRML) method was introduced as an iterative EnKF algorithm in [44]. The algorithm is formulated in a similar manner as the RML method. That is, one seeks the parameter vector that minimize (4.28). While the main computational cost of the RML algorithm is the calculation of the sensitivity matrix, the EnRML utilizes the ensemble to calculate an approximate sensitivity matrix. Contrary to the approach utilized by the EnKF and ES methods, the EnRML only updates the unknown parameters. However, there is strong similarity between the EnRML and the EnKF/ES methods, which is discussed in Paper B.

Since the EnRML only updates the parameters, we cannot consider the update of $\boldsymbol{y}$, which is incorporated in the EnKF and ES. Hence all data are given as

$$\boldsymbol{d} = H\left(G\left(z_0, \boldsymbol{m}^{prior}\right) + \boldsymbol{\eta}\right) + \boldsymbol{\epsilon}, \tag{5.22}$$

where, generally, H and G are non-linear operators. To simplify the notation, we incorporate the observation operator into the forward model; we incorporate the model error into the data error; and we remove the explicit dependence on initial value, z_0, from the forward model. The data are then given as

$$\boldsymbol{d} = G\left(\boldsymbol{m}^{prior}\right) + \boldsymbol{\xi}. \tag{5.23}$$

In similar fashion as for the EnKF, the method generates an initial ensemble of parameter models by sampling from the initial prior PDF $\boldsymbol{m} \sim N\left(\boldsymbol{\mu}_m^{prior}, Q_{m^{prior}}\right)$. An ensemble of predictions is then generated by the forward model utilizing the prior ensemble of parameters as input. Utilizing the ensemble perturbation matrices, we can

define the ensemble average sensitivity matrix, $\widetilde{\mathcal{F}}$, as the coefficient matrix relating the changes in model parameters to the changes in computed data [44]

$$\Delta G\left(M_{prior}\right) = \widetilde{\mathcal{F}}\Delta M. \tag{5.24}$$

However, the matrix ΔM is not generally invertible and we must therefore utilize the pseudo-inverse (see, e.g. [37]) to calculate the sensitivity matrix. The pseudo-inverse will throughout be denoted by a superscripted †, and the ensemble-based sensitivity matrix is then $\widetilde{\mathcal{F}} = \Delta G\left(M_{prior}\right)\Delta M^{\dagger}$.

After one has obtained the ensemble-based sensitivity matrix, the EnRML and RML are similar since the algorithms do not depend on a specific minimization algorithm. Any of the optimization methods discussed in Section 4.3.1 can be utilized, and especially the Levenberg-Marquardt method has been successfully applied to porous-media flow problems [14].

5.4 Multiple data assimilation

When considering techniques for history matching petroleum reservoirs that are based on optimization, several authors have demonstrated that taking a full iteration step might lead to a significant overcorrection of the petrophysical values [31, 32, 60]. In optimization algorithms this problem can be avoided by restricting the step length or the trust region for the first couple of iterations. Neither the EnKF nor the ES algorithms can adjust the step length, and for non-linear problems the analysis step might overcorrect the parameters. Seeking the same effect as for the optimization algorithms, the multiple data assimilation (MDA) algorithm was introduced as an extension of the EnKF and ES methods. This extension allows the algorithms to divide the full analysis step into several smaller steps in a statistically consistent way [23, 24].

In the following we discuss a single EnKF analysis step with the MDA algorithm. Consider the available data at a given time step, $\boldsymbol{d}_k$. Following the standard EnKF assumptions, these data have zero-mean Gaussian error with covariance Q_{d_k}. Instead of assimilating the data in a single step, the MDA algorithm assimilates the same data n_{mda} times. The new data are defined as $\boldsymbol{d}_i$ for $i = 1, \ldots, n_{mda}$, and the error in each data is generated utilizing an inflated data covariance matrix, $Q_{d_i^{mda}} = \varpi_i Q_d$. To guarantee that the MDA method samples correctly for the Gauss-linear case, the inflation factors for the data covariance matrix must satisfy

$$\sum_{i=1}^{n_{mda}} \frac{1}{\varpi_i} = 1. \tag{5.25}$$

The MDA can be considered as a discrete approximation to continuous analysis step applied in the mollified EnKF [8].

Recall that the Bayesian estimation problem can be formulated as finding the minimizer of (3.12). Similar to the RML objective function (4.28), the Gaussian objective function contains two terms, one quadratic corresponding to the Gaussian prior term, and one non-quadratic corresponding to the non-Gaussian likelihood. If ϖ is selected as a large value, it is clear that the objective function is dominated by the quadratic term. Hence, the MDA can be seen as a method for making the total objective function more quadratic by adding weight to the quadratic term.

Chapter 6

Evaluating sampling performance

For many problems, the posterior PDF is intractable, and we can only extract information by drawing samples. The methods described in Chapter 4 are designed to generate exact samples from any PDF, while the methods described in Chapter 5 are designed to generate an ensemble which for all cases, apart from one important exception, only represent approximate samples from the posterior PDF. The exception is in the Gauss-linear case, when the number of ensemble members goes towards infinity. For all other cases, when utilizing the methods of Chapter 5, we do not know the exact size of the error in the approximation, or if there is a similar error for the various approximate methods.

In this chapter, we will discuss some methods that allow us to gauge this approximation error. Since, as mentioned, we cannot calculate the exact posterior, all these methods are based on comparing the ensemble of approximate samples to exact samples from the posterior PDF.

6.1 Stochastic distance measures

Let us assume that the posterior ensemble represents samples from an approximation to the posterior PDF, denoted q, and let us assume that we have an analytical expression for both q and the true posterior p. A fair assessment of the approximate method would be obtained by comparing q to p. The comparison can be performed by calculating the distance between the PDFs in some norm, by the integrated mean squared error, or by some measures based on information theory, see, e.g., [86]. In the following, we consider the latter group of distance measures.

A standard method for evaluating the distance between two PDFs is the Kullback-Leibler (KL) divergence introduced by [58], which is defined as

$$I_{KL}\left(p||q\right) = \int p\left(\boldsymbol{m}\right) \log\left(\frac{p\left(\boldsymbol{m}\right)}{q\left(\boldsymbol{m}\right)}\right) \mathrm{d}\,\boldsymbol{m}. \tag{6.1}$$

This measure of dissimilarity between the PDFs is non-symmetric and does not satisfy the triangle inequality, hence it is denoted the divergence instead of the distance [106] (this is denoted by the double bar separating the arguments in (6.1)). This measure arises from information theory, and the units depend on which logarithm that is utilized. The divergence is expressed in bits if the base-2 logarithm is utilized, while it is

expressed in nats if the base-e logarithm is utilized. It is assumed that $0 \log 0/q = 0$ and $p \log p/0 = \infty$, hence the KL divergence takes values between 0 and ∞.

An alternative to the KL divergence is the Hellinger (or Bhattacharyya) distance, defined as

$$\begin{aligned} I_H(p,q) &= \left(\frac{1}{2} \int \left(\sqrt{p(\boldsymbol{m})} - \sqrt{q(\boldsymbol{m})} \right)^2 \mathrm{d}\, m \right)^{1/2}, \\ &= \left(1 - \int \sqrt{p(\boldsymbol{m})\, q(\boldsymbol{m})} \mathrm{d}\, m \right)^{1/2}. \end{aligned} \tag{6.2}$$

When the Hellinger distance is written in this form it takes values between 0 and 1.

There exist numerous other metrics for quantifying the distance between probability measures, see, e.g., [36] for an introduction and comparison of some metrics. Both the KL divergence and the Hellinger distance can be calculated by closed-form expressions if p and q are Gaussian PDFs. However, for problems where one does not know the shape of the PDFs, or when the analytical expressions cannot be evaluated, these measures must be approximated.

6.2 Density estimation

In the discussion above, it was assumed that both p and q were known and could be evaluated. However, for many problems this is not the case. Typically, we only have samples from p and samples from q. Hence, we need methods that allow for evaluation of the densities based on the available samples. Following the theory provided in [89], we give a short introduction to density estimation.

Let us assume that we have n_e samples from the n_u dimensional PDF p, stored as columns in the ensemble matrix $U = (\boldsymbol{u}_1, \ldots, \boldsymbol{u}_{n_e})$. Based on these samples we seek to estimate the PDF p. (The estimation of the PDF q will be performed in a similar manner.) The simplest approach for estimating the PDF is by the well known histogram. This method is simple and works well for univariate PDFs. However, for high-dimensional cases the histogram encounters several problems rendering it difficult to use as a density estimator.

For more complex PDFs, alternative methods must be applied. These methods, known as kernel density estimators, can all be described utilizing the same framework. The methods approximate the PDF as a sum of 'bumps' centred at each sample. The kernel density estimator of p can formally be written as

$$\widetilde{p}(\boldsymbol{u}) = \frac{1}{n_e h^{n_u}} \sum_{j=1}^{n_e} K\left(\frac{1}{h} \left(\boldsymbol{u} - \boldsymbol{u}_j \right) \right), \tag{6.3}$$

where h is the widow width, defining the width of the 'bumps', and k is the kernel, a function defining the shape of the 'bumps'. Both the window width and the kernel must be selected by the user, and this choice can affect the quality of the estimate. If, for example, h is too small the estimate will be dominated by spikes at each sample, and if h is too large the estimate will contain none of the details provided by the samples. The

choice of kernel function is also important, and one can choose among a large number of kernels satisfying

$$\int_{\mathbb{R}^{n_u}} K(\boldsymbol{u})\,\mathrm{d}\boldsymbol{u} = 1. \tag{6.4}$$

Hence, provided that K is everywhere non-negative and Borel measurable, the kernel can be chosen as any PDF, and the estimation will also be a PDF. This fact ensures that the approximation inherits all the continuity and differentiability properties of the kernel. Thus, if one seeks a smooth estimate one need to utilize a smooth kernel. A typical kernel function is the multivariate Epanechnikov kernel

$$K(\boldsymbol{u}) = \begin{cases} \frac{1}{2} c_{n_u} (n_u + 2) \left(1 - \boldsymbol{u}^T \boldsymbol{u}\right) & \text{if } \boldsymbol{u}^T \boldsymbol{u} < 1, \\ 0 & \text{otherwise,} \end{cases} \tag{6.5}$$

where c_{n_u} is the volume of the unit n_u-dimensional sphere.

An alternative density estimator is provided by the nearest neighbour estimator. Consider the samples stored in the matrix U, one can calculate the Euclidean distance, $\psi_n(\boldsymbol{u})$, from a fixed $\boldsymbol{u}$ to each sample $\boldsymbol{u}_n$. For each $\boldsymbol{u}$, one can then sort the distances according to ascending size. The distance to the r'th nearest sample (i.e., r'th nearest neighbour), $\zeta_r(\boldsymbol{u})$, is then denoted $\psi_r(\boldsymbol{u})$. In a n_u-dimensional case, this distance can be utilized to calculate the volume of a n_u-dimensional sphere, $v_r(\boldsymbol{u})$, of radius $\psi_r(\boldsymbol{u})$ centred at $\boldsymbol{u}$. This is given as $v_r(\boldsymbol{u}) = c_{n_u} \psi_r(\boldsymbol{u})^{n_u}$. With these definitions, the nearest neighbour estimator is given as

$$\widetilde{p}(\boldsymbol{u}) = \frac{r/n_e}{c_{n_u} \psi_r(\boldsymbol{u})^{n_u}}. \tag{6.6}$$

The nearest neighbour density estimator can be motivated by the observation that, for a sample of n_e members, one would expect about $n_e p(\boldsymbol{u})\, v_r(\boldsymbol{u})$ samples to fall in the sphere of radius $\psi_r(\boldsymbol{u})$ centred at $\boldsymbol{u}$. The estimate is then obtained by setting this number equal to the number of nearest neighbours, r, which, by definition, is the the number of observed samples inside the sphere.

Note that the nearest neighbour estimator at $\boldsymbol{u}$ can also be given as the kernel estimator on the form (6.3), by defining the kernel

$$K(\boldsymbol{u}) = \begin{cases} c_{n_u}^{-1} & \text{if } |\boldsymbol{u}| \leq 1 \\ 0 & \text{otherwise,} \end{cases} \tag{6.7}$$

and window width $h = \psi_r(\boldsymbol{u})$. Hence, for the estimate at a fixed point $\boldsymbol{u}$ there is no difference between the kernel methods and the nearest neighbour methods. There will, however, due to the discontinuity in the derivative of the functions $\psi_r(\boldsymbol{u})$, be differences between the methods when approximating the full PDFs.

6.3 KL with r-nearest neighbour estimator

In the following, we discuss two approximations to the KL divergence based on the r-nearest neighbour estimator. These approximations were proposed in [103, 104], and we refer the reader to these papers for details regarding asymptotic behaviour of the

methods. Let us assume that $U = (\boldsymbol{u}_1, \ldots, \boldsymbol{u}_{n_e})$ are n_u-dimensional samples drawn from p, and $V = (\boldsymbol{v}_1, \ldots, \boldsymbol{v}_{n_e})$ are n_u-dimensional samples from q. (Note that it is not necessary to have an identical number of samples from p and q) By the law of large numbers, the KL divergence (6.1) is approximated by

$$\widetilde{I}_{KL}(p||q) = \frac{1}{n_e} \sum_{j=1}^{n_e} \log \frac{\widetilde{p}\left(\boldsymbol{u}_j\right)}{\widetilde{q}\left(\boldsymbol{u}_j\right)}. \tag{6.8}$$

Inserting the r-nearest neighbour estimate for both densities, $\widetilde{p}$ and $\widetilde{q}$, estimated around the samples in U provides the following empirical estimate for the KL divergence

$$\widetilde{I}_{KL}(p||q) = \frac{n_u}{n_e} \sum_{j=1}^{n_e} \log \frac{\psi_r^v\left(\boldsymbol{u}_j\right)}{\psi_r^u\left(\boldsymbol{u}_j\right)} + \log \frac{n_e}{n_e - 1}, \tag{6.9}$$

where the superscripts u and v indicate whether the distance, $\psi_r\left(\boldsymbol{u}_j\right)$, is calculated from the fixed point $\boldsymbol{u}_j$ to the r-nearest neighbour in U or in V. This estimator was shown, under certain mild regularity assumptions, to be asymptotically unbiased and mean-square consistent [104].

An alternative estimator was proposed in [104]. Here, instead of choosing a fixed number of nearest neighbours, the estimator allowed a different choice of neighbours, r_j, for each evaluation of $\psi_{r_j}\left(\boldsymbol{u}_j\right)$. This estimator was also shown to be asymptotically unbiased and mean-square consistent.

For any density estimator, it is, as mentioned above, important to select a suitable window width. For the r-nearest neighbour estimator this corresponds to selecting a suitable number of nearest neighbours. To this end, [104] suggested that r_j should be found by fixing the nearest neighbour distance instead of the number of nearest neighbours. One then selects a distance $\epsilon\left(\boldsymbol{u}_j\right)$ and, for each point $\boldsymbol{u}_j$, one counts the number of samples from U and V that are within the ball, c, centred at $\boldsymbol{u}_j$, with radius $\epsilon\left(\boldsymbol{u}_j\right)$. Let us denote the number of samples from U as l_j, and denote the number of samples from V as k_j. If one selects the fixed distance as

$$\epsilon\left(\boldsymbol{u}_j\right) = \min\left(\psi^u\left(\boldsymbol{u}_j\right), \psi^v\left(\boldsymbol{u}_j\right)\right), \tag{6.10}$$

where the distances are defined as

$$\psi^u\left(\boldsymbol{u}_j\right) = \min_{i=1,\ldots,n_e, i \neq j} \left\|\boldsymbol{u}_j - \boldsymbol{u}_i\right\|, \tag{6.11}$$

$$\psi^v\left(\boldsymbol{u}_j\right) = \min_{i=1,\ldots,n_e} \left\|\boldsymbol{u}_j - \boldsymbol{v}_i\right\|, \tag{6.12}$$

(where, since this is not the distance to any specified neighbour, there are no subscripts). The biased reduced KL divergence estimator can be defined as

$$\widetilde{I}_{KL}(p||q) = \frac{n_u}{n_e} \sum_{j=1}^{n_e} \log \frac{\psi_{l_j}^v\left(\boldsymbol{u}_j\right)}{\psi_{k_j}^u\left(\boldsymbol{u}_j\right)} + \frac{1}{n_e} \sum_{j=1}^{n_e} \Gamma\left(k_j\right) - \Gamma\left(l_j\right) + \log \frac{n_e}{n_e - 1}, \tag{6.13}$$

where Γ is the Digamma function, added to guarantee consistency [104]. The biased reduced KL divergence estimator was utilized to evaluate sample performance in Paper C.

6.4 Nearest neighbour test for equal PDFs

All the methods described above try to estimate the distance between two high-dimensional PDFs. As an alternative, we will now briefly discuss a multivariate empirical test for equal PDFs, where the test statistic is based on nearest neighbour calculations. This discussion follows the theory outlined in [77].

Let us again consider the ensemble matrix U containing n_e samples from p, and the matrix V containing n_e samples from q. Now, for each element $\boldsymbol{u}_n$ and $\boldsymbol{v}_n$, one finds the r-nearest neighbours, $\zeta_r(\boldsymbol{u}_n)$ and $\zeta_r(\boldsymbol{v}_n)$. Based on these calculations, one can define the indicator functions

$$T_{u_n}(r) = \begin{cases} 1 & \text{if } \zeta_r(\boldsymbol{u}_n) \text{ is from } U, \\ 0 & \text{if } \zeta_r(\boldsymbol{u}_n) \text{ is from } V, \end{cases} \tag{6.14}$$

and $T_{v_n}(r)$, defined in similar manner. The 1-nearest neighbour statistics is then defined as

$$A_1 = \frac{1}{n_e} \sum_{j=1}^{n_e} T_{u_j}(1) + \frac{1}{n_e} \sum_{j=1}^{n_e} T_{v_j}(1). \tag{6.15}$$

With this method, the higher order statistics are based on the lower order. Thus, the 2-nearest neighbour statics is defined as

$$A_2 = \frac{1}{2n_e} \sum_{j=1}^{n_e} T_{u_j}(1) + T_{u_j}(2) + \frac{1}{2n_e} \sum_{j=1}^{n_e} T_{v_j}(1) + T_{v_j}(2), \tag{6.16}$$

and the r-nearest neighbour statics is

$$A_r = \frac{1}{rn_e} \sum_{j=1}^{n_e} \sum_{i=1}^{r} T_{u_j}(i) + \frac{1}{rn_e} \sum_{j=1}^{n_e} \sum_{i=1}^{r} T_{v_j}(i). \tag{6.17}$$

This test statistic can now be utilized in a test for equal PDFs. Under the hypothesis of equal PDFs, H_0, there are on average less nearest neighbours from the same sample than under hypothesis of unequal PDFs, H_1. Hence, the test is designed to reject H_0 for large values of A_r. A non-parametric bound on this statistic can then be estimated via an approximative permutation test, see, e.g. [20, 77]. The test of equal PDFs was utilized in Paper A.

6.5 Statistics in a Reproducing kernel Hilbert space

In the current section, we provide necessary theoretical foundations for the reproducing kernel Hilbert space (RKHS), introduce kernels associated with such methods, and consider several methods that compare statistical quantities in RKHS. We will keep the discussion brief and omit most theoretical results; for a more detailed introduction, see, e.g., [9, 85, 88].

6.5.1 Theory on RKHS

Let us consider a non-linear mapping, denoted the feature map,

$$\phi : \mathbb{R}^{n_m} \mapsto \mathbb{H}, \tag{6.18}$$

which maps samples from the parameter space, $\boldsymbol{m} \in \mathbb{R}^{n_m}$, into a n_h-dimensional feature space, $\phi(\boldsymbol{m}) \in \mathbb{H}$. The purpose of the mapping (6.18) is to enable calculations in the feature space that would have been difficult or impossible in the original space. Hence, we seek to convert features that are non-linear in the original space into linear features in the feature space. There are, however, some difficulties related to this approach. Firstly, to ensure that non-linear features are convert to linear features, the space $\mathbb{H}$ must be high-dimensional, or even infinite dimensional (this can be demonstrated by the mapping of monomials into a polynomial feature space [85]). Secondly, we cannot, in general, provide an explicit expression for the feature map ϕ.

Instead of an explicit evaluation in $\mathbb{H}$ via ϕ, we can use the inner product defined as

$$\langle \cdot, \cdot \rangle_{\mathbb{H}} : \mathbb{H} \times \mathbb{H} \mapsto \mathbb{R}, \tag{6.19}$$

as an indirect measure. The inner product induces a norm on $\mathbb{H}$ given as $\|\phi(\boldsymbol{m})\|_{\mathbb{H}} = \langle \phi(\boldsymbol{m}), \phi(\boldsymbol{m}) \rangle_{\mathbb{H}}$. Hence, the inner product also provides information regarding the length of an element in $\mathbb{H}$, and it can be used to measure the distance between two elements.

Unfortunately, we still need the feature map to calculate the inner product. To this end, we introduce the kernel function, $k : \mathbb{R}^{n_m} \times \mathbb{R}^{n_m} \mapsto \mathbb{R}$, such that

$$k(\boldsymbol{u}, \boldsymbol{v}) = \langle \phi(\boldsymbol{u}), \phi(\boldsymbol{v}) \rangle_{\mathbb{H}}, \tag{6.20}$$

where $\boldsymbol{u}, \boldsymbol{v} \in \mathbb{R}^{n_m}$. Assuming that the kernel is defined in a correct manner, it is possible to evaluate any inner product involving ϕ without explicit knowledge of ϕ. Algorithms defined in terms of inner products can now be expressed in terms of kernels, which greatly simplifies calculations in feature space. The substitution of inner products by kernels is typically referred to as the *kernel trick* [85].

We will now describe a space $\mathbb{H}$ where (6.20) is valid. Firstly, we require that k is a symmetric positive-definite function, and $\mathbb{R}^{n_m}$ a nonempty set. Moreover, the inner product in $\mathbb{H}$ must be defined such that the the following holds

$$\langle f, k(\boldsymbol{v}, \cdot) \rangle_{\mathbb{H}} = f(\boldsymbol{v}), \tag{6.21}$$

for all functions f in $\mathbb{H}$, in particular

$$\langle k(\boldsymbol{v}, \cdot), k(\boldsymbol{u}, \cdot) \rangle_{\mathbb{H}} = k(\boldsymbol{v}, \boldsymbol{u}). \tag{6.22}$$

This is known as the reproducing property of the kernel function k. Now, if we define the feature map as

$$\phi(\boldsymbol{u}) = k(\boldsymbol{u}, \cdot) \in \mathbb{H} \quad \forall u \in \mathbb{R}^{n_m}, \tag{6.23}$$

and insert in (6.22), we see that (6.20) holds. $\mathbb{H}$ is thus a Hilbert space of symmetric positive-definite functions with the reproducing property, denoted RKHS. This is given by the Moore-Aronszajn theorem; for more details and a rigorous proof see, e.g., [9].

Note that, every symmetric positive-definite function is a reproducing kernel. Thus, for every function k, there exists a unique corresponding RKHS, $\mathbb{H}$, for which k is a reproducing kernel. Given a symmetric positive-definite function k, there exists a function ϕ such that the evaluation of the kernel at points $\boldsymbol{u}$ and $\boldsymbol{v}$ is equivalent to taking the inner product between $\phi(\boldsymbol{u})$ and $\phi(\boldsymbol{v})$ in some Hilbert space.

By defining the kernel as a symmetric positive-definite function it is possible to perform computations in RKHS via the kernel trick. However, there are still a vast number of kernels to choose from, and there is generally no restrictions on which kernels to use for a given application. Since the kernel will implicitly define the RKHS and the mapping ϕ, it is important to choose the kernel wisely. However, for many applications the kernel must be chosen based on trial-and-error. A widely used kernel function is the radial-basis-function kernel

$$k(\boldsymbol{u},\boldsymbol{v}) = \exp\left(-\frac{1}{2a^2}\|\boldsymbol{u}-\boldsymbol{v}\|^2\right). \tag{6.24}$$

6.5.2 Maximum mean discrepancy in RKHS

The maximum mean discrepancy (MMD) in RKHS was introduced in [40] as a non-parametric test of whether two set of samples are drawn from the same PDF or not. The test is based on mapping the samples using smooth functions from a function space $\mathbb{F}$. The functions should return different values if the samples are drawn from different PDFs. The difference between the samples is then gauged by calculating the difference between the mean function values on the two samples. When this value is large, it is likely that the samples are drawn from different PDFs.

The MMD is defined by the space of smooth functions $\mathbb{F}$ utilized in the test, and this choice will affect the quality of the test. In [40], it was shown that an optimal choice of function space was the unit ball in a RKHS, with associated kernel $k(\cdot,\cdot)$. With this choice, the MMD value was shown to be zero if and only if the two PDFs were identical. Consider two samples $U = (\boldsymbol{u}_1,\ldots,\boldsymbol{u}_{n_u})$ and $V = (\boldsymbol{v}_1,\ldots,\boldsymbol{v}_{n_v})$ drawn from the PDFs p and q, respectively, the MMD test statistic, utilizing the unit ball in RKHS as function class $\mathbb{F}$, is given as

$$I^2_{mmd} = \mathbb{E}\left[k(\boldsymbol{u},\boldsymbol{u}')\right] - \mathbb{E}\left[k(\boldsymbol{u},\boldsymbol{v})\right] + \mathbb{E}\left[k(\boldsymbol{v},\boldsymbol{v}')\right], \tag{6.25}$$

where the expectation is taken over both arguments in the kernel, k. The unbiased empirical estimate of the MMD is given as [39, 40]

$$\begin{aligned} I^2_{mmd} =& \frac{1}{n_u(n_u-1)}\sum_{j=1}^{n_u}\sum_{i\neq j}^{n_u} k\left(\boldsymbol{u}_j,\boldsymbol{u}_i\right) + \frac{1}{n_v(n_v-1)}\sum_{j=1}^{n_v}\sum_{i\neq j}^{n_v} k\left(\boldsymbol{v}_j,\boldsymbol{v}_i\right) \\ & \frac{1}{n_u n_v}\sum_{j=1}^{n_u}\sum_{i=1}^{n_v} k\left(\boldsymbol{u}_j,\boldsymbol{v}_i\right). \end{aligned} \tag{6.26}$$

If the same number of samples have been drawn from the different PDFs, i.e., n_u=n_v, the empirical, and unbiased estimate can be given as

$$I^2_{mmd} = \frac{1}{n_u(n_u-1)}\sum_{j\neq i}^{n_u} h\left(\boldsymbol{z}_j,\boldsymbol{z}_i\right), \tag{6.27}$$

where $h\left(\boldsymbol{z}_j,\boldsymbol{z}_i\right) = k\left(\boldsymbol{u}_j,\boldsymbol{u}_i\right) + k\left(\boldsymbol{v}_j,\boldsymbol{v}_i\right) - k\left(\boldsymbol{u}_j,\boldsymbol{v}_i\right) - k\left(\boldsymbol{u}_i,\boldsymbol{v}_j\right)$.

As mentioned, the MMD was designed as a test of similarity between PDFs. The test statistic can therefore be utilized to differentiate between the null hypothesis, H_0, that the samples are drawn from the same PDF and the alternative hypothesis, H_1, that the samples are drawn from two different PDFs. Similar to other statistical hypothesis tests, given some upper limit α on the probability of a Type I error, one needs to calculate a limit value for the test where H_0 is rejected for MMD values higher than the limit.

This limit value for the test statistic under H_0 can be approximated in several ways. By calculating the asymptotic behaviour of I^2_{mmd} under both hypothesis, it was showed that this limit can be found by approximating the $(1-\alpha)$ quantiles of the I^2_{mmd} under the H_0 hypothesis [40]. Alternatively, based on the original samples the limit can be found using bootstrap or by fitting Pearson curves to the first moments. For more details regarding the asymptotic behaviour of I^2_{mmd} and the different approximation methods for the limit value we refer to [40].

The approximate methods, such as the EnKF, will only sample exactly in the Gauss-linear case when $n_e \to \infty$. Hence, if one seeks to compare samples from the approximate methods to exact samples for cases where these aforementioned assumptions are not met, the two samples will never be from the same PDF. The MMD can still be utilized as a measure of the distance between the PDFs, but it is not necessary to calculate the bound on the H_0 hypothesis. The MMD was used in this manner, with the radial basis function kernel (6.24), in Paper C, D and E.

6.5.3 Statistical distance measures in RKHS

For two high-dimensional PDFs p and q, one cannot, due to the high-dimensional integral, evaluate the stochastic distance measures discussed in Section 6.1. Moreover, if we only have samples from these PDFs, calculating the distance measures are even more involved, since it involves two approximations. Firstly, the density must be approximated via some estimation procedure. Secondly, the integral must be approximated via some numerical method. If, however, the PDFs p and q are Gaussian, the calculation of the distance measures are simplified significantly. This simplification arises from the fact that for Gaussian PDFs there exist closed-form expressions for the stochastic distances. By transforming the samples into a RKHS, where they are Gaussian, [108] derived closed-form expressions for a wide range of stochastic measures, including the two defined in Section 6.1. Following [108], we now discuss how an empirical estimate of the KL divergence can be formulated in RKHS.

For the special case where $p{=}N\left(\boldsymbol{\mu}_u, Q_u\right)$ and $q{=}N\left(\boldsymbol{\mu}_v, Q_v\right)$, the KL divergence is given in closed form as

$$I_{KL}\left(p||q\right) = \frac{1}{2}\left(\boldsymbol{\mu}_u - \boldsymbol{\mu}_v\right)^T {Q_v}^{-1}\left(\boldsymbol{\mu}_u - \boldsymbol{\mu}_v\right) + \frac{1}{2}\log\frac{|Q_v|}{|Q_u|} + \frac{1}{2}\,\mathrm{tr}\left(Q_u Q_v^{-1} - I\right), \quad (6.28)$$

where $|\cdot|$ denotes the matrix determinant. If samples from p and q were available, one could easily calculate an empirical estimate, $\widetilde{I}_{KL}$, of (6.28) via the standard MC estimates of mean and covariance. In the following, we investigate a similar approach. Here, $\widetilde{I}_{KL}$ is estimated in the RKHS utilizing samples from two general PDFs.

Let us assume that we have available $U = (\boldsymbol{u}_1, \ldots, \boldsymbol{u}_{n_u})$ and $V = (\boldsymbol{v}_1, \ldots, \boldsymbol{v}_{n_v})$, which are not samples from Gaussian PDFs. By applying the feature map to every sample we can represent the two samples in RKHS as

$$B_u = (\phi(\boldsymbol{u}_1), \ldots, \phi(\boldsymbol{u})), \qquad B_v = (\phi(\boldsymbol{v}_1), \ldots, \phi(\boldsymbol{v})), \tag{6.29}$$

where the samples are Gaussian by construction. The KL divergence in the RKHS can then be estimated by

$$\begin{aligned} \widetilde{I}_{KL}^{RKHS}(p||q) =& \frac{1}{2}\left(\overline{\phi(\boldsymbol{u})} - \overline{\phi(\boldsymbol{v})}\right)^T Q_{\phi(v)}^{-1}\left(\overline{\phi(\boldsymbol{u})} - \overline{\phi(\boldsymbol{v})}\right) + \frac{1}{2}\log\frac{|C_{\phi(v)}|}{|C_{\phi(u)}|} \\ &+ \frac{1}{2}\operatorname{tr}\left(C_{\phi(u)}C_{\phi(v)}^{-1} - I\right). \end{aligned} \tag{6.30}$$

Where the calculation of the empirical mean and the empirical covariance is formulated such that we never need to evaluate ϕ. Hence, it incorporates the kernel trick. For more details regarding this calculation we refer to [108]. This measure was utilized in Paper C.

6.6 Alternative methods for evaluating sampling performance

In the previous sections, one sought to estimate the distance between the full densities p and q based on samples from these PDFs. This was either performed by a standard kernel estimator method or by transforming the samples into a RKHS. These methods were non-parametric, that is, no assumptions were made regarding the PDFs p and q. Since we generally do not know the form of the posterior PDF, these methods are preferable. However, the methods are often associated with a high computational cost, and, for this reason, methods that do not estimate the full PDF may be more suitable.

For some cases, the densities p and q resemble some parametric PDF. This might be the case for a Bayesian problem if the prior model is Gaussian and the forward model is almost linear. For such cases, it is reasonable to assume that the posterior PDF is approximately Gaussian. Hence, the distance in mean and variance might be sufficient to gauge the distance between p and q. In [52], empirical estimates, calculated from samples $\boldsymbol{u}$ from p and $\boldsymbol{v}$ from q, of the relative distance in the mean with respect to the prior mean, and the relative distance in the variance were utilized to estimate the distance between p and q. These measures were defined as

$$\widetilde{I}_{\mu}(p,q) = \frac{\left\|\left(\overline{\boldsymbol{v}} - \boldsymbol{\mu}_{prior}\right) - \left(\overline{\boldsymbol{u}} - \boldsymbol{\mu}_{prior}\right)\right\|}{\left\|\overline{\boldsymbol{u}} - \boldsymbol{\mu}_{prior}\right\|}, \tag{6.31}$$

and

$$\widetilde{I}_{\text{var}}(p,q) = \frac{\|\widetilde{\text{var}}_v - \widetilde{\text{var}}_u\|}{\|\widetilde{\text{var}}_u\|}, \tag{6.32}$$

using the Euclidean norm. These measures were utilized to evaluate sampling performance in Paper C, D, and E.

As an alternative to the previous methods, which rely on the comparison of p and q, we now consider a method that only rely on the parametric form of the posterior PDF, p.

For a linear forward model, it can be shown that $2J(\boldsymbol{m}_{MAP})$ has a χ^2 distribution with n_D degrees of freedom, where J is defined in (3.13), and $\boldsymbol{m}_{MAP}$ is defined in (3.16), see, e.g., [96]. By the properties of the χ^2 distribution, $2J(\boldsymbol{m}_{MAP})$ has mean equal to n_D and variance equal to $2n_D$.

Now, the quality of approximate samples $\boldsymbol{v}$ can be gauged by comparing the sample approximation of J to the parametric value. If the samples are close to the parametric values, they are assumed to be close to the exact MAP solution. The test is performed by calculating the objective function for all approximate samples $2J(\boldsymbol{v})$. These values should be close to n_D, and typically not more than five standard deviations away from the mean, i.e.,

$$n_D - 5\sqrt{2n_D} \leq 2J(\boldsymbol{v}) \leq n_D + 5\sqrt{2n_D}. \tag{6.33}$$

This test, which only assess the approximate samples, is fundamentally different from the previous tests. Moreover, for problems with a non-linear forward model, the assumptions of this test do not hold. Despite this problem, one can utilize this measure to approximately evaluate sampling performance for cases with non-linear forward models [25], and the measure can also be utilized for convergence control when sampling the posterior via the RML method [73]. In addition, since the measure only relies on the parametric values of p, this method only require samples from q. Hence, this test is significantly less expensive that the other tests discussed in this chapter.

Chapter 7

Calculating model non-linearity

In Chapter 2, the Bayesian formulation of the inverse problem was discussed. For Gauss-linear problems the posterior PDF (the solution to the inverse problem) is Gaussian and given, in closed form, by the KF equations. However, for non-linear problems, even though the prior PDF is Gaussian, the posterior PDF is non-Gaussian and, generally, analytically intractable. Hence, we can only obtain information regarding the solution by sampling from the posterior PDF, utilizing the methods discussed in Chapter 4.

Clearly, solving an inverse problem that has a non-linear forward model is considerably more demanding than solving an inverse problem where the forward model is linear. Unfortunately, the sampling methods discussed in Chapter 4 is computationally expensive, and, for most problems, we must rely on ensemble-based methods, discussed in Chapter 5. However, these methods can only be shown to sample exactly in the limit $n_e \to \infty$, for problems with a linear forward model. Thus, for non-linear problems the ensemble-based methods will only provide approximations.

It is, however, unreasonable to only distinguish between problems based on whether the forward model is linear or non-linear. A more reasonable approach would be to consider a sliding transition from a linear forward model to a strongly non-linear forward model. Utilizing the ensemble-based methods, it is reasonable to assume that problems with weakly non-linear forward models have a lower approximation error compared to problems with strongly non-linear forward models.

For simple cases, the degree of non-linearity can be determined by inspecting the forward model, but for most cases the forward model represent a complex relationship between a high-dimensional parameters space and the data space. For such cases, one cannot determine the degree of non-linearity by inspecting the forward model. In this chapter, we introduce two measures for evaluating the forward model non-linearity: the relative curvature measure of non-linearity [6], and a stochastic measure introduced in [61].

7.1 Relative curvature measure of non-linearity

In the following section, we discuss a measure of non-linearity arising from the theory of non-linear regression. This measure, denoted the relative curvature, was introduced by [6] as an extension of the measure introduced in [7]. Our discussion of the relative

curvature measure of non-linearity will follow [87]. Consider data on the form

$$\boldsymbol{d} = \boldsymbol{\omega} + \boldsymbol{\xi}, \tag{7.1}$$

where $\boldsymbol{\omega} \in \Omega$ is a subset of the data space $\mathbb{R}^{n_d}$, and $\boldsymbol{\xi} \sim N(\mathbf{0}, Q_d)$. Typically, the data are given by (3.2), such that Ω can be described in terms of a n_m-dimensional parameter $\boldsymbol{m}$ and a forward model $G(\boldsymbol{m})$. This is written as

$$\Omega = \{\boldsymbol{\omega} : \boldsymbol{\omega} = G(\boldsymbol{m}), \boldsymbol{m} \in \mathbb{R}^{n_m}\}, \tag{7.2}$$

and, for this formulation, Ω defines a n_m-dimensional surface in the $\mathbb{R}^{n_d}$-dimensional data space. Since $\boldsymbol{\omega} \in \Omega$ will satisfy $\boldsymbol{\omega} = G(\boldsymbol{m})$ for some $\boldsymbol{m}$, the surface is known as the *solution locus* [7]. Alternatively, the surface is known as the *expectation surface* [87], since the surface contains all possible values of $\mathbb{E}[\boldsymbol{d}]$. (Note that the surface Ω is not uniquely defined by the parametrization and forward model)

To formally define the curvature measure one must consider a local approximation to $\boldsymbol{\omega}$. Assuming that $\boldsymbol{\delta}_m = \boldsymbol{m} - \boldsymbol{m}'$ is small, the quadratic Taylor approximation is

$$\boldsymbol{\omega} - \boldsymbol{\omega}' \approx \mathcal{G}\boldsymbol{\delta}_m + \frac{1}{2}\boldsymbol{\delta}_m^T \underline{H} \boldsymbol{\delta}_m, \tag{7.3}$$

where one element of the $n_m \times n_m$ matrix $\mathcal{G}$ is

$$\mathcal{G}_{j,i} = \frac{\partial G(\boldsymbol{m})_j}{\partial m_i}|_{m'}, \tag{7.4}$$

and one "face" of the $n_D \times n_m \times n_m$ tensor $\underline{H}$ is

$$\underline{H}_{\cdot,j,i} = \frac{\partial^2 G(\boldsymbol{m})}{\partial m_j \partial m_i}|_{m'}. \tag{7.5}$$

In the above, $|_{m'}$ denotes that the expressions are evaluated in $\boldsymbol{m}'$.

A linear approximation to $\boldsymbol{\omega}$ is obtained by ignoring the quadratic term in (7.3)

$$\boldsymbol{\omega} - \boldsymbol{\omega}' \approx \mathcal{G}\boldsymbol{\delta}_m. \tag{7.6}$$

This will approximate the expectation surface in the neighbourhood of $\boldsymbol{m}'$ by a tangent plane at $\boldsymbol{m}'$, and it is clear that the validity of this approximation depends on the magnitude of the quadratic term $\frac{1}{2}\boldsymbol{\delta}_m^T \underline{H} \boldsymbol{\delta}_m$ relative to the linear term $\mathcal{G}\boldsymbol{\delta}_m$. There are two aspects to curvature for non-linear models. The first is related to the bending of the expectation surface (intrinsic effects), and the second is related to the parametrization (parameter effects). When comparing the linear term and the quadratic term, these two aspects are considered by splitting $\frac{1}{2}\boldsymbol{\delta}_m^T \underline{H} \boldsymbol{\delta}_m$ into the projection onto the tangent plane (denoted with a superscripted Tan) and normal to the tangent plane (denoted with a superscripted Nor), i.e.

$$\underline{H} = \underline{H}^{\text{Tan}} + \underline{H}^{\text{Nor}}, \tag{7.7}$$

where the decomposition is obtained via the projection matrix $P|_{m'} = \mathcal{G}\left(\mathcal{G}^T\mathcal{G}\right)\mathcal{G}^T|_{m'}$, see, e.g., [87]. The degree of curvature in direction of $\boldsymbol{\delta}_m$ with respect to parameter effects and intrinsic effects where given in [6] as

$$\Theta^{\text{Par}}_{\delta_m} = \frac{\left\|\boldsymbol{\delta}_m^T \underline{H}^{\text{Tan}} \boldsymbol{\delta}_m\right\|}{\|\mathcal{G}\boldsymbol{\delta}_m\|^2}, \quad \Theta^{\text{Int}}_{\delta_m} = \frac{\left\|\boldsymbol{\delta}_m^T \underline{H}^{\text{Nor}} \boldsymbol{\delta}_m\right\|}{\|\mathcal{G}\boldsymbol{\delta}_m\|^2}. \tag{7.8}$$

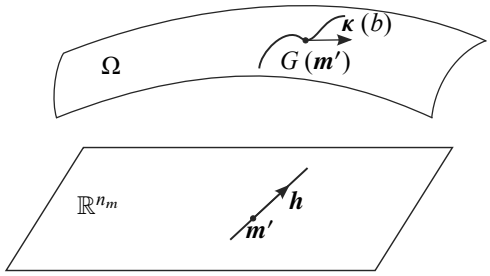

Figure 7.1: Parametric curve on solution locus

The relative measure of non-linearity can also be derived by a geometric argument, which justifies that the measures are curvatures [87]. This argument considers the parametrized curve, $\boldsymbol{\kappa}(b)$, on the expectation surface Ω

$$\boldsymbol{\kappa}(b) = G(\boldsymbol{m}(b)) = G(\boldsymbol{m}' + b\boldsymbol{h}), \tag{7.9}$$

where $\boldsymbol{m}'$ is a point, $\boldsymbol{h}$ is an arbitrary vector, and b is a real number. If G is a linear function, $\boldsymbol{\kappa}(b)$ is a straight line on the expectation surface. However, if G is a non-linear function, the curve $\boldsymbol{\kappa}(b)$ will not be a straight line, as illustrated in Figure 7.1. The tangent and acceleration at $\boldsymbol{m}'$ in direction of $\boldsymbol{h}$ are now given as $\mathcal{J}\boldsymbol{h}$ and $\boldsymbol{h}^T\underline{H}\boldsymbol{h}$. Decomposing the acceleration into its tangential and normal components provides the parameter and intrinsic curvature in direction of $\boldsymbol{h}$

$$\Theta_{\boldsymbol{h}}^{\text{Par}} = \frac{\left\|\boldsymbol{h}^T\underline{H}^{\text{Tan}}\boldsymbol{h}\right\|}{\|\mathcal{J}\boldsymbol{h}\|^2}, \qquad \Theta_{\boldsymbol{h}}^{\text{Int}} = \frac{\left\|\boldsymbol{h}^T\underline{H}^{\text{Nor}}\boldsymbol{h}\right\|}{\|\mathcal{J}\boldsymbol{h}\|^2}. \tag{7.10}$$

Finally, the measure of non-linearity introduced by [6] is obtained by maximising the scale-free curvature measures, $\Theta_{\boldsymbol{h}}^{\text{Par}}\rho$ and $\Theta_{\boldsymbol{h}}^{\text{Int}}\rho$, with respect to $\boldsymbol{h}$

$$\gamma_{\boldsymbol{h}}^{\text{Par}} = \max_{\boldsymbol{h}} \Theta_{\boldsymbol{h}}^{\text{Par}}\rho, \quad \gamma_{\boldsymbol{h}}^{\text{Int}} = \max_{\boldsymbol{h}} \Theta_{\boldsymbol{h}}^{\text{Int}}\rho. \tag{7.11}$$

Here the scale factor ρ is defined as $\rho = \sigma_d\sqrt{n_m}$, where σ_d is the data standard deviation.

The intrinsic non-linearity, $\gamma_{\delta_m}^{\text{Int}}$, provides a measure for how well a tangent plane can, locally, approximate Ω. It can be shown that this value is independent of the parametrization [87]. The parameter effect non-linearity, $\gamma_{\delta_m}^{\text{Par}}$, measure whether straight parallel equispaced lines in the parameter space map into straight parallel equispaced lines in the expectation surface. This non-linearity depends on the choice of parametrization, and significant reduction of non-linearity can be achieved by re-parametrizing the problem [6, 87].

The relative curvature measure of non-linearity has been utilized by several authors for complex systems [16, 41, 42, 43, 51, 64, 95], but there are some drawbacks to the method. Firstly, the method requires the evaluation of both the first-order and the second-order derivatives in parameter space, which are infeasible for many high-dimensional systems. Secondly, since the method arises from the study of non-linear

regression, it is designed for overdetermined problems, i.e., problems where $n_D > n_m$. It is, however, not clear how one should extend this analysis for underdetermined problems, i.e., problems where $n_m > n_D$.

7.2 Non-linearity measure for stochastic systems

A measure of non-linearity, defined for stochastic systems, was recently introduced in [61]. Contrary to the relative curvature measure discussed in the previous section, this measure assumes that all quantities are random. Hence, for this problem, it makes sense to consider whether the parameter vector, $\boldsymbol{m}$, is likely to be in a region where the non-linearity in the forward-model is high, and the measure of non-linearity is designed to mirror this.

In [61], the non-linearity in the forward model and the observation operator were assessed simultaneously by considering the vector $\boldsymbol{y}$ defined in (5.8). Note that the non-linearity in the forward-model with respect to the parameters can be assessed by substituting $\boldsymbol{y}$ with $\boldsymbol{m}$.

In similar manner as the measure discussed in the previous section, the non-linearity measure for stochastic systems attempts to quantify the deviation of the non-linear function, G, from its best linear approximation. However, the deviation from linearity is now defined in a different manner. Let $\mathbb{F}$ denote the function space containing all functions with a fixed dimension equal to G. $\mathbb{F}$ can be partitioned into two subspaces: $\mathbb{L}$ containing all linear functions, and $\mathbb{G}$ containing all non-linear functions. Clearly, the non-linear function G is contained in $\mathbb{G}$ and the measure of non-linearity is defined as the greatest lower-bound of the distance from G to all function L in $\mathbb{L}$.

The distance, $\Psi(G, G')$, between two function in $\mathbb{F}$ will be defined as the square root of the mean-square error, and the measure of non-linearity can, formally, be defined as

$$I_G = \inf_{L \in \mathbb{L}} \Psi(L, G) = \inf_{L \in \mathbb{L}} \left(\mathbb{E}\left[\| L(\boldsymbol{y}) - G(\boldsymbol{y}) \|^2 \right] \right)^{1/2}, \tag{7.12}$$

where the expectation is with regards to the random variable $\boldsymbol{y}$, and the norm is the Euclidean norm. It is possible to utilize I_G directly as a measure of non-linearity. However, [61] proposed the following normalized version

$$\gamma_G = \frac{I_G}{\sqrt{\text{tr}\left(Q_g\right)}}, \tag{7.13}$$

where Q_g is the covariance matrix of $G(\boldsymbol{y})$. The following description, regarding the values of γ_G, was provided by [61]: if $\gamma_G = 0$ the function G is linear almost everywhere, while if $\gamma_G = 1$ the function G contains roughly no linear components.

Note that any function in $\mathbb{L}$ is on the form $L(\boldsymbol{y}) = A\boldsymbol{y} + \boldsymbol{b}$, and linear model solving (7.12), denoted $\widehat{L}$, can be derived from the first-order necessary conditions [67]

$$\frac{\partial \Psi(L, G)}{\partial \boldsymbol{b}} = 2\mathbb{E}\left[A\boldsymbol{y} + \boldsymbol{b} - G(\boldsymbol{y}) \right] = \boldsymbol{0}, \tag{7.14}$$

$$\frac{\partial \Psi(L, G)}{\partial A} = 2\mathbb{E}\left[\left(A\boldsymbol{y} + \boldsymbol{b} - G(\boldsymbol{y}) \right) \boldsymbol{y}^T \right] = \boldsymbol{0}. \tag{7.15}$$

The two equations have solutions $\widehat{A} = Q_{gy}^{-1}$, and $\widehat{\boldsymbol{b}} = \boldsymbol{\mu}_g - \widehat{A}\boldsymbol{\mu}_y$, where Q_{gy} is the cross-covariance between G and $\boldsymbol{y}$. Hence, the model solving (7.12) is

$$\widehat{L} = \boldsymbol{\mu}_g + Q_{gy}Q_y^{-1}\left(\boldsymbol{y} - \boldsymbol{\mu}_y\right). \tag{7.16}$$

Inserting $\widehat{L}$ into (7.12) gives the following expression for the measure of non-linearity

$$\begin{aligned} I_G &= \left(\mathbb{E}\left[\left(\widehat{L} - G\left(\boldsymbol{y}\right)\right)^T\left(\widehat{L} - G\left(\boldsymbol{y}\right)\right)\right]\right)^{1/2}, \\ &= \left(\text{tr}\left\{\mathbb{E}\left[\left(\widehat{L} - G\left(\boldsymbol{y}\right)\right)\left(\widehat{L} - G\left(\boldsymbol{y}\right)\right)^T\right]\right\}\right)^{1/2}, \\ &= \left(\text{tr}\left\{Q_g - Q_{gy}Q_y^{-1}Q_{gy}^T\right\}\right)^{1/2}, \end{aligned} \tag{7.17}$$

and the normalized measure of non-linearity is

$$\gamma_G = \sqrt{1 - \frac{\text{tr}\left\{Q_{gy}Q_y^{-1}Q_{gy}^T\right\}}{\text{tr}\left\{Q_g\right\}}}. \tag{7.18}$$

The measure has range $[0,1]$ since $\text{tr}\left\{Q_g\right\} \geq \text{tr}\left\{Q_{gy}Q_y^{-1}Q_{gy}^T\right\} \geq 0$ for all choices of G and $\boldsymbol{y}$.

The non-linearity measure for stochastic systems does not require any high-order derivatives in parameter space, and it is therefore suited for large-scale problems. Clearly, the computationally demanding part of this non-linearity measure is the calculation of the covariance matrices, and, for most realistic problems, the covariance matrices cannot be calculated analytically. For such problems, it is possible to use empirical estimates of the covariance matrices.

The non-linearity measure for stochastic systems is highly suited for the ensemble-based methods introduced in chapter 5, since these methods approximate the covariance matrices in the forecast step. However, similar to the ensemble-based methods, both the covariance approximation and the measure of non-linearity depend on the number of ensemble members. A higher number of ensemble members provide a better estimate of the non-linearity measure.

When the empirical covariance matrix is used in the non-linearity measure, there is a requirement on the number of ensemble members. Let us consider the numerator in the second term under the square root in (7.18), and insert the expression for the empirical covariance matrices

$$\text{tr}\left\{C_{gy}C_y^{-1}C_{gy}^T\right\} = \frac{1}{n_e - 1}\,\text{tr}\left\{\Delta G \Delta Y^T\left(\Delta Y^T\right)^{-1}\Delta Y^{-1}\Delta Y \Delta G^T\right\}. \tag{7.19}$$

Recall that ΔY is, generally, not square and, for this reason, we need to utilize the pseudo-inverse, $\Delta Y^{\dagger}$. To define the pseudo-inverse, we start by writing ΔY in terms of the truncated singular value decomposition (SVD) expansion (see, e.g., [37])

$$\Delta Y = U_p S_p V_p^T. \tag{7.20}$$

Here $p \leq \min\left(n_y, n_e\right)$ is the number of positive singular values of ΔY, the diagonal matrix $S_p \in \mathbb{R}^{p\times p}$ holds the positive singular values, while the columns of $U_p \in \mathbb{R}^{n_y \times p}$

and $V_p \in \mathbb{R}^{n_e \times p}$ contain the left- and right-singular vectors, respectively. The left- and right-singular vectors are orthogonal and normalized

$$U_p^T U_p = I_p, \quad V_p^T V_p = I_p, \tag{7.21}$$

where $I_p \in \mathbb{R}^{p \times p}$ is the identity matrix, while, generally,

$$U_p U_p^T \neq I_p, \quad V_p V_p^T \neq I_p. \tag{7.22}$$

If p=n_y, the first of the inequalities in (7.22) becomes an equality. Likewise, if $p = n_e$, the second inequality in (7.22) becomes an equality. Utilizing the SVD, the pseudo-inverse is given as

$$\Delta Y^\dagger = V_p S_p^{-1} U_p^T. \tag{7.23}$$

Inserting $\Delta Y^\dagger$, and expanding all the ΔY terms in (7.19) gives

$$\text{tr}\left\{C_{gy} C_y^{-1} C_{gy}^T\right\} = \frac{1}{n_e - 1} \text{tr}\left\{\Delta G V_p S_p U_p^T U_p S_p^{-1} V_p^T V_p S_p^{-1} U_p^T U_p S_p V_p^T \Delta G^T\right\} \tag{7.24}$$

$$= \frac{1}{n_e - 1} \text{tr}\left\{\Delta G V_p V_p^T \Delta G^T\right\}. \tag{7.25}$$

Hence, for cases where the second inequality of (7.22) turns to an equality, the non-linearity measure is useless since $\text{tr}\left\{C_{gy} C_y^{-1} C_{gy}^T\right\} = \text{tr}\left\{C_g\right\}$ and $\gamma_G = 0$ for all G. Now, since ΔY is an ensemble perturbation matrix, its columns sum to zero, and ΔY has at most $p = \min\left(n_e - 1, n_y\right)$ positive singular values [62]. Hence, at the outset $V_p V_p^T \neq I_p$. Unfortunately, for cases where $n_e \leq n_y + 1$, it is possible to show that $\Delta G \Delta G^T = \Delta G V_p V_p^T \Delta G^T$ (see Appendix A in Paper B). For this reason, the measure of non-linearity utilizing the empirical covariance matrices requires that $n_e > n_y + 1$.

The non-linearity measure for stochastic systems, utilizing the empirical covariances, was applied in Paper C, D, and E.

Chapter 8

Two-phase flow in porous media

The investigation conducted in this thesis focuses on problems that have a non-chaotic forward-model that depends, non-linearly, on a high-dimensional parameter vector. One such type of problems, where the ensemble-based methods have been extensively applied, is multiphase flow in porous media [1, 70]. In the following chapter, we introduce the mathematical equations describing two-phase flow in a porous media; we discuss how these equations can be solved via numerical models; and we discuss how observations of flow in the wells can be predicted by the numerical models.

8.1 Mathematical model

Mathematical models describing the fluid flow in a porous media are based on the conservation of mass, momentum and energy. In this section, we briefly introduce the mathematical equations governing the simultaneous flow of two immiscible fluid phases in an incompressible porous media. There exists a wide range of literature on this topic, and for more details we refer the reader to, e.g., [5, 15, 74].

Assuming that both phases are present in the reservoir, one phase will wet the porous medium more than the other. This phase is denoted the wetting phase and is indicated by a subscript w. The other phase is denoted the non-wetting phase and is indicated by a subscript nw. In a typical North-sea reservoir the wetting phase is water and the non-wetting phase is oil.

Let us assume that the mass of each fluid phase is conserved. This is expressed in differential form as

$$\phi \frac{\partial \rho_\alpha S_\alpha}{\partial t} = -\nabla \cdot (\rho_\alpha \boldsymbol{u}_\alpha) + q_\alpha, \quad \alpha = \text{w, nw}, \tag{8.1}$$

where the saturation of each phase is denoted S_α, the density of each phase is denoted ρ_α, the Darcy velocity of each phase is denoted $\boldsymbol{u}_\alpha$, the source/sink terms for each phase is denoted q_α, and the porosity of the porous media is denoted as ϕ. Darcy's law, which is valid for single phase flow, can be extended directly to two-phase flow

$$\boldsymbol{u}_\alpha = -\frac{1}{\mu_\alpha} \boldsymbol{k}_\alpha \left(\nabla p_\alpha - \rho_\alpha \vartheta \nabla z\right), \quad \alpha = \text{w, nw}, \tag{8.2}$$

where $\boldsymbol{k}_\alpha$, p_α, and μ_α are the effective permeability, pressure, and viscosity for phase α; ϑ denotes the magnitude of gravitational acceleration; and z denotes the vertical

coordinate. Due to the simultaneous presences of two phases, the effective permeability of either phase is lower than the absolute permeability, $\boldsymbol{k}$. The effective permeability is, therefore, represented via the relative permeability, $k_{r\alpha}$,

$$\boldsymbol{k}_\alpha = k_{r\alpha}\boldsymbol{k}, \quad \alpha = \text{w, nw}. \tag{8.3}$$

Moreover, we assume that the two fluids jointly fill the void within the porous media, hence,

$$S_w + S_{nw} = 1. \tag{8.4}$$

Also, due to forces working on the interface between the two phases, the pressure in the wetting fluid is less than the pressure in the non-wetting fluid. This pressure difference is given by the capillary pressure, assumed to be a function of the saturation,

$$p_c\left(S_w\right) = p_{nw} - p_w. \tag{8.5}$$

Finally, we define the constitutive relationships for the parameters

$$k_{r\alpha} = k_{r\alpha}\left(S_w\right), \tag{8.6}$$
$$\rho_\alpha = \rho_\alpha\left(p_w\right), \tag{8.7}$$
$$\mu_\alpha = \mu_\alpha\left(p_w\right), \tag{8.8}$$

and note that the number of sources and sinks are finite. Hence, by inserting (8.2) into (8.1) and utilizing (8.4)–(8.8), we obtain a complete set of equations. This can be solved for two of the four main unknowns: p_α and S_α for $\alpha = \text{w, nw}$.

It is possible to formulate the fluid equations in several forms. The choice of formulation depends on the main variables, solution procedure, and the amount of coupling between the variables. However, provided suitable boundary and initial conditions, the equations can only be solved analytically if additional assumptions are made. For all other cases, the solution must be found by numerical techniques.

8.2 Numerical model

The models for fluid flow in a porous media consist of a large coupled system of non-linear, time-dependent partial differential equations. Designing a suitable numerical scheme for such problems is not trivial. The equations must be discretized in both time and space, and problems, such as coupling between the equations, must be handled by the numerical method. In this section, we briefly discuss some issues regarding the numerical solution strategies; for further details, see, e.g., [2, 5, 15].

The temporal discretization in the numerical model can be designed to evaluate the different terms either implicitly or explicitly. Commercial simulators generally prefer full implicit strategies due to their robustness [2]. The non-linear equations are typically solved utilizing iterative methods, such as the Newton-Raphson scheme. These methods typically converges after a few iterations. However, for each iteration a large linear system of equations needs to be solved. Hence, solving the flow equations requires the solution of many linear systems, and can therefore be computationally expensive. For realistic reservoir cases, as much as 80-90% of the computational time can be spent solving linear systems [15]. A good linear solver is therefore crucial for an efficient

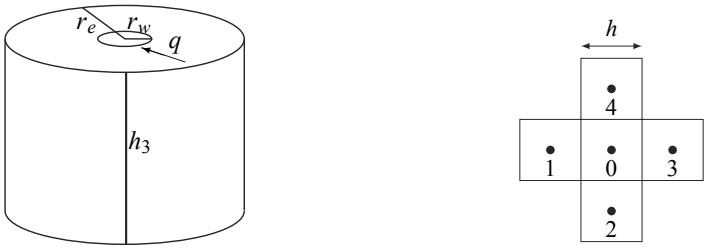

(a) (b)

Figure 8.1: Flow models near the well. (a): radial flow in analytical model. (b): five-point stencil for numerical approximation.

numerical method, and methods utilized for realistic reservoir models favours iterative Krylov subspace methods [84] like, e.g., the conjugate gradient method [49].

A less time consuming method is to decouple the equations and solve them sequentially. In this approach, the equation for the pressure and saturation are solved separately, where one can utilize different methods for the different equations. One example of such a method is IMPES (implicit pressure, explicit saturation). For these methods smaller time-steps are often required to meet the time-step restrictions associated with the explicit solution method [59]. Moreover, a few extra iterations might be needed to remove the error caused by decoupling the equations. Hence, even though each time-step is in general much faster to solve, the time-step restrictions can remove the efficiency of the IMPES method.

8.3 Well model

In the flow equations, the source and sink terms are included as q_α for $\alpha = \mathrm{w}, \mathrm{nw}$. These terms represent the transfer of mass for all fluids entering or exiting the reservoir, and they need to be included in the numerical model. Any well model must describe the flow into the wellbore accurately, and the well equations must allow the computation of bottom hole pressure (BHP) when the production or injection rate is given, and the fluid rate when the BHP is known. The main difficulty when modelling wells is the difference in scale between the large grid block and the small region surrounding the well where there are large pressure gradients.

We will now illustrate how wells can be modelled in the computational grid. This derivation is one of the approaches given in [75], and the approach is based on combining the numerical and the analytical solution of the well flow. We start by deriving an analytical model that approximate the fluid flow near the well. Here, we assume single phase, incompressible, steady-state, horizontal flow, within a homogeneous and isotropic reservoir where the fluid viscosity and density are constant. Moreover, we assume that the flow is radial in a small neighbourhood around the well (see Figure 8.1a). With these assumptions, the conservation equation is

$$\nabla \cdot (\rho \boldsymbol{u}) = q\delta(x), \tag{8.9}$$

where $\delta(x)$ is the Dirac delta function representing a well placed at the origin, and Darcy's law is given as

$$\boldsymbol{u} = -\frac{1}{\mu}\boldsymbol{k}\nabla p. \tag{8.10}$$

Since the fluid flow is radial around the well, it is possible to derive an analytical flow model, given as [15]

$$p(r) = p\left(r^0\right) - \frac{\mu q}{2\pi\rho k h_3}\ln\left(\frac{r}{r^0}\right). \tag{8.11}$$

Here, r^0 is a reference point (usually the well radius r_w), and h_3 is the height of the reservoir (grid block) containing the well.

We now derive the numerical well equation utilizing a cell-centred finite difference method on a square grid with a grid size h (see, Figure 8.1b). Let us start by solving (8.9) and (8.10) by a five-point stencil scheme [15]

$$\frac{\rho k h_3}{\mu}(4p_0 - p_1 - p_2 - p_3 - p_4) = q. \tag{8.12}$$

Because of the symmetry of the solution, i.e., $p_1 = p_2 = p_3 = p_4$, we obtain

$$\frac{\rho k h_3}{\mu}(p_0 - p_1) = \frac{q}{4}. \tag{8.13}$$

Assuming that the pressure, p_1, in the gridblock adjacent to the well block is computed exactly by the analytical well model, and given a value for the BHP, p_{bhp}, it follows that

$$p_1 = p_{bhp} - \frac{\mu q}{2\pi\rho k h_3}\ln\left(\frac{h}{r_w}\right). \tag{8.14}$$

Inserting (8.14) into (8.13) gives

$$\begin{aligned} p_0 &= p_{bhp} - \frac{\mu q}{2\pi\rho k h_3}\ln\left(\frac{h}{r_w}\right) + \frac{q\mu}{4\rho k h_3}, \\ &= p_{bhp} + \frac{\mu q}{2\pi\rho k h_3}\left(\ln\left(\frac{r_w}{h}\right) + \frac{\pi}{2}\right), \\ &= p_{bhp} + \frac{\mu q}{2\pi\rho k h_3}\ln\left(\frac{r_w}{\alpha h}\right), \end{aligned} \tag{8.15}$$

where $\alpha = \exp\left(-\frac{\pi}{2}\right) = 0.20788...$. Rearranging (8.15) gives the well known as Peaceman's well model

$$q = \frac{2\pi\rho k h_3}{\mu\ln\left(r_e/r_w\right)}\left(p_{bhp} - p\right), \tag{8.16}$$

where the equivalent radius is given as $r_e = \alpha h$ and $p = p_0$.

This well model is easily extended to account for anisotropic media, horizontal wells and for flow containing multiple phases. For the latter case the well equations, for phase α is given as

$$q_\alpha = \frac{2\pi k h_3}{\ln\left(r_e/r_w\right)}\frac{\rho_\alpha k_{r\alpha}}{\mu_\alpha}\left(p_{bhp} - p_\alpha\right), \quad \alpha = \text{w, nw}. \tag{8.17}$$

Note that this well model is derived utilizing a specific numerical method and a specific grid. However, the same procedure, combining the analytical and numerical solution, can be utilized to derive alternative well equations for alternative numerical methods and grids, see, e.g., [15].

8.4 Data

In this work, given realizations of the poorly known petrophysical parameters, the numerical models are utilized to generate numerical predictions of the fluid flow. The reservoir models are then history matched by comparing the predictions to real observations. Predictions of the pressure and saturation in every grid cell can be utilized to match seismic, electromagnetic, and gravimetric observations. However, for most reservoirs, the wells are the primary source of information regarding the subsurface. All well-data, used for history matching the reservoir model, are given by (8.17), but the explicit expressions for the different data types depend on the well controls. In the following, we briefly summarize the different well controls and potential data types. For some selected data types, we comment on the functional relationship between the data and the petrophysical parameters. For simplicity we assume that the wetting phase is water, denoted by a subscript w, and the non-wetting phase is oil, denoted by a subscript o.

Let us consider a well that injects water into the reservoir. This well can either be controlled by BHP or water injection rate. If the injector is controlled by BHP, and since only water is injected through the well, the water injection rate is the only available data. The injection rate is given by (8.17) as

$$q_w = \frac{2\pi k h_3}{\ln\left(r_e/r_w\right)} \frac{\rho_w k_{rw}}{\mu_w} \left(p_{bhp} - p_w\right). \tag{8.18}$$

If the well is controlled by water injection rate the BHP is the only available data, given by rearranging (8.18)

$$p_{bhp} = \frac{\ln\left(r_e/r_w\right)}{2\pi k h_3} \frac{\mu_w}{\rho_w k_{rw}} q_w + p_w. \tag{8.19}$$

A well block containing an injector will (with the exception of the first time steps) have a constant saturation, and both data available for a injection well will depend on the pressure of the water phase in the well block. Hence, with the exception of the direct dependence on the absolute permeability in the well block, the data depends on the fields petrophysical quantities through the pressure values.

Let us consider a well producing both oil and water from the reservoir. The production well can either be controlled by BHP or total production rate, given as the sum of oil and water production rate,

$$\begin{aligned} q_t &= q_o + q_w \\ q_t &= \frac{2\pi k h_3}{\ln\left(r_e/r_w\right)} \left(\frac{\rho_o k_{ro}}{\mu_o} + \frac{\rho_w k_{rw}}{\mu_w}\right) \left(p_{bhp} - p\right) \end{aligned} \tag{8.20}$$

where we for simplicity have assumed no capillary pressure. If the well is controlled by BHP, the available data are the water production rate, oil production rate, and the total production rate given by (8.20). Since the well produce multiple phases, it is also possible to measure the water cut (WCT) , that is, the water rate divided by the total production rate. If the well is controlled by total production rate, the available data is BHP, oil production rate, water production rate, and WCT. As an example, we now give the expression for the water production rate for a well controlled by total

production in the case with no capillary pressure. By comparing (8.18) and (8.20) the water production rate is given as

$$q_w = \frac{\frac{\rho_w k_{rw}}{\mu_w}}{\left(\frac{\rho_o k_{ro}}{\mu_o} + \frac{\rho_w k_{rw}}{\mu_w}\right)} q_t. \tag{8.21}$$

An equivalent expression can be derived for the oil production rate. Generally, the production data depend on the petrophysical quantities via both the pressure and the saturation values. Moreover, for some data, such as the water production rate given in (8.21), there is no dependence on the absolute permeability in the well block.

Chapter 9

Summaries of Papers

A number of scientific papers have been produced as a part of this work. In the following chapter, we present summaries of the Papers A – E, including the main results and future works.

9.1 Summary of Paper A

Title: *Numerical Comparison of Ensemble Kalman Filter and Randomized Maximum Likelihood*
Authors: K. Fossum, T. Mannseth, D. S. Oliver, and H. J. Skaug

In Paper A, we perform a numerical comparison of EnKF and RML type methods in a petroleum reservoir model small enough to allow a reference MCMC run. For cases where the forward model is non-linear the EnKF and RML methods sample differently. To understand this difference, three model characteristics, summarizing the main features of the EnKF and the RML, were defined. The effect of each of these characteristics were then assessed by a numerical investigation. Paper A was presenter at the 2012 ECMOR conference in Biarritz, France.

The comparison of EnKF and RML revealed the following difference in the three characteristics: (i) whether or not gradients are used, (ii) whether data are assimilated sequentially or simultaneously, and (iii) whether the method iterates or not. By considering the EnKF (the HIEnKF was utilized in this study), the RML (using the Levenberg-Marquardt optimization method), and two related methods, the ES and the RML1 (RML with one Gauss-Newton iteration), the effect of each of the characteristics could be assessed with respect to the sampling capabilities.

The numerical study was performed on the PUNQ-S3 case, a small-scale synthetic reservoir model, and the vertical log permeability, the horizontal log permeability, and the porosity were estimated by all four methods, applying a moderately sized ensemble. The methods were evaluated by comparing the posterior ensemble to samples obtained from an MCMC run. In this paper, we employed numerous parallel runs of a variable-at-a-time M-H algorithm. However, no rigorous evaluation of the MCMC convergence was performed. The assessment was based on comparing the data-match, the prediction capabilities, and the parameter match obtained from the four approximate methods to the corresponding MCMC values.

The numerical investigation showed that the RML and the EnKF gave equally good data-match, while the ES and RML1 obtained worse results. The result obtained by comparing data-match indicated that sequential assimilation of data or iterations are needed to obtain a good result.

All methods gave reasonable predictions of the cumulative oil recovery which captured the reference solution. The EnKF and the RML results were almost identical to the MCMC result, the RML1 result was unbiased with a significant variance, and the ES result was biased with less variance.

The comparison of the parameter values showed large differences between the methods. Generally, the RML gave parameter values that were closest to the MCMC solution. In the assessment of the parameter values, several effects caused by the moderate ensemble size were observed.

Paper A showed that different methods could have large variation in the estimated parameters even though the data-match and prediction of cumulative oil recovery were similar. It was concluded that extended investigations, including studies on very simple models, were needed to further assess the approximate methods.

9.2 Summary of Paper B

Title: *Parameter sampling capabilities of sequential and simultaneous data assimilation. Part I: analytical comparison*
Authors: K. Fossum, and T. Mannseth

In Paper B, we perform an analytical comparison of the parameter sampling capabilities for ensemble-based methods that only differ with respect to how data are assimilated. This paper is strongly connected to its companion paper, Paper C, which assess the difference between the parameter sampling capabilities of these methods numerically.

The investigation in this paper is focused on the difference between parameter estimation utilizing comparable versions of the EnKF and ES, i.e., methods that only differ with respect to how data are assimilated. However, it turns out that the RML type methods are more suitable for the analysis. For this reason, we also consider comparable versions of the RML method. The comparable methods were found to be the HIEnKF, ES, and the EnRML using one full step Gauss-Newton iteration. To establish if any results obtained from the RML type methods are valid for the EnKF type methods, the different methods were compared thoroughly.

The comparison of the methods showed that, for non-linear models, the EnKF type methods are identical to the EnRML type methods if the parameter ensemble perturbation matrix ΔM has $n_e - 1$ positive singular values. However, the difference between the methods depend on the degree of non-linearity in the forward model, and for linear forward models the methods are identical, independent of the matrix ΔM.

Utilizing the EnRML methods and considering the assimilation of one weakly non-linear data group and one linear data group, it was shown that the parameter update from the sequential assimilation scheme is identical to the parameter update from the simultaneous scheme if the weakly non-linear data group is assimilated prior to the linear data group. For the reverse case, the sequential and simultaneous schemes were shown to produce different results.

Following this, some theoretical considerations, related to the case where the methods differ, were presented. Considering the Bayesian objective function, we argue that the sequential approach will gradually increase the weight on the quadratic term in the objective function; hence, gradually linearizing the problem. This argument indicates that the maximum effect of the linearization is obtained when the data group with the highest degree of non-linearity is assimilated last. Assimilating the data sequentially ordered after ascending degree of non-linearity should, by this argument, provide a lower approximation error than simultaneous assimilation of the data or by sequential assimilation with an alternative ordering of the data.

All results, obtained in paper B, were derived using the EnRML with one full Gauss-Newton step and a high number of ensemble members. However, the investigation of the difference between the EnRML methods and EnKF methods shows that the results carry over to the EnKF methods for weakly non-linear problems. The results in this paper are summarized by the following three claims, all assuming that a sufficiently large number of ensemble members are utilized for estimating the unknown parameters.

- When assimilating one weakly non-linear data group prior to assimilating one linear data group with HIEnKF, the sampling capability corresponds to that of ES.

- When assimilating one linear data group prior to the assimilation of one weakly non-linear data group with HIEnKF, HIEnKF will outperform ES.

- When assimilating two or more weakly non-linear data groups, HIEnKF will outperform ES, particularly if the data groups are ordered according to ascending degree of non-linearity

9.3 Summary of Paper C

Title: *Parameter sampling capabilities of sequential and simultaneous data assimilation. Part II: statistical analysis of numerical results*
Authors: K. Fossum, and T. Mannseth

In Paper C, we assess the sampling capabilities of the HIEnKF, a method that assimilates the data sequentially, and the ES, a method that assimilate the data simultaneously. This paper is strongly connected to its companion paper, Paper B, which compares the two assimilation strategies analytically. The numerical investigation is specifically designed to evaluate the three claims made in Paper B.

We only wish to assess the difference in sampling capabilities caused by the different assimilation strategies. The numerical study evaluates the comparable methods HIEnKF and ES. This ensures that any difference in the sampling capabilities is caused by the difference between sequential and simultaneous assimilation. Similar to Paper A, the sampling performance of the methods are assessed by comparison with an MCMC run. However, contrary to Paper A, we perform a statistical analysis of the parameter estimation properties for all the methods. The methods are compared utilizing four different sample based measures for the performance. The non-linearity, for all data

in all experiments, was evaluated by an ensemble approximation to the non-linearity measure for stochastic models.

Applying a large number of ensemble members, the two methods were compared for both toy models and small-scale reservoir models. The toy models were all characterized by low computational requirements and easily controllable data non-linearity. To gradually increase the model complexity, the number of unknown parameters in the toy models were increased, and for each degree of complexity two setups were considered. The first setup considered the assimilation of one linear and one weakly non-linear data group, while the second setup considered the assimilation of ten weakly non-linear data groups with varying degree of non-linearity. With this flexible setup, the toy models assessed all three claims made in Paper B.

Two reservoir models were considered, the first model allowed flow in one direction while the second model allowed flow in two spatial directions. For each reservoir case we considered the assimilation of two weakly non-linear data groups with a significant difference in non-linearity. Thus, the reservoir model setup would only assess the third claim made in Paper B.

The results of the toy model experiments clearly and consistently supported all the three claims made in Paper B, while results for the reservoir models primarily showed strong and consistent support of the last claim.

9.4 Summary of Paper D and E

Paper D
Title: *Evaluation of ordered sequential assimilation for improved EnKF sampling*
Authors: K. Fossum, and T. Mannseth

Paper E
Title: *Assessment of ordered sequential data assimilation*
Authors: K. Fossum, and T. Mannseth

For many problems, several different, non-linear, data types are assimilated utilizing the ensemble-based methods. Each data group can be considered as a non-linear map from parameter space to the data space, where each map has a unique degree of non-linearity. In Paper D and E, we investigate sequential and simultaneous assimilation strategies for numerous data types representing a large variation in the degree of non-linearity. The numerical investigation considers both simple and complex forward models, with adjustable and varying degree of non-linearity. There is a special emphasis on the effect of sequential assimilation of weakly non-linear data groups ordered according to ascending degree of non-linearity. The investigation is motivated by the third claim made in Paper B, which states that there is a potential for reducing the sampling error if weakly non-linear data are assimilated sequentially ordered after ascending degree of non-linearity. A high number of ensemble members were applied in all numerical experiments, and all experiments were assessed by a stochastic measure comparing the approximate samples to samples from a MCMC run. Paper D was presented at the 2014 ECMOR conference in Catania, Italia. Paper E is an extension of Paper D and includes several additional experiments with a greater variation of non-linear forward models.

However, some numerical experiments are included in both papers.

Both Paper D and Paper E divided the numerical investigation into two parts. In the first part, Paper D and E evaluate the parameter sampling capabilities for the different assimilation strategies applied to toy models. The design of the toy models allowed a controllable variation in the degree of data non-linearity. This experimental setup could therefore assess the various assimilation strategies for a high number of numerical experiments, representing data with a wide range of non-linearity.

In the second part of the numerical study, both Paper D and Paper E investigated multiple 2D synthetic reservoir models. Here, we could not vary the degree of non-linearity in a controlled manned, but the experiments showed a large spread in the non-linearity values for the various data types and production strategies. For each experiment, a selection of data groups were assimilated using the different assimilations strategies.

The experiments illustrated that, for weakly non-linear data groups with a significant difference in the degree of non-linearity between the data groups, assimilating the data sequentially ordered after ascending degree of non-linearity provided the lowest approximation error. For cases with a low difference in non-linearity between the data groups, the various assimilation methods gave virtually identical results, and for strongly non-linear cases the results produced no consistent ranking of the methods.

Two counter examples were included in Paper E. These illustrate that the optimal assimilation strategy cannot be determined for all cases, especially if there is a significant variation in the degree of non-linearity ranging from strongly non-linear to weakly non-linear depending on the position in the parameter space.

9.5 Future work

The work presented in this thesis shows that for weakly non-linear parameter estimation problems, using ensemble-based methods, it is beneficial to assimilate the data sequentially ordered after ascending degree of non-linearity. Experiments illustrated this effect for several toy models and small synthetic reservoir cases. However, some counter examples demonstrated that there exists cases where the optimal assimilation strategy could not be determined. An interesting, but computationally demanding, follow-up of this work would be to assess sequential assimilation of ordered data for a high number of reservoir cases with a wide range of potential data. The numerical experiments could be extended to test more complex cases, this could, e.g., be cases with alternating well controls, or cases with infill well. Such investigations could, gradually, build a data-base of results, and illuminate the difference between assimilation strategies for a wide range of models and data types. A sufficiently large data-base of results could then be used to indicate rules-of-thumb for the selection of an optimal assimilation strategy.

In all the experiments presented in this work, we have used a high number of ensemble members. When ensemble-based methods are used for parameter estimation in realistic reservoir models there are strict restrictions on the number of ensemble members, and $n_e \ll n_m$. Hence, we cannot utilize the empirical approximation to the measure of non-linearity for stochastic systems. A potential follow-up of this work would be to assess the sensitivity of the results with respect to the ensemble size. Such investigations could be performed in several manners. The most natural investigation would

be an assessment of a dual experiment, using a high and a low number of ensemble members. Here, the data must be ordered after the degree of non-linearity, calculated from the case with a high number of ensemble members. Such investigation must be preformed on a synthetic reservoir case small enough to allow a high number of ensemble members. Alternatively one could select a subspace of important parameters $\boldsymbol{m}'$, such that $n_e > n_{m'} + 1$, and calculate the measure of non-linearity of the data with regards to these parameters. By applying this measure, sequential and simultaneous assimilation can be assessed for realistic reservoir cases.

For realistic reservoir cases, simultaneous assimilation of the data provides the computationally most robust and flexible approach. The essential drawback of the sequential assimilation strategy is caused by the restart step. For traditional EnKF schemes, the restart is known to cause severe convergence problems in the reservoir model. For the HIEnKF, which restarts from initial time, there are no convergence problems, but an additional computational cost related to the restart of the reservoir model. To achieve a sufficiently good result, the simultaneous assimilation algorithms usually includes some sort of iteration, either via EnRML algorithms or ES with MDA. An interesting topic for future work would be to combine sequential assimilation of ordered data with an iterative simultaneous approach. One such combination could be to first assimilate the data with a low degree of non-linearity in a sequential manner, and then assimilate the data with a higher degree of non-linearity simultaneously using an iterative approach.

Bibliography

[1] Aanonsen, S. I., Nævdal, G., Oliver, D. S., Reynolds, A. C., and Vallès, B. The Ensemble Kalman Filter in Reservoir Engineering–a Review. *SPE J. 14*, 3 (2009), 393–412.

[2] Aarnes, J. E., Gimse, T., and Lie, K. An Introduction to the Numerics of Flow in Porous Media using Matlab. In *Geom. Model. Numer. Simulation, Optim.*, G. Hasle, K. Lie, and E. Quak, Eds. Springer Berlin Heidelberg, 2007, pp. 265–306.

[3] Arulampalam, M., Maskell, S., Gordon, N., and Clapp, T. A tutorial on particle filters for online nonlinear/non-Gaussian Bayesian tracking. *IEEE Trans. Signal Process. 50*, 2 (2002), 174–188.

[4] Aster, R. C., Borchers, B., and Thurber, C. H. *Parameter Estimation and Inverse Problems*, vol. 90 of *International Geophysics Series*. Elsevier Academic Press, 2005.

[5] Aziz, K., and Settari, A. *Petroleum Reservoir Simulation*. Elsevier Applied Science, New York, 1979.

[6] Bates, D. M., and Watts, D. G. Relative curvature measures of nonlinearity. *J. Roy. Stat. Soc. B Met. 42*, 1 (1980), 1–25.

[7] Beale, E. M. L. Confidence Regions in Non-Linear Estimation. *J. R. Stat. Soc. Ser. B 22*, 1 (1960), 41–88.

[8] Bergemann, K., and Reich, S. A mollified ensemble Kalman filter. *Q. J. R. Meteorol. Soc. 136*, 651 (2010), 1636–1643.

[9] Berlinet, A., and Thomas-Agnan, C. *Reproducing Kernel Hilbert Spaces in Probability and Statistics*. Springer US, Boston, MA, 2004.

[10] Bertino, L., Evensen, G., and Wackernagel, H. Sequential Data Assimilation Techniques in Oceanography. *Int. Stat. Rev. 71*, 2 (2007), 223–241.

[11] Brooks, S., Gelman, A., Jones, G. L., and Meng, X.-L., Eds. *Handbook of Markov Chain Monte Carlo*. Chapman and Hall / CRC, 2011.

[12] Brooks, S. P., and Gelman, A. General Methods for Monitoring Convergence of Iterative Simulations. *J. Comput. Graph. Stat. 7*, 4 (1998), 434.

[13] Burgers, G., van Leeuwen, P. J., and Evensen, G. Analysis scheme in the ensemble Kalman filter. *Mon. Weather Rev. 126*, 6 (1998), 1719–24.

[14] Chen, Y., and Oliver, D. S. Levenberg–Marquardt forms of the iterative ensemble smoother for efficient history matching and uncertainty quantification. *Comput. Geosci.* (2013).

[15] Chen, Z., Huan, G., and Ma, Y. *Computational Methods for Multiphase Flows in Porous Media*. Computational Science and Engineering. Society for Industrial and Applied Mathematics, Philadelphia, 2006.

[16] Cheng, H., Datta-Gupta, A., and He, Z. A Comparison of Travel-Time and Amplitude Matching for Field-Scale Production-Data Integration: Sensitivity, Nonlinearity, and Practical Implications. *SPE J. 10*, 1 (2005), 5–8.

[17] Cotter, S. L., Roberts, G. O., Stuart, A. M., and White, D. MCMC Methods for Functions: Modifying Old Algorithms to Make Them Faster. *Stat. Sci. 28*, 3 (2013), 424–446.

[18] Cowles, M. K., and Carlin, B. P. Markov Chain Monte Carlo Convergence Diagnostics: A Comparative Review. *J. Am. Stat. Assoc. 91*, 434 (1996), 883–904.

[19] Cox, H. On the estimation of state variables and parameters for noisy dynamic systems. *IEEE Trans. Automat. Contr. 9*, 1 (1964), 5–12.

[20] Davison, A. C., and Hinkley, D. V. *Bootstrap methods and their applications*. Cambridge Series on Statistical and Probabilistic Mathematics. Cambridge University Press, Cambridge, 1997.

[21] Douc, R., and Cappe, O. Comparison of resampling schemes for particle filtering. In *Proc. 4th Int. Symp. Image Signal Process. Anal.* (2005), IEEE, pp. 64–9.

[22] European Centre for Medium-Range Weather Forecasts. *http://www.ecmwf.int/en/research/data-assimilation/assimilation-methods*.

[23] Emerick, A. A., and Reynolds, A. C. History matching time-lapse seismic data using the ensemble Kalman filter with multiple data assimilations. *Comput. Geosci. 16*, 3 (2012), 639–59.

[24] Emerick, A. A., and Reynolds, A. C. Ensemble smoother with multiple data assimilation. *Comput. Geosci. 55* (2013), 3–15.

[25] Emerick, A. A., and Reynolds, A. C. Investigation of the sampling performance of ensemble-based methods with a simple reservoir model. *Comput. Geosci. 17*, 2 (2013), 325–50.

[26] Engl, H. W., Hanke, M., and Neubauer, A. *Regularization of Inverse Problems*, vol. 375 of *Mathematics and Its Applications*. Kluwer Academic Publishers, Dordrecht, 2000.

[27] Evensen, G. Sequential data assimilation with a nonlinear quasi-geostrophic model using Monte Carlo methods to forecast error statistics. *J. Geophys. Res. 99*, C5 (1994), 10143.

[28] Evensen, G. *Data Assimilation*. Springer Berlin Heidelberg, Berlin, Heidelberg, 2009.

[29] Evensen, G., Dee, D. P., and Schröter, J. Parameter Estimation in Dynamical Models. In *Ocean Model. Parameterization*, E. P. Chassignet and J. Verron, Eds., NATO Science Series. Springer Netherlands, 1998, ch. 16, pp. 373–398.

[30] Evensen, G., and van Leeuwen, P. J. An Ensemble Kalman Smoother for Nonlinear Dynamics. *Mon. Weather Rev. 128*, 6 (2000), 1852–67.

[31] Fossum, K., Mannseth, T., Oliver, D. S., and Skaug, H. J. Numerical Comparison of Ensemble Kalman Filter and Randomized Maximum Likelihood. In *13th Eur. Conf. Math. Oil Recover. (ECMOR XIII)* (Biarritz, France, 2012).

[32] Gao, G., and Reynolds, A. C. An Improved Implementation of the LBFGS Algorithm for Automatic History Matching. *SPE J. 11*, 01 (2006), 5–17.

[33] Gelman, A., Roberts, G. O., and Gilks, W. Efficient metropolis jumping Rules. *Bayesian Stat. Oxford Univ. Press 5* (1996), 599–607.

[34] Gelman, A., and Rubin, D. B. Inference from iterative simulation using multiple sequences. *Stat. Sci. 7*, 4 (1992), 457–72.

[35] Geweke, J. Bayesian Inference in Econometric Models Using Monte Carlo Integration. *Econometrica 57*, 6 (1989), 1317–39.

[36] Gibbs, A. L., and Su, F. E. On Choosing and Bounding Probability Metrics. *Int. Stat. Rev. 70*, 3 (2002), 419–435.

[37] Golub, G. H., and Van Loan, C. F. *Matrix Computations*. Johns Hopkins series in the mathematical sciences. The Johns Hopkins University Press, Baltimore, 1983.

[38] Gordon, N. J., Salmond, D. J., and Smith, A. F. M. Novel approach to nonlinear/non-Gaussian Bayesian state estimation. *Radar Signal Process. IEE Proc. F 140*, 2 (1993), 107–113.

[39] Gretton, A., Borgwardt, K. M., Rasch, M. J., Schölkopf, B., and Smola, A. J. A Kernel Two-Sample Test. *J. Mach. Learn. Res. 13* (2012), 723–73.

[40] Gretton, A., Borgwardt, K. M., Schölkopf, B., and Smola, A. J. A kernel method for the two sample problem. In *Adv. Neural Inf. Process. Syst. 19*, B. Schölkopf, J. Platt, and T. Hoffman, Eds., no. 157. MIT Press, 2007, pp. 513 – 20.

[41] Grimstad, A.-A., Kolltveit, K., Mannseth, T., and Nordtvedt, J.-E. Assessing the validity of a linearized accuracy measure for a nonlinear parameter estimation problem. *Inverse Probl. 17*, 5 (2001), 1373–90.

[42] Grimstad, A.-A., and Mannseth, T. Nonlinearity, Scale, and Sensitivity for Parameter Estimation Problems. *SIAM J. Sci. Comput. 21*, 6 (2000), 2096–2113.

[43] Grimstad, A.-A., Mannseth, T., Nævdal, G., and Urkedal, H. Adaptive multiscale permeability estimation. *Comput. Geosci. 7*, 1 (2003), 1–25.

[44] Gu, Y., and Oliver, D. S. An Iterative Ensemble Kalman Filter for Multiphase Fluid Flow Data Assimilation. *SPE J. 12*, 4 (2007), 438–46.

[45] Haario, H., Saksman, E., and Tamminen, J. An adaptive Metropolis algorithm. *Bernoulli 7*, 2 (2001), 223–242.

[46] Hadamard, J. Sur les problèmes aux dérivées partielles et leur signification physique. *Princet. Univ. Bull. 13* (1902), 49—-52.

[47] Hager, W. W. Updating the Inverse of a Matrix. *SIAM Rev. 31*, 2 (1989), 221–39.

[48] Hastings, W. K. Monte Carlo sampling methods using Markov chains and their applications. *Biometrika 57*, 1 (1970), 97–109.

[49] Hestenes, M., and Stiefel, E. Methods of conjugate gradients for solving linear systems. *J. Res. Natl. Bur. Stand. (1934). 49*, 6 (1952), 409.

[50] Houtekamer, P. L., Mitchell, H. L., Pellerin, G., Buehner, M., Charron, M., Spacek, L., and Hansen, B. Atmospheric Data Assimilation with an Ensemble Kalman Filter: Results with Real Observations. *Mon. Weather Rev. 133*, 3 (2005), 604–620.

[51] Hvidevold, H. K., Alendal, G., Johannessen, T., and Mannseth, T. Assessing model parameter uncertainties for rising velocity of CO_2 droplets through experimental design. *Int. J. Greenh. Gas Control 11* (2012), 283–89.

[52] Iglesias, M. A., Law, K. J. H., and Stuart, A. M. Evaluation of Gaussian approximations for data assimilation in reservoir models. *Comput. Geosci. 17*, 5 (2013), 851–85.

[53] Jazwinski, A. H. *Stochastic Processes and Filtering Theory*. Academic Press, New York, 1970.

[54] Kalman, R. E. A new approach to linear filtering and prediction problems. *J. Basic Eng. 82*, 1 (1960), 35–45.

[55] Kitanidis, P. K. Quasi-Linear Geostatistical Theory for Inversing. *Water Resour. Res. 31*, 10 (1995), 2411.

[56] Kovalenko, A., Mannseth, T., and Nævdal, G. Error Estimate for the Ensemble Kalman Filter Analysis Step. *SIAM J. Matrix Anal. . . . 32*, 4 (2011), 1275–1287.

[57] Kovalenko, A., Mannseth, T., and Nævdal, G. Sampling error distribution for the ensemble Kalman filter update step. *Comput. Geosci. 16*, 2 (2011), 455–466.

[58] Kullback, S., and Leibler, R. On Information and Sufficiency. *Ann. Math. Stat. 22*, 1 (1951), 79–86.

[59] Leveque, R. J. *Finite Volume Methods for Hyperbolic Problems*. Cambridge University Press, Cambridge, 2002.

[60] Li, R., Reynolds, A. C., and Oliver, D. S. History Matching of Three-Phase Flow Production Data. *SPE J. 8*, 4 (2003), 11–4.

[61] Li, X.-R. Measure of nonlinearity for stochastic systems. In *15th Int. Conf. Inf. Fusion* (2012), no. c, pp. 1073–80.

[62] Livings, D. M., Dance, S. L., and Nichols, N. K. Unbiased ensemble square root filters. *Phys. D 237*, 8 (2008), 1021–8.

[63] Mandel, J., Cobb, L., and Beezley, J. D. On the convergence of the ensemble Kalman filter. *Appl. Math. 56*, 6 (2011), 533–41.

[64] Mannseth, T. Permeability Identification from Pressure Observations: Some Foundations for Multiscale Regularization. *Multiscale Model. Simul. 5*, 1 (2006), 21–44.

[65] Maybeck, P. S. *Stochastic Models, Estimation, and Control*, vol. 141-2 of *Mathematics in science and engineering*. Academic Press, New York, 1982.

[66] Metropolis, N., Rosenbluth, A. W., Rosenbluth, M. N., Teller, A. H., and Teller, E. Equation of State Calculations by Fast Computing Machines. *J. Chem. Phys. 21*, 6 (1953), 1087.

[67] Nocedal, J., and Wright, S. J. *Numerical Optimization*, 2nd ed. Springer Series in Operation Research and Financial Engineering. 2006.

[68] Øksendahl, B. *Stochastic differential equations*, 6th ed. Springer-Verlag Berlin Heidelberg, 2007.

[69] Oliver, D. S. Minimization for conditional simulation: Relationship to optimal transport. *J. Comput. Phys. 265* (2014), 1–15.

[70] Oliver, D. S., and Chen, Y. Recent progress on reservoir history matching: a review. *Comput. Geosci. 15*, 1 (2010), 185–221.

[71] Oliver, D. S., Cunha, L. B., and Reynolds, A. C. Markov chain Monte Carlo methods for conditioning a permeability field to pressure data. *Math. Geol. 29*, 1 (1997), 61–91.

[72] Oliver, D. S., He, N., and Reynolds, A. C. Conditioning Permeability Fields to Pressure Data. In *5th Eur. Conf. Math. Oil Recover.* (1996).

[73] Oliver, D. S., Reynolds, A. C., and Liu, N. *Inverse Theory for Petroleum Reservoir Characterization and History Matching*. Cambridge University Press, 2008.

[74] Peaceman, D. W. *fundamentals of numerical reservoir simulation*. Elsevier scientific publishing company, 1977.

[75] Peaceman, D. W. Interpretation of Well-Block Pressures in Numerical Reservoir Simulation. In *52nd Annu. Fall Tech. Conf. Exhib.* (Denver, 1977), vol. 18, Society of Petroleum Engineers.

[76] Rauch, H. E., Striebel, C. T., and Tung, F. Maximum likelihood estimates of linear dynamic systems. *AIAA J. 3*, 8 (1965), 1445–1450.

[77] Rizzo, M. L. *Statistical Computing with R*. Computer Science and Data Analysis Series. Chapman and Hall / CRC, Boca Raton, 2008.

[78] Robert, C. P. Convergence Control Methods for Markov Chain Monte Carlo Algorithms. *Stat. Sci. 10*, 3 (1995), 231–253.

[79] Roberts, G. O., Gelman, A., and Gilks, W. R. Weak convergence and optimal scaling of random walk Metropolis algorithms. *Ann. Appl. Probab. 7*, 1 (1997), 110–120.

[80] Roberts, G. O., and Rosenthal, J. S. Optimal scaling for various Metropolis-Hastings algorithms. *Stat. Sci. 16*, 4 (2001), 351–367.

[81] Roberts, G. O., and Rosenthal, J. S. General state space Markov chains and MCMC algorithms. *Probab. Surv. 1* (2004), 20–71.

[82] Roberts, G. O., and Rosenthal, J. S. Coupling and ergodicity of adaptive Markov chain Monte Carlo algorithms. *J. Appl. Probab. 44*, 2 (2007), 458–475.

[83] Roberts, G. O., and Rosenthal, J. S. Examples of Adaptive MCMC. *J. Comput. Graph. Stat. 18*, 2 (2009), 349–67.

[84] Saad, Y. *Iterative Methods for Sparse Linear Systems Second Edition*, 2nd ed. Society for Industrial and Applied Mathematics, 2003.

[85] Schölkopf, B., and Smola, A. J. *Learning with Kernels*. MIT Press, Cambridge, 2002.

[86] Scott, D. W., Ed. *Multivariate Density Estimation*. Wiley Series in Probability and Statistics. John Wiley and Sons, Inc., Hoboken, NJ, USA, 1992.

[87] Seber, G. A. F., and Wild, C. J. *Nonlinear Regression*. Wiley Series in Probability and Statistics. John Wiley and Sons, Inc., Hoboken, NJ, USA, 1989.

[88] Shawe-Taylor, J., and Cristianini, N. *Kernel Methods for Pattern Analysis*. Cambridge University Press, Cambridge, 2004.

[89] Silverman, B. W. *Density Estimation for Statistics and Data Analysis*. Chapman and Hall / CRC, 1986.

[90] Simon, D. *Optimal state estimation: Kalman, H infinity, and nonlinear approaches*. Wiley-Interscience, 2006.

[91] Skjervheim, J.-A., and Evensen, G. An Ensemble Smoother for assisted History Matching. In *Proc. SPE Reserv. Simul. Symp.* (2011), no. 2003, Society of Petroleum Engineers, pp. 1–15.

[92] Skjervheim, J.-A., Evensen, G., Aanonsen, S. I., Ruud, B. O., and Johansen, T.-A. Incorporating 4D Seismic Data in Reservoir Simulation Models Using Ensemble Kalman Filter. *SPE J. 12*, 03 (2007), 282–92.

[93] Stordal, A. S., Karlsen, H. A., Nævdal, G., Skaug, H. J., and Vallès, B. Bridging the ensemble Kalman filter and particle filters: the adaptive Gaussian mixture filter. *Comput. Geosci. 15*, 2 (2010), 293–305.

[94] Stuart, A. M. Inverse problems: A Bayesian perspective. *Acta Numer. 19* (2010), 451–559.

[95] Sylte, A., Ebeltoft, E., Grimstad, A.-A., Kulkarni, R., Nordtvedt, J.-E., and Ted Watson, a. Design of Two-Phase Displacement Experiments. *Inverse Probl. Eng. 10*, 1 (2002), 65–84.

[96] Tarantola, A. *Inverse Problem Theory and Methods for Model Parameter Estimation*. Other Titles in Applied Mathematics. (Philadelphia: Society for Industrial and Applied Mathematics), Jan. 2005.

[97] Thulin, K., Li, G., Aanonsen, S. I., and Reynolds, A. C. Estimation of Initial Fluid Contacts by Assimilation of Production Data With EnKF. In *Proc. SPE Annu. Tech. Conf. Exhib.* (2007), no. i, Society of Petroleum Engineers.

[98] Tikhonov, A. N., and Arsenin, V. Y. *Solution of ill-posed problems*. Scripta series in mathematics. V. H. Winston and Sons, Washington : John Wiley and Sons, New York, 1977.

[99] Tortorelli, D. a., and Michaleris, P. Design sensitivity analysis: Overview and review. *Inverse Probl. Sci. Eng. 1*, 1 (1994), 71–105.

[100] Trotter, H. F., and Tukey, J. W. Conditional Monte Carlo for normal samples. In *Symp. Monte Carlo Methods* (Florida, 1956), H. A. Meyer, Ed., Wiley: New York, pp. 64–79.

[101] UK Met Office. *http://www.metoffice.gov.uk/research/areas/data-assimilation-and-ensembles/4d-var-research*.

[102] van Leeuwen, P. J., and Evensen, G. Data Assimilation and Inverse Methods in Terms of a Probabilistic Formulation. *Mon. Weather Rev. 124*, 12 (1996), 2898–913.

[103] Wang, Q., Kulkarni, S. R., and Verdu, S. A Nearest-Neighbor Approach to Estimating Divergence between Continuous Random Vectors. In *2006 IEEE Int. Symp. Inf. Theory* (2006), no. x, IEEE, pp. 242–246.

[104] Wang, Q., Kulkarni, S. R., and Verdu, S. Divergence Estimation for Multidimensional Densities Via k-Nearest-Neighbor Distances. *IEEE Trans. Inf. Theory 55*, 5 (2009), 2392–2405.

[105] Wang, Y., Li, G., and Reynolds, A. C. Estimation of Depths of Fluid Contacts and Relative Permeability Curves by History Matching Using Iterative Ensemble-Kalman Smoothers. *SPE J. 15*, 2 (2010).

[106] Yustres, A., Asensio, L., Alonso, J., and Navarro, V. A review of Markov Chain Monte Carlo and information theory tools for inverse problems in subsurface flow. *Comput. Geosci. 16*, 1 (2011), 1–20.

[107] Zafari, M., and Reynolds, A. C. Assessing the Uncertainty in Reservoir Description and Performance Predictions With the Ensemble Kalman Filter. *SPE J. 12*, 3 (2007).

[108] Zhou, S. K., Chellappa, R., and Zhao, W. *Unconstrained Face Recognition*, vol. 5 of *International Series on Biometrics*. Springer US, 2006.